**Title**
Neurophysiological Oscillations as Biomarkers of Neurodevelopmental Disorders



**Author**
Frohlich, Joel

**Publication Date**
2018

Peer reviewed|Thesis/dissertation

UNIVERSITY OF CALIFORNIA

Los Angeles

# Neurophysiological Oscillations as Biomarkers of Neurodevelopmental Disorders

A dissertation submitted in partial satisfaction

of the requirements for the degree

Doctor of Philosophy in Neuroscience

by

Joel Frohlich

2018

ABSTRACT OF THE DISSERTATION

Neurophysiological Oscillations as Biomarkers
of Neurodevelopmental Disorders

by

Joel Frohlich
Doctor of Philosophy in Neuroscience
University of California, Los Angeles, 2018
Professor Shafali Spurling Jeste, Chair

Mechanism-based biomarkers are needed to guide clinical trials for neurodevelopmental disorders by indexing disease pathology or a treatment response. In this dissertation, I describe electroencephalogram (EEG) biomarkers in two neurodevelopmental disorders, Dup15q syndrome and Angelman syndrome. Dup15q syndrome is caused by duplications of 15q11.2-q13.1, including *UBE3A*—a paternally imprinted gene involved in synapse development—and several gamma-aminobutyric acid type-A ($GABA_A$) receptor subunit genes. In Angelman syndrome, the majority of cases are caused by deletions of 15q11.2-q13.1, though some cases are caused by *UBE3A* dysfunction alone. Both disorders are characterized by epilepsy, intellectual disability, and phenotypic overlap with autism spectrum disorder (ASD).

In Chapter 1, I introduce biomarkers and neurodevelopmental disorders. In Chapter 2, I infer the emergence of stable oscillations from neural noise in typically developing (TD)

preschool age children. In Chapter 3, I describe a beta EEG phenotype of Dup15q syndrome, which distinguishes children with this disorder from TD and nonsyndromic ASD controls. In Chapter 4, I compare this phenotype with beta oscillations induced with midazolam, a $GABA_A$ modulator, in healthy adult participants. Furthermore, two cases of paternal Dup15q syndrome (i.e., duplications of the *UBE3A*-silenced allele) also show this EEG phenotype, suggesting that it is a marker of GABAergic pathology. In Chapter 5, I describe a delta EEG phenotype of Angelman syndrome (previously described by Sidorov and colleagues in 2017) that is stronger in children with a deletion genotype than those with a non-deletion genotype. Furthermore, I find lower beta power and higher theta power in the deletion genotype. Thus, beta power and theta power appear to reflect GABAergic dysfunction, whereas delta power appears to reflect *UBE3A* dysfunction but is modulated by $GABA_A$ receptor gene deletion. Chapter 6 summarizes this work and provides a discussion about implications and next steps.

In conclusion, neurophysiological oscillations are likely markers of gene-specific disease pathology in Dup15q syndrome and Angelman syndrome. Clinical trials targeting specific gene products (e.g., $GABA_A$ receptors) may utilize these EEG measures as biomarkers of target engagement or surrogate endpoints.

The dissertation of Joel Frohlich is approved.

Carrie E. Bearden

Peyman Golshani

Andrei Irimia

Richard W. Olsen

Shafali Spurling Jeste, Committee Chair

University of California, Los Angeles

2018

# DEDICATION

This work is dedicated to those who have supported me the most, my parents and my wife. I'm incredibly lucky to have parents who always encouraged me to do and become what I wanted growing up. Without their nurturing attitude towards my quirky interests, I would never have found myself here today. During my internship at Hoffmann-La Roche in Basel, Switzerland, my wife, Katharina, entered my life. Katharina has been incredibly nurturing and supportive as I balance dissertation writing with our move around the globe. She and my parents are the foundation that my academic work stands on.

# TABLE OF CONTENTS

## List of Figures

### Chapter 1



### Chapter 2



### Chapter 3

## Chapter 4



## Chapter 5

## List of Tables

### Chapter 2



### Chapter 3



### Chapter 4



### Chapter 5

ACKNOWLEDGEMENTS

Chapter 2 is a version of: Frohlich J, Irimia A, Jeste SS. Trajectory of frequency stability in typical development. Brain imaging and behavior. 2015 Mar 1;9(1):5-18. http://doi.org/10.1097/WCO.0000000000000181. Specific contributions: Joel Frohlich developed the analysis, preprocessed and analyzed the data, and wrote the manuscript; Andrei Irimia guided the development of the analysis and contributed to the writing and preparation of the manuscript; Shafali S. Jeste oversaw the study as the principal investigator, guided development of the analysis, and contributed to the preparation of the manuscript.

Chapter 3 is a version of: Frohlich J, Senturk D, Saravanapandian V, Golshani P, Reiter LT, Sankar R, Thibert RL, DiStefano C, Huberty S, Cook EH, Jeste SS. A quantitative electrophysiological biomarker of duplication 15q11. 2-q13. 1 syndrome. PloS one. 2016 Dec 15;11(12):e0167179. https://doi.org/10.1371/journal.pone.0167179. Specific contributions: Joel Frohlich collected some of the data, preprocessed, and analyzed the data, and wrote the manuscript; Damla Senturk performed the statistical analysis; Charlotte Distefano collected data and performed behavioral testing of children; Scott Huberty collected data; Vidya Saravanapandian, Peyman Golshani, Larry T. Reiter, Raman Sankar, Ronald L. Thibert, Edwin H. Cook, Charlotte DiStefano, and Damla Senturk contributed to the discussion of the results and the preparation of the manuscript; Shafali S. Jeste oversaw and designed the study as the principal investigator, guided the analysis, and contributed to the writing and preparation of the manuscript.

Chapter 4 is a version of Frohlich J, Reiter LT, Saravanapandian V, DiStefano C, Huberty S, Chamberlain S, Bearden CE, Golshani P, Irimia A, Olsen RW, Hipp JF, Jeste SS. Neuronal *UBE3A* overexpression is not necessary for the Dup15q syndrome beta EEG phenotype. Manuscript in preparation. Specific contributions: Joel Frohlich collected some of the data, preprocessed, and analyzed the data, and wrote the manuscript; Larry T. Reiter provided data and contributed to the discussion of the results and the preparation of the manuscript; Vidya Saravanapandian, Charlotte DiStefano, and Scott Huberty collected some of the data; Stormy Chamberlain, Carrie E. Bearden, Peyman Golshani, Andrei Irimia, and Richard W. Olsen contributed to the discussion of results and the preparation of the manuscript; Joerg F. Hipp was co-supervisor of the study, helped design the study and analysis, provided, preprocessed, and analyzed data, and oversaw the writing of the manuscript; Shafali S. Jeste was co-supervisor of the study, helped design the study and analysis, and oversaw the writing of the manuscript.

Chapter 5 is a version of: Frohlich J, Miller M, Bird LM, Garces P, Purtell H, Hoener MC, Philpot BD, Sidorov MS, Tan WH, Hernandez MC, Rotenberg A, Jeste SS, Krishnan M, Khwaja O, Hipp JF. Electrophysiological Phenotype in Angelman Syndrome Differs Between Genotypes. Manuscript in preparation. Specific contributions: Joel Frohlich preprocessed and analyzed the data; Joerg F. Hipp supervised the study, designed the analysis, wrote code for pre-processing tools; Joel Frohlich and Joerg F. Hipp both wrote the manuscript and generated figures; Meghan Miller coordinated collaborations between researchers; Lynne M. Bird and Alexander Rotenberg were principal investigators of data collection sites; Pilar Garces contributed code that was used in

the analysis; Shafali S. Jeste reviewed participant medications; all authors contributed to the discussion of results and the preparation of the manuscript.

I am deeply grateful to all children and parents who volunteered their time to advance our knowledge of both typical and atypical development. There also many colleagues and mentors to whom I am especially thankful. Firstly, I am very grateful to my dissertation advisor and committee chair, Dr. Shafali Spurling Jeste, for her mentorship, as well as her generous flexibility in allowing me to pursue opportunities abroad while a student in her lab. I also warmly thank the other members of dissertation committee, Dr. Carrie E. Bearden, Dr. Peyman Golshani, Dr. Andrei Irimia, and Dr. Richard W. Olsen, for their time and mentorship. I also thank Dr. Joerg Hipp for both his mentorship to me at Hoffmann-La Roche and his valuable assistance in allowing me to return to Basel, Switzerland in a visiting researcher capacity several months after completing an internship under his supervision. I would also like to thank my former officemate, Dr. Iman Mohammad-Rezazadeh, for his mentorship to me in EEG signal processing and his much-needed comic relief when times were stressful in the lab. I thank Dr. Mikhail Rabinovich, Dr. Ted Hutman, Dr. Carrie E. Bearden for their comments on a draft of the manuscript adapted into Chapter 2, and Dr. Amaya Miquelajauregui for her comments on a draft of the manuscript adapted into Chapter 3. I would also like to thank my friend Nima Chenari for his kind help producing Figure 1.1., Figure 2.1, Figure 2.11, and Figure 5.1., as well as my current and former labmates Christina Shimizu, Andrew Sanders, Amanda Noroña, Scott Huberty, and Charlotte DiStefano for their patience and professionalism in assisting with data collection.

The work herein was supported by a number of sources, including NIMH K23MH094517-01, grant 20144605 from the Dup15q Alliance, R01 GM111378-01A1 from the National Institute of General Medical Sciences NIGMS (NIH), NIMH K23MH094517-01, and IDDRC U54HD087101. Work in Chapter 4 was also supported by a Shainberg Neuroscience Fund award to Lawrence T. Reiter. Work in Chapter 5 was also supported by NIH U54RR019478 (awarded to Arthur Beaudet) and U54HD061222 (awarded to Alan Percy). For ten months of my graduate training, I participated in the Roche Internships for Scientific Exchange (RISE) program as an employee of Hoffmann-La Roche in Basel, Switzerland. Another portion of my graduate training was supported by National Institute of Mental Health of the National Institutes of Health under Award Number T32MH073526. The content of this dissertation does not necessarily represent the official views of the National Institutes of Health.

# VITA

**Education**

2009 - 2012 **College of William and Mary, B.S. 2012 Neuroscience**

2008 - 2009 **University of Maryland, College Park**

**Additional Training**

2016 – 2017 **Roche internships for Scientific Exchange (RiSE) program**

F. Hoffmann-La Roche Ltd., Basel, Switzerland

2018 **Visiting researcher**

F. Hoffmann-La Roche Ltd., Basel, Switzerland

**Teaching**

2015 **Instructor - N215 Human Electrophysiology** *Professor: Shafali S. Jeste, UCLA*

2014-2015 **Teaching assistant - Neuroscience M101A** *Professor: Scott Chandler, UCLA*

**Awards**

2016 **Society for Neuroscience Next Generation Award**

Recognizes outstanding contributions to public communication in neuroscience

2015 – 2016 **Neurobehavioral Genetics T31 Training Grant**

NIMH training grant through the Center for Neurobehavioral Genetics at UCLA

2015 **Neuroimaging Training Program Offer**

Offered training grant under RFA DA-06-011

Declined due to conflict with other funding

**Publications** **Frohlich, J.**, Senturk, D., Saravanapandian, V., Golshani, P., Reiter, L. T., Sankar, R., … & Jeste, S. S. (2016). A Quantitative Electrophysiological Biomarker of Duplication 15q11. 2-q13. 1 Syndrome. PLoS One, 11(12), e0167179. https://doi.org/10.1371/journal.pone.0167179

Mohammad-Rezazadeh, I., **Frohlich, J.**, Loo, S. K., & Jeste, S. S. (2016). Brain Connectivity in Autism Spectrum Disorder. Current Opinion in Neurology, 29(2), 137–147. http://doi.org/10.1097/WCO.0000000000000301

Jeste, S. S., **Frohlich, J.**, & Loo, S. K. (2015). Electrophysiological biomarkers of diagnosis and outcome in neurodevelopmental disorders. Current Opinion in Neurology. 28 (2), 110-116 http://doi.org/10.1097/WCO.0000000000000181

**Frohlich, J.**, Irimia, A., & Jeste, S. S. (2015). Trajectory of frequency stability in typical development. Brain Imaging and Behavior, 9(1), 5–18. http://doi.org/10.1007/s11682-014-9339-3

**Frohlich, J.**, & van Horn, J. D. (2014). Reviewing the ketamine model for schizophrenia. Journal of Psychopharmacology (Oxford, England), 28(4), 287–302. http://doi.org/10.1177/0269881113512909

**Book chapters**

Coben, R., Mohammad-Rezazadeh, I., **Frohlich, J.**, Jurgiel, J., & Michelini, G. (2017). Imaging brain connectivity in autism spectrum disorder. In Casanova, M.F., El-Baz, A., Suri, J.S. (Ed.) Autism Imaging and Devices. Pages 245-286. CRC Press.

**Frohlich, J**, Van Horn, J.D. (2016) Chapter 60: Ketamine and the Dissociatives: Comparisons with Schizophrenia. In Preedy VR (Ed.) Neuropathology of Drug Addictions and Substance Misuse, Volume 2: Stimulants, Cub and Dissociative Drugs, Hallucinogens, Steroids, Inhalants and International Aspects. Part III: Dissociative Drugs, Section C: Structural and Functional Aspects. Pages 649-660. Academic Press.

# Chapter 1: Introduction

## 1.1 Behavior and the Brain

The story of understanding the brain is the story of understanding ourselves. In the brain, we search for data to explain our thoughts, desires, and illnesses. Humans dating back to at least Galen and Hippocrates have understood a link between the brain and behavior. Yet even in the twenty-first century, the bridge between neurobiology and disorders such as autism and schizophrenia is often submerged in a foggy ravine, difficult to transverse without our best scientific tools.

Galen of Pergamum, born in 129 AD, was among the first people to clearly record a relationship between the brain and behavior (Freemon 1994; Gross 1987). A physician to the Roman gladiators, Galen wrote that brain injury "at once makes men both motionless and without feeling." Correlations Galen witnessed in his patients between brain lesions and paralysis likely informed this observation. Galen also demonstrated that cutting the recurrent laryngeal nerve silences screaming animals. Crude experiments like this one supported a hypothesis put forth by the Greek physician Hippocrates several centuries prior, who postulated that the brain is the seat of mental function. By confirming that the brain is indeed the locus of sensation and the controller of movement, Galen was possibly the first person to attribute specific neurological disorders to specific brain regions. For instance, he attributed epilepsy to the posterior ventricles (Gross 1987) and noted that coma could be induced through pressure on the fourth ventricle (Freemon 1994).

Galen's understanding of movement disorders in terms of basic physiological markers has led us, over many centuries, towards an understanding of mental function in terms of brain anatomy and function. This realization—that mental illness is also physical illness—brings us to the final frontier of medicine: psychiatry. Psychiatry is the branch of medicine that treats mental disorders. We understand today that depressed mood and psychotic hallucinations are not the working of evil demons but, rather, a dysregulated brain interacting with the environment. Yet, at present, mental disorders are defined by behavioral criteria that hardly consider dimensions such as brain function and genetics (American Psychiatric Association 2013). To be sure, looking at the brain is often unnecessary for evaluating a psychiatric patient. But to deeply understand a disease, we grasp in the dark to find biological handles for psychiatric disorders, handles that open the door to disease mechanisms and treatments. Just as Galen connected brain injury to paralysis, epilepsy and coma, we seek biomarkers that connect brain function and genetics to psychiatric disorders.

What are biomarkers? An NIH Biomarkers Definitions Working Group once defined a biomarker as "a characteristic that is objectively measured and evaluated as an indication of normal biological processes, pathogenic processes, or pharmacologic responses to a therapeutic intervention" (Biomarkers Definitions Working Group et al. 2001). In other words, biomarkers are biological substances or signals that relate to a healthy or disease state.

Today, investigators commonly seek biomarkers that are quantitative, varying continuously across a population and subject to the tools of statistical analysis; furthermore, today's investigators are often looking for mechanism-based biomarkers (Shafali Spurling Jeste et al. 2015). A mechanism-based biomarker reflects the actual etiology of the disease and is not

merely correlated with the disease in a trivial sense. For instance, obesity is correlated with major depressive disorder (Dixon et al. 2003), yet one would hesitate to consider a measure such as body mass index (BMI) a biomarker of depression. Weight gain is likely a symptom of depressed mood, and an intervention that improves BMI may not directly improve mood in a patient with depression. Perhaps depressed mood sometimes results from a complex interaction between brain chemistry, metabolic factors (influenced by weight and diet), and body image. In this case, chemical markers such as brain-derived neurotrophic factor (BDNF) are likely closer to the mechanistic root of depressed mood. As such, biomarkers rooted in mechanism may inform drug treatments for a disorder by elucidating a molecular treatment target. Changes in mechanism-based biomarkers are also likely to reliably track changes in symptom severity or a treatment response. For instance, BDNF level changes induced by antidepressant drugs are associated with changes in depressive symptom scores (Matrisciano et al. 2009).

**1.2 Why do we need biomarkers?**

The story so far demonstrates two purposes of biomarkers: guiding drug development and indexing a treatment response. In fact, biomarkers serve several additional purposes beyond these, such as stratifying a disease population along clinically meaningful subgroups, predicting outcomes for patients, and linking disease pathology to symptoms. Biomarkers may also detect circuit-level treatment changes that precede behavioral changes in short clinical trials. Such clinical trials are often unable to observe long-term behavioral changes that may only be measurable months after a drug treatment. This allows biomarkers to sometimes serve

as surrogate endpoints in clinical trials, i.e., endpoints that substitute for more reliable yet challenging clinical endpoints as target outcomes.

To better understand the purposes and challenges of biomarkers, this introduction continues in the 1970s with the publication of a paper in *Science* (Rosenhan 1973) titled "On being sane in insane places." The Stanford psychologist David Rosenhan argued that psychiatric hospitals of his era failed to recognize symptom improvements in patients diagnosed with psychiatric disorders. In his *Science* paper's abstract, he wrote that it "is clear that we cannot distinguish the sane from the insane in psychiatric hospitals." (In a clinical context, one would today use the term "mentally ill" rather than "insane"). In what is now referred to as the "Rosenhan experiment," Rosenhan himself and several other participants called psychiatric hospitals and feigned auditory hallucinations. After gaining admission to 12 different psychiatric hospitals, the participants, or "pseudopatients," stopped simulating hallucinatory symptoms and behaved normally. Despite this, none of the pseudopatients were detected. Each was discharged with a diagnosis of "schizophrenia in remission" after an average stay of 19 days, with a minimum stay of 7 days and a maximum stay of 52 days.

In fact, Rosenhan's experiment was more a critique of diagnostic labels (Fontaine 2013) than a call for biologically-informed psychiatry. Nonetheless, it was among the first works to powerfully challenge the validity of behaviorally diagnosed mental disorders. Behavioral symptoms of psychiatric disorders such as schizophrenia are often overt, debilitating, and measurable. Yet without a biological handle on the disease, psychiatrists struggle to properly treat or understand mental disorders. In the case of the Rosenhan experiment, a poor health care system may even fail to discriminate health from illness. To this day, frustrations continue

with the Diagnostic and Statistical Manual of Mental Disorders or DSM (American Psychiatric Association 2013), which defines mental disorders almost entirely in terms of behavioral criteria. Former NIMH director Thomas Insel described its latest edition, DSM-5, as "at best, a dictionary, creating a set of labels" in a 2013 blog post on the official NIMH website (Insel 2013). The post continues:

> "Unlike our definitions of ischemic heart disease, lymphoma, or AIDS, the DSM diagnoses are based on a consensus about clusters of clinical symptoms, not any objective laboratory measure. In the rest of medicine, this would be equivalent to creating diagnostic systems based on the nature of chest pain or the quality of fever. Indeed, symptom-based diagnosis, once common in other areas of medicine, has been largely replaced in the past half century as we have understood that symptoms alone rarely indicate the best choice of treatment."

With the goal of transcending behavioral diagnoses and revolutionizing psychiatric nosology, NIMH has launched the Research Domain Criteria (RDoC) project (Insel et al. 2010). RDoC does not aim to replace behavioral diagnostic criteria with biological criteria, but rather to build a classification system informed by both biological and behavioral levels of understanding mental illness. Categorical labels still hold practical value: they allow us to identify specific forms of mental suffering, refer patients to an appropriate clinician, and deal with rigid, bureaucratic insurance companies. Indeed, DSM diagnoses are not disappearing anytime soon.

Yet if we want to understand or treat disease, RDoC holds promise by digger deeper, beneath the labels.

By escaping the DSM framework, RDoC may also be more sensitive to the complaints of patients. NIMH calls for "[c]linical trials [that] might study all patients in a mood clinic rather than those meeting strict major depressive disorder criteria," (Insel 2013). Indeed, such a reconceptualization of psychiatric illness as a phenotypic continuum rather than a diagnostic dichotomy may also result in a greater acceptance of patients' perspectives that were ignored in the rigid DSM framework. The new direction is one that Rosenhan might be applauding today, though he sadly died in 2012 during RDoC's infancy.

What role will biomarkers play in tracking the continuum of psychiatric disorders? An explicit assumption of RDoC is that "[m]apping the cognitive, circuit, and genetic aspects of mental disorders will yield new and better targets for treatment" (Insel 2013). Here, genetic and circuit level biomarkers promise to stratify patients into clinically meaningful subgroups rooted in different etiologies and thus responding to different treatments. Mechanism based biomarkers also promise to reveal molecular targets for drug treatments. The biomarker signal itself may be changed by the treatment, thus indexing target engagement or a treatment response.

While the RDoC framework will crucially depend on biomarkers, it is worth first considering their limitations and potential misuses. Biomarkers inform our understanding and treatment of psychiatric disorders and may soon guide efforts towards reconceptualization of diagnostic categories (e.g., RDoC). While biomarkers may soon assist in guiding and informing psychiatric diagnosis, they are not intended to replace symptom-based diagnosis in the near

future. This is in part because one cannot realistically expect perfect specificity of a biomarker for any particular psychiatric illness, i.e., only manifesting in that disorder. Given the complexity of the brain and the noisiness of EEG and neuroimaging data, one also cannot expect a biomarker to be perfectly sensitive to any particular psychiatric disorder, i.e., manifesting in all instances of that disorder. Specificity and sensitivity are thus important parameters that should be evaluated in early investigation of a biomarker, along with test-retest reliability

Ignoring the specificity of a biomarker may lead to fallacious use of reverse inference in EEG or neuroimaging. Reverse inference is the informal inference of a mental process or illness from a neuroimaging signature associated with it (Poldrack 2006). In what is perhaps the most notorious misuse of reverse inference, UC Irvine neuroscientist James Fallon informally diagnosed himself with psychopathy (Fallon 2013) after identifying hypofrontality—a marker of antisocial and violent behavior (Yang and Raine 2009)—in a positron emission tomography (PET) scan of his brain. This does not mean, however, that biomarkers have no use in the absence of symptoms, where they may be used to evaluate a patient's risk for a particular disorder. In some cases, biomarkers may also be used to prognosticate or indicate a treatment response before long-term behavioral changes have taken effect. Yet nothing brings with it the dangers of Rosenhan's world of sane people in insane places more so than the premature prospect of psychiatric diagnoses based entirely on EEG or neuroimaging. A marriage of behavior and biology in the future of psychiatry.

I sincerely hope that this dissertation will advance our scientific understanding of the relationship between the brain and behavior through biomarkers. The story begun centuries ago by Galen is still continuing, and patients are yearning for a fuller mapping of the brain-

behavior relationship. Our progress depends on patience, innovation, self-skepticism, and large-scale collaborations that facilitate productive feedback and reproducible science. Guided by such principles, I hope the work that my colleagues and I have contributed may illuminate dark caverns at the frontiers of neuroscientific knowledge, thus serving, to quote the late astronomer Carl Sagan, "as a candle in the dark" (Sagan 2011).

**1.3 Neurodevelopmental disorders**

Neurodevelopmental disorders (NDDs) are a family of conditions defined by DSM-5 that emerge during childhood development, typically before a child begins school. This period coincides with important changes in synaptic architecture (Stiles and Jernigan 2010). Biomarkers offer to revolutionize the field of NDDs, in which genetic testing is yielding an increasing proportion of cases with causative genetic variants, from single gene mutations to copy number variation (CNV) (Gaugler et al. 2014; Schaefer and Mendelsohn 2013; Tammimies et al. 2015). These genetically defined subpopulation may respond differently to treatment; thus, patient stratification using biomarkers will likely guide inclusion criteria for clinical trials.

For instance, consider autism spectrum disorder (ASD), a NDD characterized by deficits in social communication and social interaction, as well as restricted interests and repetitive behaviors (American Psychiatric Association 2013). As of DSM-5, several DSM-IV disorders—autistic disorder, Asperger's disorder, childhood disintegrative disorder, Rett disorder, and pervasive developmental disorder-not otherwise specified (PDD-NOS)—are consolidated into ASD. This consolidation admits of a phenotypic autism spectrum, but DSM-5 stops short of biologically informed criteria for diagnosing autism. The genetics of ASD are complex and involve hundreds of genes, including common variants with mild penetrance and rare variants

with strong penetrance (Geschwind 2008). There are currently no pharmaceutical treatments for the core deficits of ASD, thus emphasizing the need for biomarkers that guide ASD drug development. As mentioned above, such biomarkers might identify subpopulations of patients with specific etiologies that would respond to specific drugs. In fact, myriad CNVs and single nucleotide variants (SNVs) have been identified which are highly penetrant for ASD, though few variants account for more than 1% of cases (de la Torre-Ubieta et al. 2016).

During early development, a huge number of new synapses are born, peaking in the first year of life before being reined in by synaptic pruning, the process that eliminates extraneous synapses (Stiles and Jernigan 2010). Given the huge changes in synaptic architecture that occur during the first year of life, the path towards typical development is a thin and narrow trajectory. NDDs occur when dysregulation derails these typical processes; thus, many genes associated with ASD govern synaptic development. Given that most synapses in the brain are chemical synapses, a large number of genes associated with ASD also encode neurotransmitter receptor subunits. Despite this tremendous biological heterogeneity, several key players emerge. Many genes are associated with multiple NDDs and even other psychiatric and neurological disorders (Li et al. 2016). Given their penetrance for a variety of brain disorders, such genes are likely to be especially active in synaptic development, thus making them attractive targets for pharmaceutical interventions. In particular, two such genes—*UBE3A* and *GABRB3*—reside on the q-arm of chromosome 15 (Buiting et al. 2016; Finucane et al. 2016). Duplications and deletions of this genetic locus result in distinct genetic disorders that are highly penetrant for NDDs.

### 1.3.1 Dup15q syndrome

Duplication 15q11.2-q13.1 syndrome, or Dup15q syndrome, is a genetic disorder that is highly penetrant for NDDs such as ASD and intellectual disability. Dup15q syndrome also confers strong risk for epilepsy, sleep problems, and hypotonia (Finucane et al. 2016). It is commonly identified as the most common genetic variant associated with ASD, accounting for > 1% of cases (Abrahams and Geschwind 2008). Two duplication types exist: 1) interstitial duplications, in which the extra genetic material remains on chromosome 15, and 2) isodicentric ("idic") duplications, in which two copies of extra genes dissociate from chromosome 15, ligate end-to-end, and form an extranumerary chromosome. Interstitial duplications are generally instances of partial trisomy while isodicentric duplications are generally instances of partial tetrasomy and confer a more severe clinical phenotype (Cook Jr et al. 1997).

The 15q11.2-q13.1 region encompasses several genes that are involved in synaptic development and synaptic transmission (Fig. 1.1). The imprinted gene *UBE3A* is a ubiquitin protein ligase that is silenced from the paternal allele. It is also the causative gene of Angelman syndrome (described in the next section). Additionally, this locus contains a gamma-aminobutryic acid type-A ($GABA_A$) receptor β3/α5/γ3 subunit gene cluster. These genes, *GABRB3*, *GABRA5*, and *GABRG3* are nonimprinted (i.e., expressed biallelically) and associated with ASD (Cook Jr et al. 1998; McCauley et al. 2004) and epilepsy (Feucht et al. 1999; Tanaka et al. 2008, 2012). Different subunits display different expression profiles, e.g., the α5 subunit is expressed frontotemporally in humans (McGinnity et al. 2017). Other notable genes, whose roles in the disease pathology are poorly understood, include *HERC2* and *CYFIP1*. *HERC2*

encodes an E3 ubiquitin ligase and is associated with ASD and global developmental delay (Finucane et al. 2016; Puffenberger et al. 2012). *CYFIP1* interacts with the mammalian target of rapamycin (mTOR) pathway (Oguro-Ando et al. 2015), which is important in other causative genetic syndromes such as Fragile X syndrome (Sharma et al. 2010) and tuberous sclerosis complex (TSC) (Inoki et al. 2005). Increased CYFIP1 gene dosage also alters dendritic morphology (Oguro-Ando et al. 2015).

The Dup15q syndrome EEG is characterized by beta (12-30 Hz) frequency oscillations (Al Ageeli et al. 2014; Urraca et al. 2013) that may relate to overexpression of the duplicated β3/α5/γ3 subunit gene cluster. Given that drugs which modulate $GABA_A$ receptors often produce a beta EEG signature (Greenblatt et al. 2004; van Lier et al. 2004; Domino et al. 1989), the beta EEG phenotype in Dup15q syndrome is likely a mechanism-based biomarker of GABAergic pathology in this disorder. As such, it may soon be deployed as a marker of target engagement, treatment response, or surrogate endpoint in clinical trials targeting $GABA_A$ receptors in Dup15q syndrome.

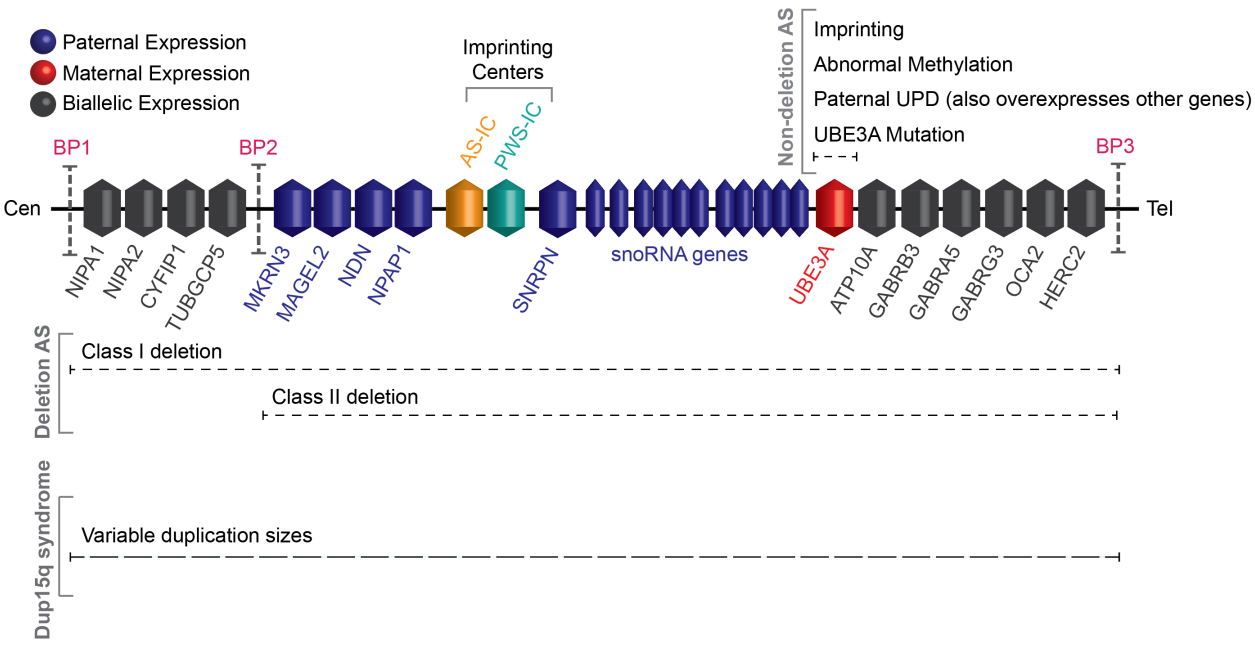


***Figure 1.1 Schematic of 15q11-q13.*** *The maternally expressed (i.e., paternally imprinted) gene UBE3A is shown in red, paternally expressed (i.e., maternally imprinted) genes are shown in blue. Genes shown in black are non-imprinted (i.e., biallelically expressed). Dup15q syndrome is caused by 15q11-q13 duplications which vary in length and may even extend beyond BP3. Angelman syndrome is caused by either 15q11-q13 deletions or mechanisms that principally impact UBE3A, such as imprinting defects, abnormal methylation, paternal uniparental disomy (UPD), and UBE3A mutations. Paternal UPD also overexpresses maternally imprinted genes. Deletion AS may encompass BP1-BP3 (Class I deletion) or BP2-BP3 (Class II deletion).*

### 1.3.2 Angelman syndrome

Angelman syndrome (AS) is a neurogenetic disorder that, like Dup15q syndrome, is characterized by seizures, intellectual disability, sleeping difficulties, phenotypic overlap with ASD, facial abnormalities, ataxia, and an abnormal electroencephalogram (EEG) (Bird 2014; Clayton-Smith 1993; Sidorov et al. 2017; Thibert et al. 2013; Trillingsgaard and Østergaard 2004;

Williams 1995). The majority of AS cases (~75%) are caused by deletions of 15q11-q13, thus mirroring the Dup15q syndrome genotype. The remaining cases principally impact *UBE3A* (Buiting et al. 2016; Clayton-Smith and Laan 2003). These include *UBE3A* mutations and imprinting defects. Paternal uniparental disomy (UPD) also results in loss of functional *UBE3A* while also impacting maternally imprinted genes, which should logically be overexpressed (Fig. 1.1).

The AS EEG phenotype is characterized by high amplitude, low frequency activity. It is thus more noticeable than the Dup15q syndrome beta EEG phenotype and was identified earlier in the literature (Boyd et al. 1988; Laan and Vein 2005; Williams 2005). Most descriptions of the phenotype were qualitative until a recent study by Sidorov and colleagues quantified the AS EEG phenotype in relation to typically developing (TD) controls (Sidorov et al. 2017). The study determined that the delta EEG phenotype in this disorder is robust to state changes (e.g., sleep) and translates well from rodent to human. However, it has remained hitherto unknown how the AS delta EEG phenotype varies between deletion and non-deletion (e.g., *UBE3A* mutation or paternal UPD) AS genotypes, a question addressed by Chapter 5 of this dissertation. Answering this question will help determine the extent to which the delta EEG phenotype is modulated by genes beyond *UBE3A*. A

A complex relationship exists between *UBE3A* and GABA in AS, even in cases where only *UBE3A* is directly affected. Animal models of AS which knockout *UBE3A* yield 1) cortical hyperexcitability, as revealed by low seizure threshold and a recapitulated delta EEG phenotype and 2) reduced GABAergic input onto layer 2/3 (L2/3) pyramidal cells (Judson et al. 2016). Surprisingly, these effects appear to be independent in rodents: knocking out *UBE3A* in only

GABAergic cells yields the cortical excitability phenotype while knocking out *UBE3A* in only glutamatergic cells yields the reduced inhibitory L2/3 input. This animal model does not explore the added complexity of deleting the $GABA_A$ receptor β3/α5/γ3 subunit gene cluster, nor other 15q genes that are deleted in the AS deletion genotype. Nonetheless, it reveals a complex interaction between *UBE3A* and GABA that must be carefully considered in order for clinical trials in AS to succeed. Studies examining EEG phenotypes in AS patients with both deletion and non-deletion genotypes should reveal the extent to which *UBE3A* and the β3/α5/γ3 subunit gene cluster contribute to clinical and EEG phenotypes in AS.

### 1.4 Neurophysiological oscillations as biomarkers

Nineteenth-century observations of oscillations in electrophysiological activity recorded from animals predate Hans Berger's 1929 description of the human EEG (Berger 1929). In 1890, Polish physiologist Adolf Beck observed fluctuating activity that varied with sensory stimulation in electrophysiological recording from the brains of animals (Beck 1890), thus reproducing similar work performed in monkeys by Richard Canton (Coenen et al. 2014). What were these squiggles recorded by early pioneers of EEG? EEG recorded from the scalp or cortical surface reflects the synchronous activity of millions of pyramidal cells (Nunez and Srinivasan 2006). The parallel orientation of these neurons' apical dendrites allows their postsynaptic potential (PSP) fields to summate, resulting in a signal that is recordable from the scalp when the apical dendrites are perpendicular to the surface of the scalp. Oscillations of this field thus reflect the simultaneous rise and fall of pyramidal cell PSPs as these neurons receive synchronized inputs. Why are inputs synchronized in this manner? Such synchronization by oscillation allows for both a receiving phase and a transmitting phase for neurons. During the receiving phase,

neurons are ready to receive and integrate synaptic stimulation; this is a state of high input gain. During the transmitting phase, neurons are spiking and deaf to new inputs; this is a state of low input gain (Buzsáki 2006; Fries 2015). Thus, neurophysiological oscillations are believed to be an energy efficient mechanism for temporal coordination of information transfer. Neuronal coherence (i.e., phase coordination) is a mechanism allowing for the effective exchange of information between neuronal populations (Fries 2015). Given that neurophysiological oscillations are a mechanistic phenomenon, neurophysiological oscillations measured in EEG signals may be utilized as mechanism-based biomarkers reflecting network dysfunction in NDDs.

The human EEG features oscillatory activity at many frequencies, with periods ranging from more than a second to mere milliseconds. Five frequencies bands are commonly identified in the literature, referenced by Greek letter names, though the divisions between these bands are in some respects as arbitrary as the boundaries between mental disorders defined by the DSM. To quote neurophysiologist György Buzsáki, "the borders between the different bands were evenly and arbitrarily drawn […] like the straight-line country borders between the African nations drawn by the colonialists" (Buzsáki 2006). The canonical EEG frequency bands are: delta, 0.5–4 hertz; theta, 4–8 hertz; alpha, 8–12 hertz; beta, 12–30 hertz; gamma, > 30 hertz (Buzsáki 2006). Different frequency bands generally reflect different neurophysiological and/or cognitive processes. Delta is associated with sleep and states of reduced consciousness (Simon and Emmons 1956). Theta is associated with exploratory behavior when recorded from hippocampus and working memory when recorded from the frontal midline of the scalp (Mitchell et al. 2008). Alpha is associated with idling or inhibition of neural computations, e.g.,

in visual cortex when the eyes are shut (Pfurtscheller et al. 1997; Ritter et al. 2009). Beta is associated with sensorimotor integration or "recalibrating the system following a movement" (Baker 2007), but is also associated with pharmacological modulation of $GABA_A$ receptors (Domino et al. 1989). Gamma is associated with cognition and binding of different features of stimuli in consciousness awareness (Tallon-Baudry and Bertrand 1999).

The boundaries between these oscillatory rhythms vary across different age groups and species. For instances, alpha is a slower rhythm in children than in adults (Lindsley 1939). In rats, the alpha rhythm is virtual absent (Buzsáki 2006), but the rat hippocampal theta rhythm is much faster (up to 14 Hz) than in other species (Buzsáki 2006; Mitchell et al. 2008). Furthermore, different oscillations of the same frequency reflect different processes in different contexts. For example, beta oscillations are often associated with arousal, yet they are also induced by benzodiazepine sedatives acting on the GABAergic system; this apparent contradiction is known as "pharmacological disassociation" (van Lier et al. 2004). Thus, an analogy between the EEG spectrum and the electromagnetic spectrum breaks down upon inspection: the significance of an EEG oscillation cannot always be identified by its frequency, unlike infrared or X-ray bands of electromagnetic radiation. For this reason, my colleagues and I advocate for a data-driven approach towards identifying neurophysiological oscillations based on peak frequencies in the EEG power spectrum. This approach is utilized in Chapter 4 and Chapter 5 of this dissertation. Spectral peaks are best identified when the EEG power spectrum is visualized with both frequency and power on a log scale. This is a useful space for visualizing the EEG power spectrum because (1) neurophysiological oscillations are equidistant in a log frequency (Buzsáki and Draguhn 2004) and (2) the "pink noise" that best describes background

EEG activity decays linearly with frequency in a log-log space, thus allowing rhythms emerging from this pink noise to be easily identified as deviations from the linear slope (Buzsáki and Draguhn 2004).

### 1.5 EEG biomarkers of neurodevelopmental disorders

EEG is well suited for studying neurodevelopment in children, as it is a noninvasive technique that circumvents some of the challenges of using magnetic resonance imaging (MRI) in pediatric populations prone to motion artifacts (Zaitsev et al. 2015). The EEG power spectrum changes over the course of development, with a general increase in power at higher frequencies (Uhlhaas et al. 2009, 2010) and a decrease in power at lower frequencies (Uhlhaas et al. 2010; Whitford et al. 2007). Neurophysiological oscillations may also reflect a maturation of synaptic architectures in early development. Infancy is characterized by a period of synaptic exuberance, in which new synapses are still being formed between neurons (Huttenlocher and de Courten 1987), thus facilitating the maturation of neural synchronization. One expects this process to sculpt oscillations from neural noise as neuronal populations wire up to one another and begin oscillating coherently. The emergence of oscillations from the buzz of dysynchronous noise should also result in changes in the complexity of the EEG signal as it evolves from a state of high entropy to a state of low entropy. The complexity of spontaneous EEG signals is thus a measure which may reflect cortical maturation. Bosl and colleagues have shown the potential of EEG complexity—as measured using modified multiscale entropy (mMSE)—to detect ASD risk in the first two years of life (Bosl et al. 2011). Chapter 2 of this dissertation explores cross-sectional changes in frequency variance—a measure that reflects the balance between EEG noise and oscillations—in a cohort of TD preschool age children.

What neurophysiological oscillations emerge—or fail to emerge—in NDDs such as ASD? Given that ASD has many etiologies and exists on a phenotypic spectrum, it is difficult, if not misguided, to look for EEG effects in the heterogenous ASD cohorts used by many studies. Furthermore, replicability of reported findings is often hindered by researchers using different EEG systems, reference channels, processing pipelines, and normalizations (i.e., relative versus absolute power). Nonetheless, EEG research in children with ASD has generally revealed deficient resting alpha power compared with TD controls, and excessive power in slower bands (i.e., delta and theta) has also been reported in the resting state by some studies (Cantor et al. 1986; Chan et al. 2007; Pop-Jordanova et al. 2010; Stroganova et al. 2007; J. Wang et al. 2013). The exact physiological processes that drive these changes remain unclear. Although many children with ASD (5-38%) have comorbid epilepsy epilepsy (Levisohn 2007) which may induce interictal EEG slowing (Noachtar and Rémi 2009), many EEG studies of ASD that exclude children with seizures still find excess slowing. Furthermore, a large study of EEGs from 889 children with ASD but without seizures (mean age 5.3 years) found epileptiform patterns in 60.7% of participants (Chez et al. 2006). Thus, ASD and epilepsy may share common etiologies rooted in GABAergic dysfunction and hyper-synchronization that disrupt typical development in the former and cause seizures in the latter (Jeste and Tuchman 2015).

The heterogeneity of ASD continues to frustrate efforts to identify biomarkers that simultaneously reflect many ASD etiologies. While different causative mechanisms might converge on common pathways (Geschwind 2008) and thus common biomarkers, much work still remains to be done in understanding how electrophysiology bridges genes with behavior in

subpopulations with common etiologies. Thus, causative genetic syndromes such as Dup15q syndrome represent an initial foothold in the search for ASD biomarkers.

### 1.6 Overview of dissertation

Scientific understanding changes over time. Nervous systems were once considered smooth, continuous networks (Cimino 1999). DNA sequences not coding for protein were once considered junk DNA (Pennisi 2012). Neither of these views are still considered valid. Likewise, our understanding of NDD biomarkers has changed over the course of the work that produced this dissertation. It is crucial to disclose several points where the interpretation of results shared by my colleagues and me has evolved since these results were first published. These points are disclosed in Chapter 6 of this dissertation. The other chapters (2-5) of this dissertation are manuscripts (either published, submitted, or in preparation) which not only tell the story of this work but also reflect our evolving interpretation and understanding of EEG biomarkers of NDDs. These chapters are archival records of manuscripts that have either been published or are currently being submitted for publication.

This story begins with the maturation of cortical networks in early childhood. Such maturation takes the form of synaptic changes that reorganize cortical networks for more efficient neural synchronization and communication. This maturation should be reflected by the emergence of neurophysiological oscillations from neural noise in spontaneous EEG signals. How can we quantify this neural reorganization? Chapter 2 of this dissertation describes frequency variance ($f_v$), a measure of EEG dynamics that is inversely related to the stability of EEG oscillations. Because neurophysiological oscillations are believed to emerge and stabilize in the first several years of life, $f_v$ is also inversely related to age in typically developing preschool

age children. It is thus a marker of typical development that underscores the importance of neurophysiological oscillations in cortical maturation.

What happens when cortical maturation goes awry? Persistent neurophysiological oscillations that are minimally modulated by task or state may be indicators of anomalous brain development and cortical dynamics. A healthy brain should switch flexibly between oscillatory states with changes in task or cognitive processes, as neuronal populations adjust their effective connectivity with other neuronal populations. For example, the EEG alpha rhythm is modulated by opening and closing the eyes. In fact, more subtle examples of this switching are observed even in task-free or resting EEG (Koenig et al. 2002; Lehmann et al. 2009), perhaps as a consequence of the fact that perceptual and cognitive processes that occur during rest take place on a sub-second timescale. The balance between hyper-stability (e.g., hypersynchrony during an epileptic seizure) and instability (e.g., random noise in immature neuronal networks) is referred to as metastability. The $f_v$ metric is a measure of metastability, as it increases almost linearly with the number of phase resets in a signal: events which interrupt neurophysiological oscillations and allow neuronal populations to rapidly desynchronize and resynchronize.

Extreme examples of hypersynchrony are observed during an epileptic seizure, when large neuronal populations fire almost simultaneously and the ictal EEG displays very high amplitude, low frequency neurophysiological oscillations. A subtler instance of anomalous brain synchrony is the beta EEG phenotype observed in Dup15q syndrome. As stated earlier in this introduction, patients with Dup15q syndrome have duplications of three $GABA_A$ receptor subunit genes, the overexpression of which may alter the decay constant of $GABA_A$ receptors. This shift in the decay constant might in turn alter the period of neurophysiological oscillations

such as gamma, slowing the frequency towards a resonant frequency at which the oscillatory amplitude greatly increases. Chapter 3 of this dissertation quantitatively describes this beta EEG phenotype in a cohort of children with Dup15q syndrome, comparing the phenotype to EEG power in age-matched TD children, as well as age-and-IQ-matched children with nonsyndromic ASD. Chapter 4 of this dissertation explores the extent to which duplications of $GABA_A$ receptor subunits genes and another gene, *UBE3A*, are necessary or sufficient for the beta EEG phenotype in Dup15q syndrome. Both chapters explore the potential utilization of the beta EEG phenotype as a biomarker that may guide drug development and clinical trials in Dup15q syndrome.

If duplications of 15q result in excessive beta oscillations, would 15q deletions result in deficient beta oscillations? If so, might disorders caused by 15q deletions such as AS benefit from EEG biomarkers that utilize EEG beta power as an index of disease pathology or treatment response? The suggested answer to both of these questions is yes, as explored in Chapter 5 of this dissertation. As stated earlier in this introduction, AS is a genetic disorder with similar clinical features to Dup15q syndrome. It is caused by disruptions of the paternally imprinted *UBE3A* gene, which may result from *UBE3A* point mutations, paternal UPD, imprinting defects, or deletions of 15q11-q13. All etiologies show greatly enhanced EEG delta power compared with TD children; however, this phenotype is stronger in children with a deletion genotype. Furthermore, the AS deletion genotype shows both excessive theta power and deficient beta power as compared with the non-deletion genotype. Thus, delta power may be applied to AS as a biomarker reflecting *UBE3A*-related pathology, whereas beta and theta power may be applied as biomarkers reflecting GABAergic pathology.

Eighty-nine years after the invention of EEG by Hans Berger, we are just learning to unlock the full potential of this tool for studying the brain and understanding disease. Like a secret code, the EEG disguises a cornucopia of information as sinusoids floating in pink noise. Whether the next generation of electroencephalographers continue to interrogate EEG with traditional methods such as Fourier transforms and Morlet wavelets, or, alternatively, explore measures of complexity such as mMSE and $f_v$, I sincerely hope this dissertation lays a foundation for future researchers, my colleagues, and myself. Indeed, Galen's project of linking behavior to the brain is still being actively realized today in the twenty-first century.

# Chapter 2: Trajectory of Frequency Stability in Typical Development

## 2.1 – Introduction

The electroencephalogram (EEG) signal recorded from scalp electrodes in humans can be understood in terms of state variables including amplitude, frequency, and topographic distribution. EEG state variables are known to be relatively static and dynamic at different temporal scales (Freeman et al. 2003; Freeman and Kozma 2010; Freeman 2004; Kaplan et al. 2005; Thatcher et al. 2008; Thatcher et al. 2009; Thatcher et al. 2009): this seemingly paradoxical balance between stability and instability is known as metastability. The prefix *meta-* generally modifies the stem of a word by raising to a higher level of abstraction (Hofstadter 1979); for instance, *metadata* is data about data, and *metacognition* is cognition about cognition. Thus, metastability is the realization that the condition of stability is often unstable. An unresolved question in brain development is, how does the degree of this instability (i.e., the balance between stationarity and nonstationarity at different temporal scales) change with age and cortical maturation? Addressing this question in typical development is necessary to understand brain stability in relation to cognitive flexibility in neurodevelopmental disorders such as autism spectrum disorder (ASD). Furthermore, a greater balance between opposing stable and unstable inclinations in functional brain data implies greater brain complexity, a concept that, while variously defined (Coffey 1998; Janjarasjitt et al. 2008; Manor and Lipsitz 2012; Meyer-Lindenberg 1996; Sporns 2011; Tononi and Edelman 1998), has already shown potential as a biomarker of ASD (Bosl et al. 2011; Catarino et al. 2011; Eldridge et al. 2014; Ghanbari et al. 2013).

In dynamical systems theory, a metastable state is transiently stable until the system which exhibits it is perturbed to another—typically lower—energy state. This can be conceptualized as a ball stuck in a depression along the slope of a hill (Fig. 2.1): the ball remains at rest until a small perturbation dislodges it and it continues to the bottom of the hill. In neuroscience, the concept of metastability provides a theoretical foundation for explaining the observed coexistence of neural sensitivity to sensory input and robustness to intrinsic noise

(Rabinovich et al. 2008) and, furthermore, it is the biophysical principle underlying the continuous emergence of new cell assemblies (Hebb 1949) through transient phase locking of neurons (Sporns 2011; Varela 1995; Werner 2007). Assuming that different cell assemblies are substrates for correspondingly different cognitive states (Varela 1995), metastability can be seen as a mechanism which endows the brain with cognitive flexibility by allowing it to shift between its seemingly opposing tendencies towards functional segregation and integration (Friston 1996, 2000; Werner 2007).

The duration of individual metastable epochs is challenging to directly measure, with most methods constrained by the need for long recordings of clean data. In studies of children, often limited by physiological artifact and variable compliance with testing, proxies of metastability are needed. Some examples include multiscale sample entropy (MSE, i.e., signal complexity) and dimensionality as estimated by principal component analysis (PCA) (Lippé et al. 2009; McIntosh et al. 2008). Another potential proxy of metastability not yet studied in early development is frequency variance. This measure can capture the synchronization and desynchronization of cell assemblies underlying cognitive states. Previous work by Freeman and colleagues has described large changes in instantaneous frequency (i.e., the time derivative of

the analytic phase) of the resting-state EEG signal; these leaps, known as phase resets, are thought to represent transitions between metastable frequency states (Freeman et al. 2003; Freeman 2003, 2004; Freeman et al. 2006; Freeman and Holmes 2005; Freeman 2004). Importantly, the measurement of frequency variance may not require clean data in every channel, as it can be examined on a channel by channel basis.

The objectives of our study were, firstly, to establish a method for measuring instantaneous frequency variance as a proxy for the phase resetting phenomenon described above and, secondly, to utilize this method to study cross-sectional development (by correlating Fv with age) in a cohort of children of ages 2 – 6. Specifically, we applied this method to brain-related independent components (ICs) yielded from an independent component analysis (ICA) decomposition of high density resting-state EEG recordings from sensors in a modified 10-20 montage. The preschool age group was chosen for our cohort as it is the age at which large gains in executive function are achieved and the frontal lobes increase steadily in gray and white matter volumes (De Luca and Leventer 2010). Moreover, it is the age at which the clinical features of neurodevelopmental disorders such as ASD emerge (Cox et al. 1999; Fountain et al. 2011; Hertz-Picciotto and Delwiche 2009, p.). We hypothesized that this method would serve as a proxy for artificial phase resets in surrogate signals and, in empirical signals, yield similar results when applied to minimal data (less than half a minute) and longer data (several minutes) from the same subjects, thus establishing it as useful and valid method for pediatric populations. Furthermore, we hypothesized that frequency stability would decrease with age, reflecting faster synchronization and desychronization of cell assemblies, the repertoire of which should expand with development. Finally, we believe that this method of quantifying

frequency stability has possible advantages over methods that measure phase locking between EEG sensors (Thatcher et al. 2008; Thatcher et al. 2009; Thatcher et al. 2009) and, thus, disregard the effective simultaneity of phase resets across large scalp distances (Freeman et al. 2003).

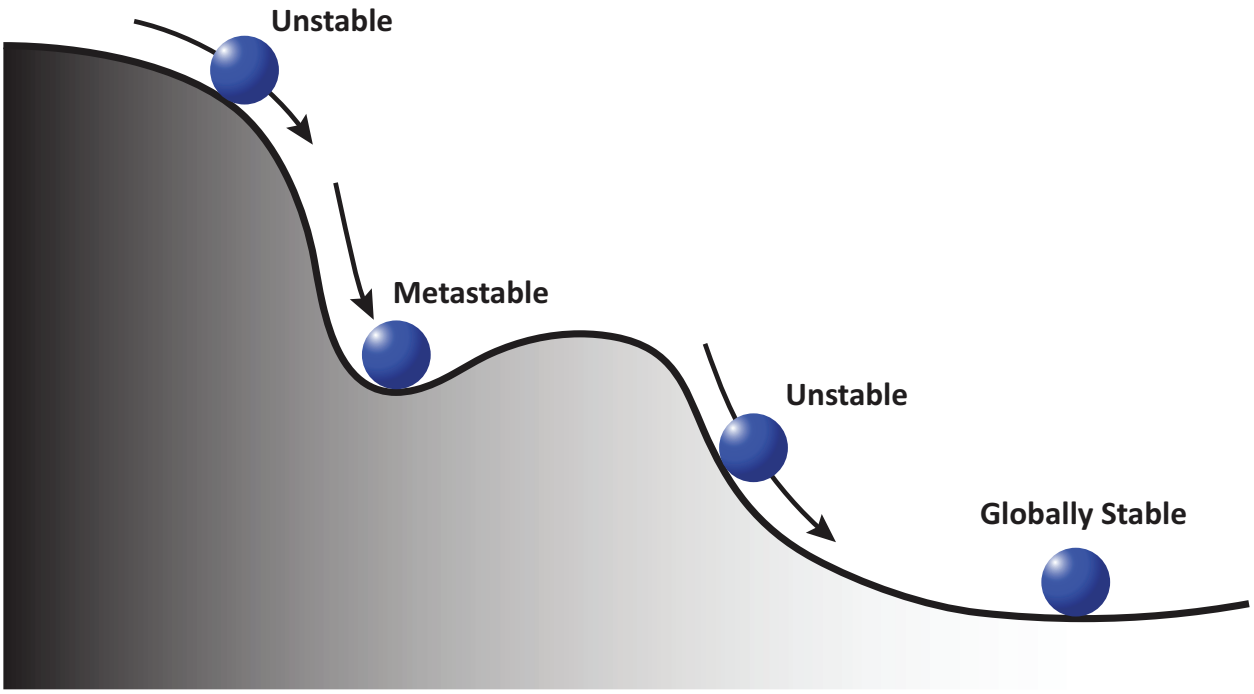


***Figure 2.1 Diagram of metastability.*** *A metastable state is analogous to a ball caught in a depression along a hill: the state is transiently stable until perturbed to a lower energy state.*

## 2.2 – Methods

Our study examined frequency variance $f_v$ in two contexts: surrogate signals, for which the number of phase resets could be directly manipulated, and brain-related ICs from resting-

state EEG recordings of typically developing children with a scalp topography consistent with a left-posterior cortical source. For each empirical dataset, the IC of interest was isolated and the fast Fourier transform (FFT) was then used to filter recordings into the 12-48 Hz bandpass, chosen so as to include beta-gamma oscillations which are known to be carrier waves for phase resets in human scalp EEG (Freeman et al. 2003). After filtering, the Hilbert transform was applied and the distribution of instantaneous frequencies was computed for the subject. The variance $f_v$ of this distribution was then investigated as a proxy for phase resetting. To ensure that $f_v$ was not influenced by the length $N$ of the signal, three separate analyses were performed using each subject's IC of interest, one using detrended segments and controlling for $N$, another using all artifact-free detrended segments, and a third taking the mean intra-segment $f_v$ value for each subject without detrending segments.

**2.2.1 - Data collection and processing**

Resting-state EEG signals were recorded using an array of 128 Ag/AgCl electrodes (Electrical Geodesics, Inc., Eugene, OR, USA) while children watched a video of bouncing soap bubbles. The Mullen Scales of Early Learning (MSEL) (Mullen 1995) or Differential Ability Scales Second Edition (DAS II) (Elliot CD 2007) were performed to verify that children had cognitive skills in the typical range. Children ages 2 - 6 ($N$ = 39, age = 53.0 ± 13.6 months, IQ = 118 ± 14.2) viewed abstract shapes on a computer monitor to capture attention for one session 120 s in duration. Recordings were amplified, digitized at a sampling rate of 250 Hz, and collected using Net Station (Electrical Geodesics, Inc., Eugene, OR, USA). Signals were bandpass filtered from 1 – 50 Hz and partitioned into 256 sample segments, in view of the fact that segments containing a number of data points equal to a power of 2 are ideal for use with the FFT. Sensors which did

not function properly either during individual recording segments or throughout the entire recording were marked as such using a 200 μV threshold and their signals were interpolated from neighboring channels. To limit the proportion of interpolated data, an upper limit was established such that the number of interpolated data points in a segment should not exceed the square root of the total number of data points. Accordingly, segments with more than 11 channels whose recordings needed to be inferred via interpolation were rejected on these grounds. Both channels that were interpolated only in a given segment and interpolated throughout the entire recording were counted towards this threshold for a given segment. Preprocessed signals were exported to MATLAB and analyzed using the EEGLAB toolbox (Delorme and Makeig 2004), where they were visually inspected so that segments containing ocular or muscle artifacts could be rejected.

**2.2.2 – Independent component analysis**

Subsequent to signal preprocessing, a combined approach involving PCA followed by ICA was utilized to identify one or more brain-related ICs in the recordings. This was accomplished using the modified infomax ICA algorithm provided by the EEGLAB toolbox (Amari S-I et al. 1996; Bell and Sejnowski 1995; Delorme and Makeig 2004; T. W. Lee et al. 1999). Recordings acquired using 20 sensors approximately corresponding to the international 10-20 montage were concatenated across subjects prior to PCA/ICA in order to ensure that (A) each subject had the same signal decomposition and that (B) subsequent analysis results would not be confounded by distinct ICA decompositions across subjects. Because recordings were vertex-referenced, sensors immediately anterior (Fcz) and posterior (CpZ) to Cz were substituted for Cz in this approximation of the 10-20 montage. Use of this montage serves as a spatial filter and

increases the ratio between the number of time points in each signal to the number of variables in each dataset, which is an important consideration for assessing the validity of PCA and ICA decompositions (Onton et al. 2006). We first performed a dimensionality reduction to 8 principal components (PCs), which were subsequently decomposed into 8 sub-Gaussian ICs.

**2.2.3 – Frequency variance**

As an inverse measure of frequency stability and as a proxy for the phase reset phenomenon, we examined the variance of the instantaneous frequencies exhibited by each IC during the resting-state. To investigate frequency metastability, we used the Hilbert transform, which is a linear transform similar to the Fourier transform but with higher temporal resolution and lower frequency resolution. This higher temporal resolution is necessary for estimating the instantaneous frequency of the signal. The Hilbert transform $H(u)$ of some signal $u(t)$ is given by the integral equation

$$H(u) = \frac{1}{\pi}\text{P.V.}\int_{-\infty}^{+\infty} u(t')/(t-t')dt' \quad (1)$$

where P.V. is the Cauchy principal value needed to solve the improper integral. The imaginary solution together with the real signal $u(t)$ yields the analytic signal $V(t)$ by the following relation:

$$V(t) = u(t) + iH(u) \quad (2)$$

From these real and imaginary components of the analytic signal, it is trivial to compute the analytic phase, $\Phi(t)$:

$$\phi(t) = \operatorname{atan}\left(\frac{H(u)}{u(t)}\right), \phi(t) \in [-\pi, +\pi] \quad (3)$$

For the purpose of taking the time derivative of $\Phi(t)$, it is necessary to unwrap the phase angles so that they are no longer bounded between –π and +π. This is accomplished by the unwrap function, which adds multiples of ± 2π at temporal differences in $\Phi(t)$ greater than a tolerance value of π. The instantaneous frequency, $f(t)$, is the time derivative of the unwrapped analytic phase of the signal:

$$\text{unwrap}\,[\Delta\phi_i(t)] = \begin{cases} \Delta\phi_i(t) + 2\pi, & \Delta\phi_i(t) \leq -\pi \\ \Delta\phi_i(t), & -\pi < \Delta\phi_i(t) < -\pi \\ \Delta\phi_i(t) - 2\pi, & \Delta\phi_i(t) \geq \pi \end{cases} \quad (4)$$

$$f(t) = \frac{d\text{unwrap}[\phi(t)]}{dt} \quad (5)$$

One can imagine the analytic phase (i.e, the antiderivative of instantaneous frequency) of the EEG signal in the context of turbulent ascent by a passenger jet into the air. Normally, the ascent is smooth and altitude is a monotonically increasing function of time. However, occasional turbulence causes large dips and jumps in the altitude of the jet. Such dips and jumps (analogous to phase resets, Fig. 2.2A) bracket periods of otherwise stable ascent velocity (analogous to frequency, Fig. 2.2B).

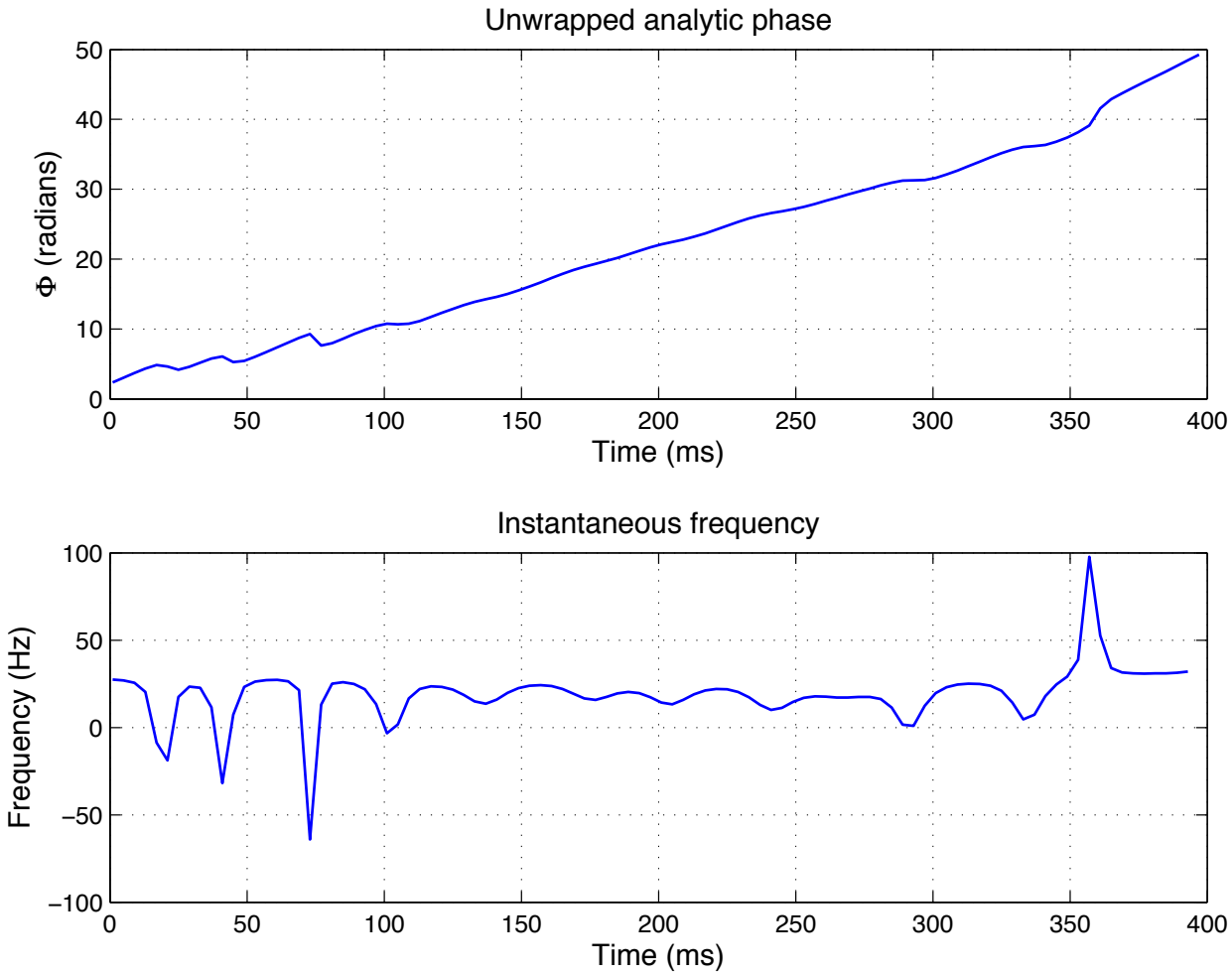


***Figure 2.2 Instantaneous phase and instantaneous frequency.*** *Unwrapping the analytic phase of a bandpass-filtered EEG signal yields an almost monotonically increasing ramp function (A). Small discontinuities in the otherwise smooth ramp are phase resets. The time derivative of the unwrapped analytic phase is the instantaneous frequency of the signal (B). Instantaneous frequencies obtained from the analytic phase are instances of angular frequency and, as such, can assume negative values.*

To emphasize local variance, a normalization operation was performed whereby the mean instantaneous frequency was subtracted from all instantaneous frequency values.

$$f_N = f_j(t) - \frac{1}{N}\sum_{j=1}^{N} f_j(t) \quad (6)$$

The variance $f_v$ of the normalized instantaneous frequency $f_N$ can be conceptualized as a surrogate measure of phase reset, and the frequency stability $f_s$ of the signal is defined as the inverse of $f_v$:

$$f_v = \mathrm{var}(f_N) \quad (7)$$

$$f_s = 1/f_v \quad (8)$$

To ensure that $f_v$ is a good proxy of phase resetting, we induced the latter in several surrogate signals of length *N* at random time points using amplitude inversion and measured $f_v$ as a function of the number of phase resets *n*. Four types of surrogate signals were used: sinusoids, pink (power-law) noise, white noise, and the logistic map. The logistic map is a 2nd degree polynomial mapping that demonstrates chaotic behavior, or extreme sensitivity to initial conditions, for certain parameter values. Unlike colored noise, the logistic map mimics deterministic chaos in the EEG signal (Fell et al. 1993; Meyer-Lindenberg 1996; Soong and Stuart 1989; Stam 2005; X. Wang et al. 2010). It is expressed by the following recurrence relation:

$$x_{n+1} = rx(1 - x_n) \quad (9)$$

Our logistic map surrogate signal used parameter values $x_0$ = 0.3, r = 3.7, a point in parameter space that yields chaotic solutions.

Unlike the logistic map, the complexity of colored noise signals is the result of a stochastic process. Pink noise signals are colored noise with power spectral density inversely proportional to the frequency of the signal raised to some power a. For our surrogate signals, we used pink noise with a = 2. Pink noise surrogate EEG signals were generated using MATLAB code by Little and colleagues (Little et al. 2007), distributed for free online at http://www.maxlittle.net/software/.

Having measured $f_v$ as a function of $n$ in surrogate signals, we held $n/N$ constant at 0.04, mimicking physiological resets rates at a sampling rate of 250 Hz, and measured $f_v$ ($N$) over 10 simulated trials to infer the minimum value of $N$ for which $f_v$ ($N$) assumes a relatively constant value in the limit of large $N$.

For empirical datasets, three separate analyses were performed using the subject's left-posterior IC. For each analysis, the IC signal was beta-gamma filtered from 12 to 48 Hz using inverse FFT filtering. Because ICA was used in conjunction with traditional methods of artifact removal to isolate brain-related activity, the IC of interest is an exquisitely clean signal, with virtually any artifact escaping the first round of rejection removed by ICA. For the first analysis, the first 29 segments of the IC signal were examined, with 29 corresponding to the number of clean segments in the smallest dataset. Linear trends were removed from all 29 segments to eliminate spurious phase resets possibly created by concatenating discontinuous segments. A single $f_v$ value for the entire IC signal was then computed. In the second analysis, the length of the IC signal was not controlled for and all clean segments were used. As with the first analysis,

each segment was detrended and a single $f_v$ value computed for the entire signal. Because the possibility of spurious phase at discontinuities created by concatenation cannot be entirely eliminated even by detrending segments, a third and final analysis was performed in which $f_v$ was computed for each clean segment of the signal and the mean intrasegment $f_v$ value was then taken as a measure of frequency variance for each subject. In all three analyses, directional statistics (Berens 2009) were utilized to examine the direction variance *S* of signal phases in the IC.

**2.3 – Results**

**2.3.1 – Surrogate EEG signals**

In surrogate signals, we found that, for sinusoids, pink noise (i.e., power law-distributed noise) with power law exponent a = 2, and a signal with deterministic chaos properties (logistic map, $x_0$ = 0.3, r = 3.7) the curve $f_v$ (*n*) increases monotonically with added noise (Fig. 2.3). The only signal for which $f_v$ did not increase as a function of *n* was Gaussian white noise. Subsequently, $f_v$ (*N*) was measured while holding *n*/*N* constant at 0.04 to ascertain the minimum length of data for which meaningful measurement of $f_v$ can be made. We found that the $f_v$ (*N*) curve follows the behavior of a damped, noisy oscillation when examined as a function of the independent variable *N* (Fig. 2.4). To find the value of *N* where the oscillation asymptotes, we examined the cumulative variance of $f_v$ (*N*), i.e., the variability of the instantaneous frequency variance, or "metavariance," as a function of signal length. The metavariance monotonically decreases following a power law and as a function of signal length after ~$2 \times 10^3$ samples (Fig. 2.5).

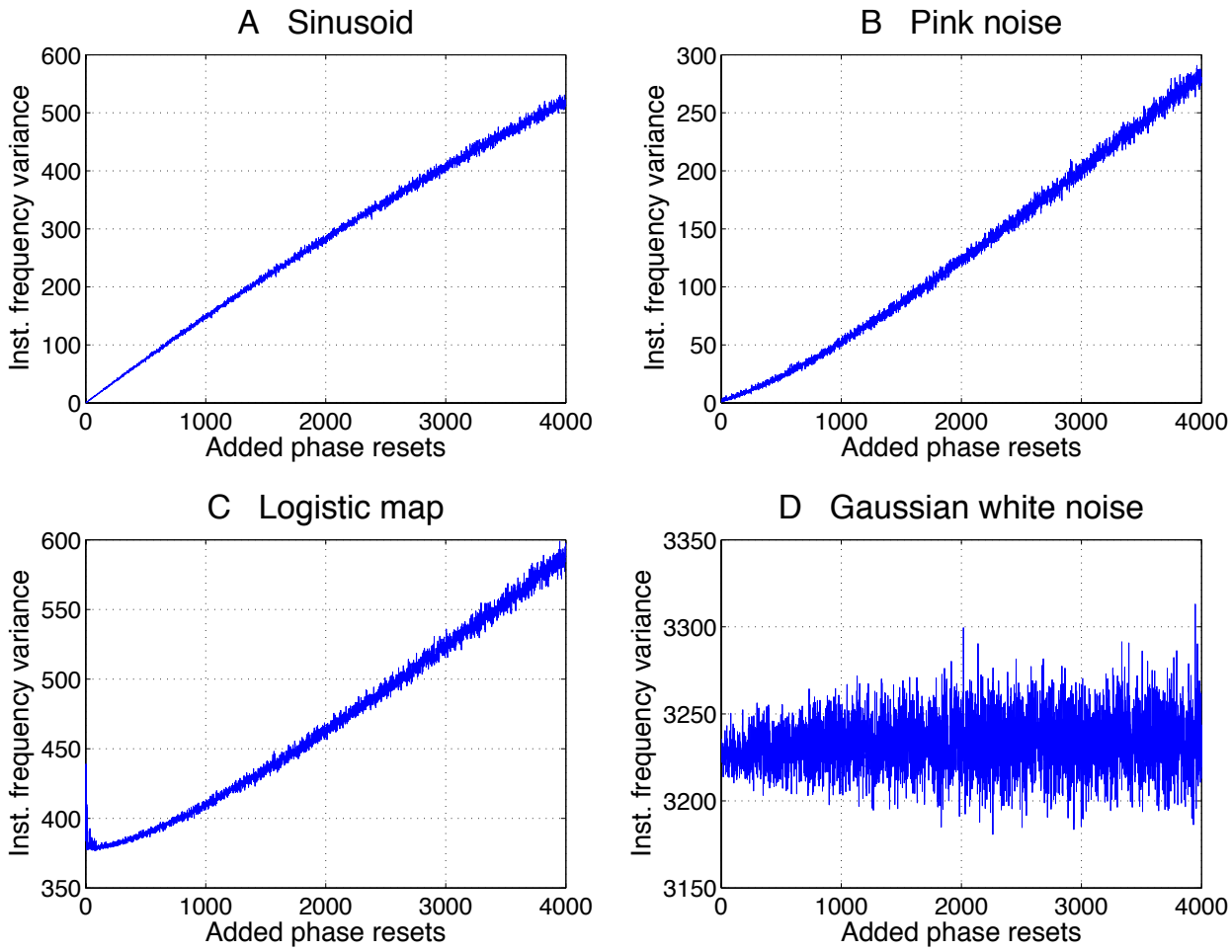


***Figure 2.3 Frequency variance in surrogate signals.*** *Four surrogate signals consisting of 5 × $10^4$ time points each were used to assess frequency variance as a proxy of phase resets. Shown are the profiles of the instantaneous frequency variance as a function of phase resets in the surrogate signal: (A) sinusoid, (B) pink (power law) noise with power law exponent α = 2, (C) signal exhibiting deterministic chaos generated using a one-dimensional logistic map ($x_0$ = 0.3, r = 3.7), and (D) Gaussian white noise with a signal mean of zero and unity variance. Phase resets were added to surrogate signals at random time points using the amplitude inversion method. As expected, frequency variance is seen to increase almost monotonically with the number of phase resets for all surrogate signals except in the case of Gaussian white noise.*

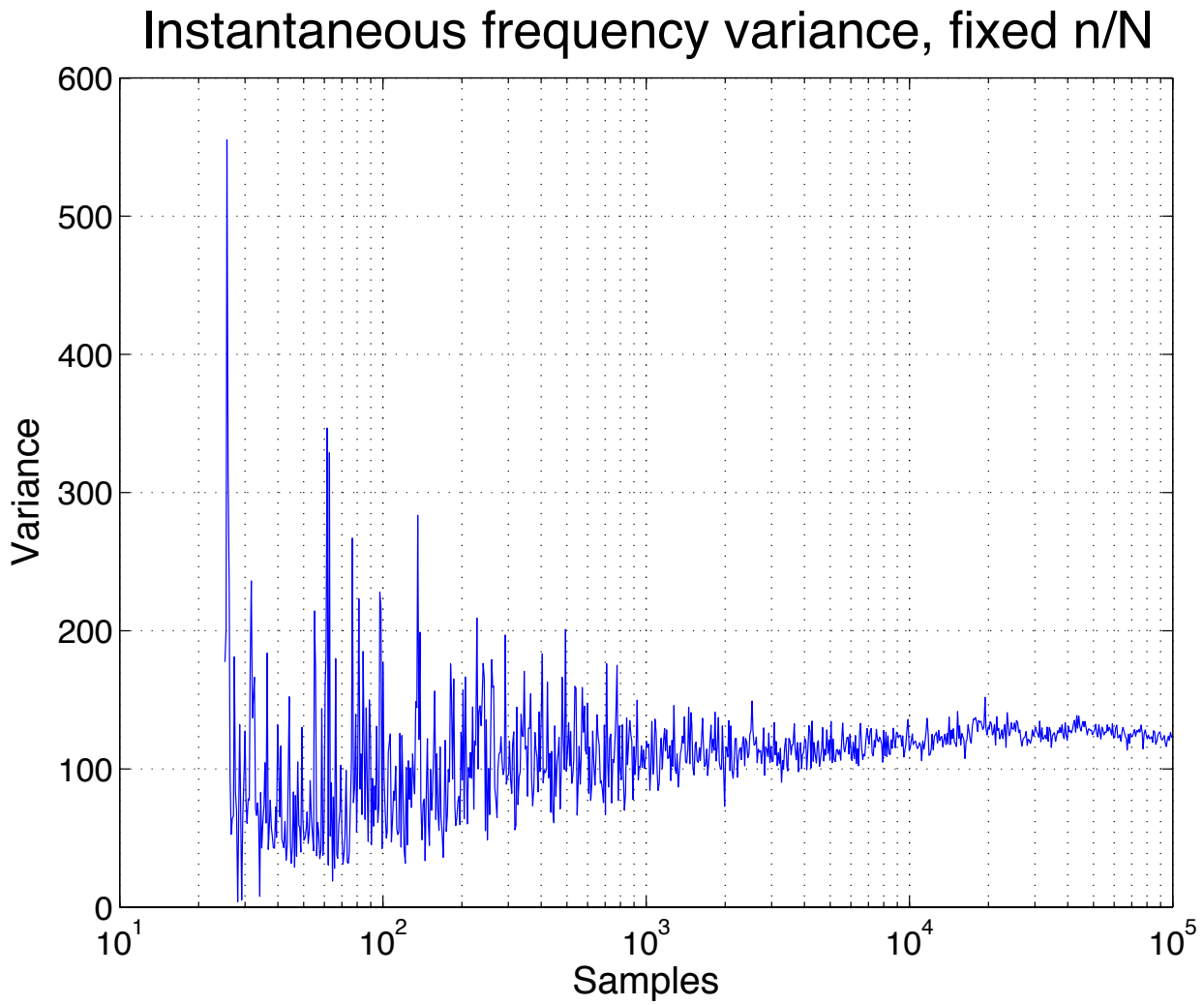


***Figure 2.4 Frequency variance reaches an asymptote after $10^3$ samples.*** *Pink (power law) noise with a power law exponent of a = 2 was used as a surrogate signal. The number of phase resets per sample (n/N) was held constant at 0.04 so as to observe the asymptotic behavior of $f_v$ as the number of points in the signal increased. Results are plotted on a semi-logarithmic scale to emphasize that the $f_v$ variance ("metavariance") can be accurately captured from ~$10^3$ samples.*

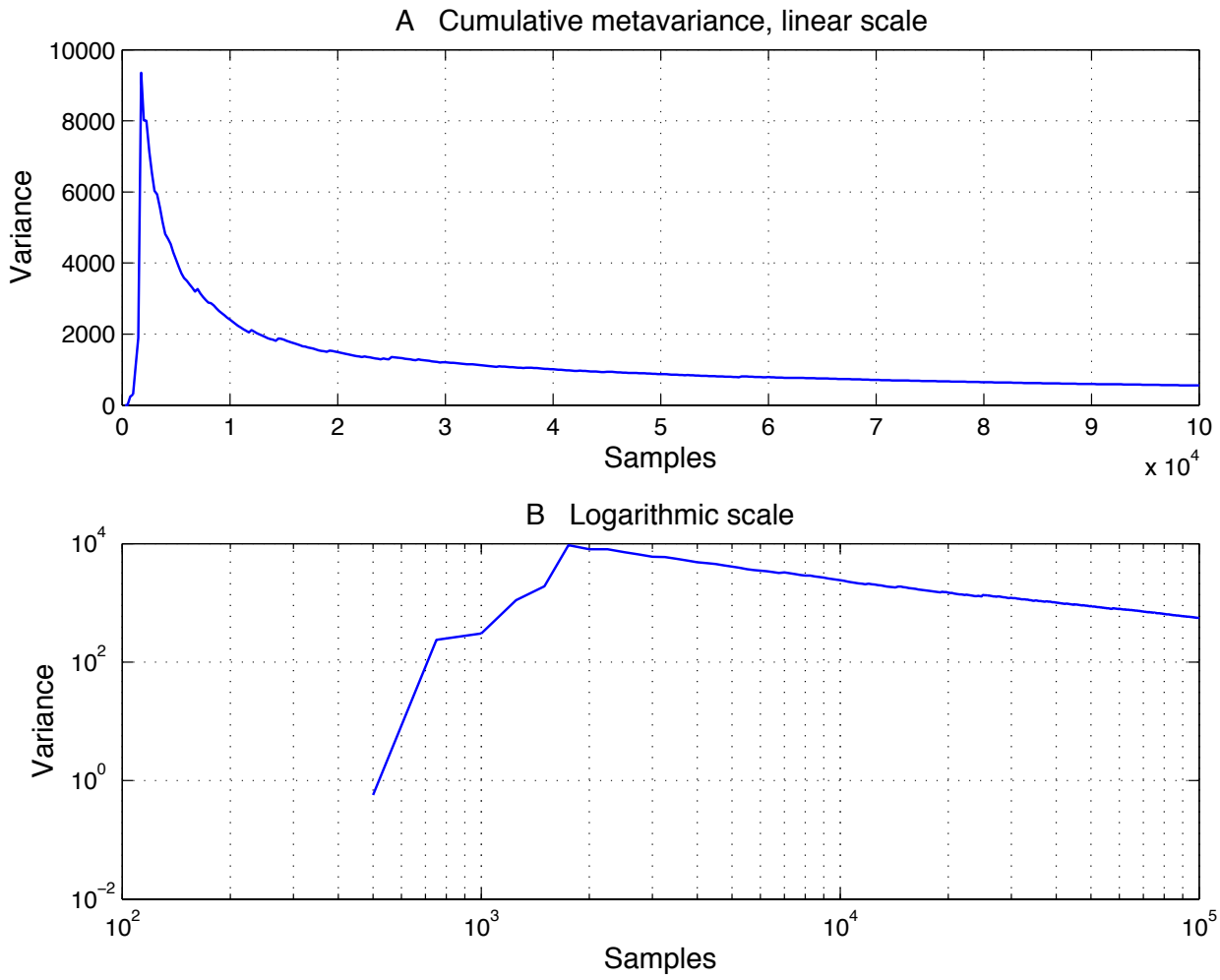


***Figure 2.5 Cumulative metavariance as function of signal length.*** *Cumulative $f_v$ variance ("metavariance") for a surrogate pink noise signal with n/N = 0.04 averaged over 10 trials (A). Plotting in log-log coordinates (B) reveals a power law relationship (linear region) after $N \approx 2 \times 10^3$. This number is thus a useful estimate of the minimum data length necessary for meaningful measurement of $f_v$.*

### 2.3.2 –Resting-state EEG signals

Data from all subjects were concatenated for the decomposition, thus all subjects shared precisely the same ICA weights matrix. Most ICs were found to be associated with noise and artifacts, such as blinks, saccades, and the presence of excessive noise in peripheral channels (Fig. 2.6). However, one IC which was most likely related to brain activity was identified in the decomposition of the concatenated data, corresponding to a dipolar pattern over the left posterior region of the head (Fig. 2.7). Unpublished data from our lab has found differences in theta (4-7 Hz) power in this scalp region between high and low functioning children with ASD. The remainder of our analysis is consequently focused exclusively on this IC whose topology resembles that of a left posterior dipole. Averaging the power spectral density (PSD) of this IC from each subject showed that posterior alpha rhythms occur at 8-9 Hz in our cohort of children (Fig. 2.8).

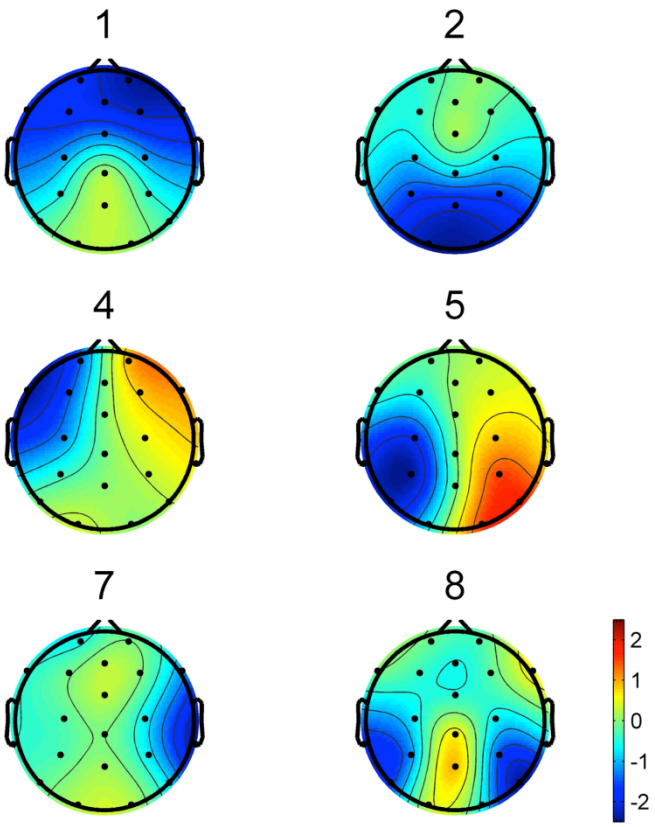


***Figure 2.6 Topography of ICA components.*** *A combined PCA and ICA decomposition yielding 8 ICs. Only $IC_5$ features a strong, dipole-like scalp topography indicative of a brain-related component. Other ICs feature scalp topographies indicative of ocular artifacts ($IC_4$, $IC_6$), or were otherwise ambiguous in origin ($IC_1$, $IC_2$, $IC_3$, $IC_7$, $IC_8$).*

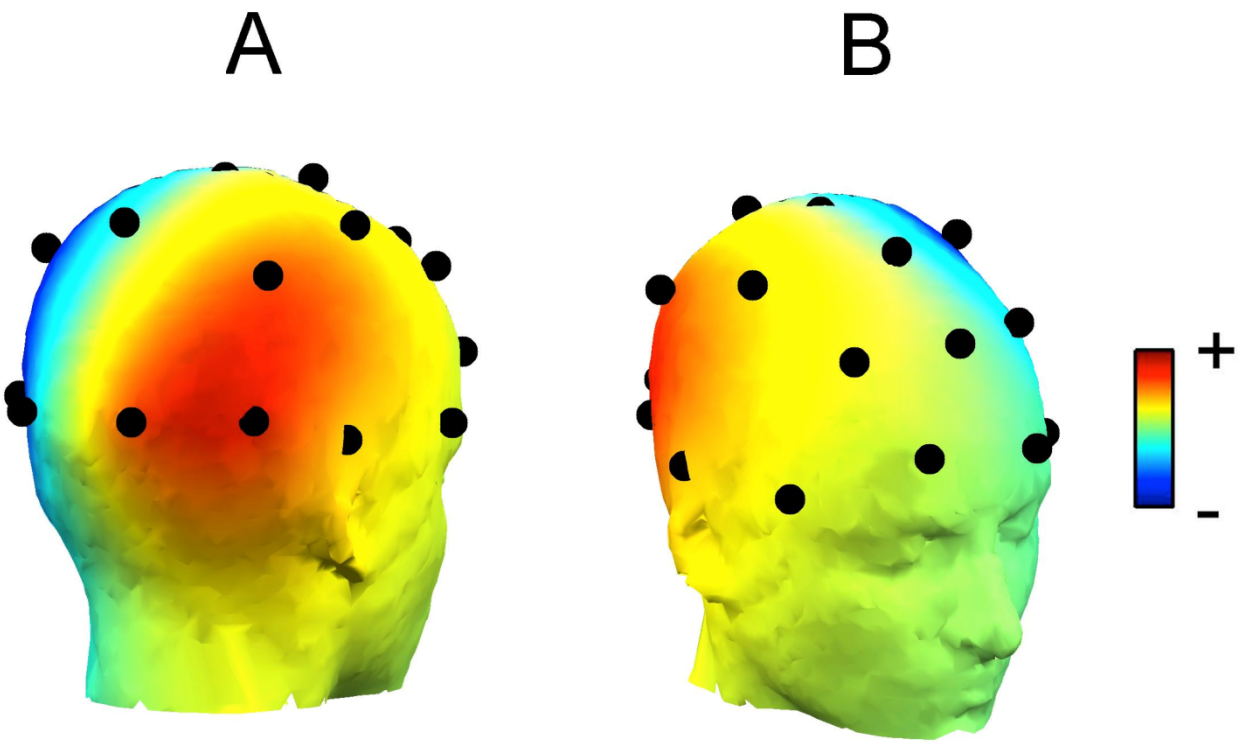


***Figure 2.7 Left posterior IC.*** *A left posterior IC was selected from the ICA decomposition as the focus for our analysis of frequency metastability and projected onto a sample head model*

Although there was no significant correlation between $f_v$ and signal length $N$ in the analysis which did not control for $N$ ($r$ = 0.25, $p$ = 0.12), we nonetheless took the precaution described in the methods section of performing three separate analyses, one controlling for $N$, another using all clean segments of the IC signal, and a third which also used all clean IC signal segments but computed $f_v$ as the mean intrasegment frequency variance.

In the analysis controlling for $N$, the first 29 segments ($N$ = $7.42 \times 10^3$) of artifact-free recordings from each subject were examined (this corresponded to the length of the shortest artifact-free dataset). Using these IC segments, a significant negative correlation between age and $f_v$ ($r$ = -0.38, $p$ = 0.018; Fig. 2.9A) was found. The IC of interest showed little to no phase

preference as measured by directional variance $S$ ($\mu_S$ = 0.99, $\sigma_S$ = 0.0046), where $S$ = 0 indicates absolute phase preference and $S$ = 1 indicates zero phase preference. Furthermore, there was no significant correlation between phase preference as measured by $S$ and $f_v$ ($r$ = -0.13, $p$ = 0.94).

In the analysis using the entire IC signal composed of all clean segments, we also found a significant negative correlation between age and $f_v$ ($r$ = -0.41, $p$ = 0.010; Fig. 2.9B). As with the first analysis, the IC signal showed no phase preference as measured with $S$ ($\mu_S$ = 0.99, $\sigma_S$ = 0.0035), nor did $S$ correlate with $f_v$ ($r$ = 0.020, $p$ = 0.90).

In the final analysis, in which linear trends were not removed from segments and the mean intrasegment frequency variance was taken as $f_v$, a negative correlation between age and $f_v$ was found which was both significant and stronger than that discovered in the previous two analyses ($r$ = -0.47, $p$ = 0.0028; Fig. 2.9C). Once again, no phase preference was revealed by $S$ ($\mu_S$ = 0.96, $\sigma_S$ = 0.0023), and $S$ showed no correlation with $f_v$ ($r$ = 0.022, $p$ = 0.89).

**2.4 – Discussion**

Our study had two principal aims: to establish a method for measuring metastable brain dynamics in children, and to use this new measure to study development in a cross-sectional cohort of young children of ages 2 – 6. Our method improves on other studies of brain metastability in development by (A) using frequency variance as a variable that corresponds to synchronization of cell assemblies, (B) is useful for minimal data with missing channels, and (C) avoids using phase relations between EEG sensors, which are not sensitive to global phase

resets. Using surrogate signals with artificially induced phase resets, we showed that $f_v$ is a good proxy for phase resetting. Having established the utility of the method, we showed that $f_v$ correlates with age in young children and gives similar results with different lengths of recordings (Fig. 3.9), thus showing promise as a biomarker of typical, and by extension, atypical development.

As stated previously, our new method for measuring frequency stability shows strong advantages for studying pediatric populations, in which children yield minimal data, over methods that directly measure the duration of metastable states, which are vulnerable to missing data. Our method allows noisy channels to be discarded with little consequence and can be applied to "virtual channels" such as brain-related ICs. Furthermore, our method takes into account the long range spatial correlations of phase resets, a consideration disregarded by a similar methodology practiced by Thatcher and colleagues (Thatcher et al. 2008; Thatcher et al. 2009; Thatcher et al. 2009). Our method is also well suited for the short datasets often obtained from children, as it gives similar results with both maximal and truncated EEG recordings.

We demonstrated that $f_v$ increases monotonically with noise as a function of the number of artificially induced phase resets in three surrogate signals: sinusoids, pink noise, and the logistic map (deterministic chaos) (Fig. 2.3). The relationship between $f_v$ and the number of phase resets $n$ is almost linear for small phase reset rate $n/N$, where $N$ is length of data. For large $n/N$, the $f_v$ ($n$) curve shows the relaxation characteristic of a hyperbolic tangent function with added noise. In a physiologically plausible scenario, an EEG signal with a sampling rate of 250 Hz and aperiodic alpha-frequency (10 Hz) phase resets (Freeman et al. 2003), $n/N$ = 0.04,

which is a sufficiently small ratio to approximate the $f_v$ ($n$) curve as linear. For the fourth surrogate signal, Gaussian white noise, $f_v$ did not increase as a function of $n$. Because the power spectrum of human EEG is power-law distributed (pink noise) rather than uniform (white noise) (Pritchard 1992), white noise is a poor model of EEG, and the finding that $f_v$ does not increase with the number of artificially induced phase resets in white noise signals should not affect the validity of our subsequent analysis using empirical data better modeled as pink noise. Having established that $f_v$ is a good proxy for phase resetting in surrogate signals with similar properties to human EEG, we measured $f_v$ while holding the rate of phase resets constant and increasing the length of surrogate data. The cumulative variance ("metavariance") was computed for the instantaneous frequency variance $f_v$ averaged across signals from 10 simulated trials (Fig. 2.5). The curve follows a power law after $N \approx 2 \times 10^3$ points, as evidenced by the linearization of the curve observed after applying the logarithmic transform. Power law relationships are scale-invariant and thus lack a time constant. The identification of a power law relationship between metavariance and the number of points in the simulated signal after $N \approx 2 \times 10^3$ suggests that this is the minimum number of points needed to compute $f_v$ with accuracy. Assuming that the minimal $N$ necessary for accurate measurement of $f_v$ depends on the number of phase resets in the recording, an inverse linear relationship between phase reset rate and minimum necessary recording length can be inferred. For instance, a signal with phase resets occurring at an average rate of 5 Hz would require $N \approx 4 \times 10^3$, twice the number of samples specified above.

In the second half of our study, all 39 subjects had artifact-free recordings longer than the minimum signal length $N = 2 \times 10^3$ established by the surrogate signal analysis ($\mu = 2.19 \times$

$10^4$ ± 9.78 × $10^3$; min = 7.42 × $10^3$, max = 4.91 × $10^4$). A left posterior brain-related IC was identified from the ICA decomposition of all subjects' EEG recordings and selected as the target for remainder of our analysis. Inspection of the average PSD computed from this IC signal shows a spectral peak around 8.5 Hz indicative of alpha rhythms (Fig 8 A). Presuming that phase resets occur, on average, at alpha frequencies (Freeman et al. 2003), our model of 10 Hz phase resetting in surrogate signals closely matches the frequency of alpha oscillations in the children herein examined (Fig. 2.8B). Furthermore, the beta and gamma frequency bands of this averaged PSD show no spectral peaks indicative of electromyography (EMG) artifacts, supporting the conclusion that this IC signal is generated by brain-related activity. Using signals from this IC, we were successful in correlating $f_v$ with age in children ages 2 – 6, implying that frequency stability changes across early development. By applying the same methods while controlling for length of signal in the first analysis and using all artifact-free recordings in the second analysis, we obtained virtually identical results, indicating that our method works well with the minimal-length signals often obtained from children. Taking the mean intrasegment $f_v$ value for each subject without removing linear trends from individual segments yielded an even stronger correlation between age and $f_v$ as compared with the first two analyses (Fig. 3.9), both of which detrended segments. A likely explanation for this finding is that removing linear trends from signals decreases variance in the data and is therefore detrimental to measuring $f_v$. Thus, for signals with discontinuities created by concatenation, we believe the approach exercised in the third analysis is the most reliable method for measuring $f_v$. Instantaneous frequency values for the left posterior IC examined in this study typically followed a leptokurtic distribution (Fig.

2.10), with values in the center of the distribution reflecting metastable frequency states and values in the small tails of the distribution reflecting state transitions.

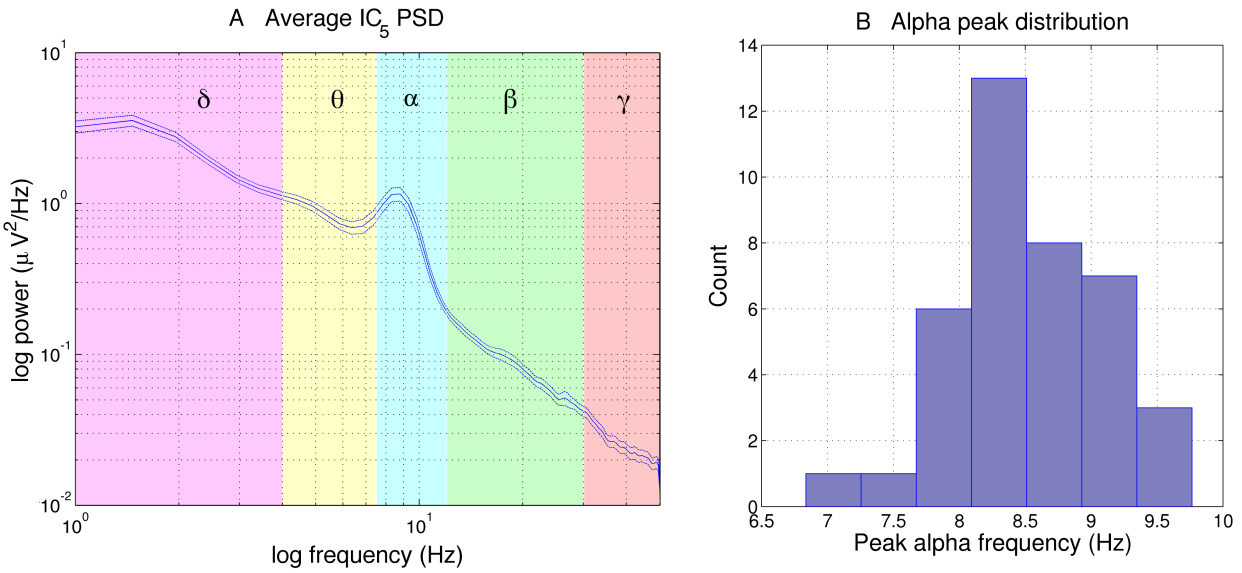


***Figure 2.8 $IC_5$ power spectrum and alpha peak frequency distribution.*** *The PSD of each subject's $IC_5$ signal was computed via Welch's method, and the grand average of all PSDs plotted on a log-log scale (A), where dotted lines indicate standard error of the mean. Frequency bands are color coded for easy interpretation: delta (1 – 4 Hz; purple), theta (4 – 7.5 Hz; yellow), alpha (7.5 – 12 Hz; blue), beta (12 – 30 Hz, green), and gamma (30 – 50 Hz, red). The grand average PSD gave little indication of muscle noise at beta or gamma frequencies, supporting our conclusion that data were sufficiently cleaned to remove muscle artifact. Furthermore, we observed that children had alpha rhythms within the traditional limits of the alpha bandpass, suggesting that phase resets also occurred within this frequency range. A histogram of peak alpha frequencies ($\mu$ = 8.6 Hz, $\sigma$ = 0.67 Hz) for all 39 subjects further supports this conclusion (B).*

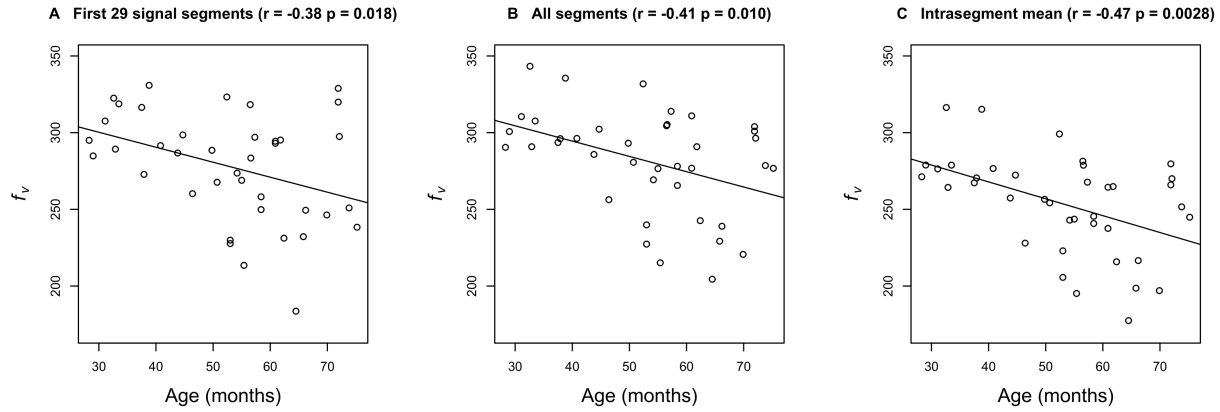


***Figure 2.9 Correlation of age with frequency variance.*** *Three different correlation analyses of $f_v$ and age were performed, one controlling for length of the IC signal (A), another all clean segments of the IC signal (B), and a third using the intrasegment mean $f_v$ of all segments from the IC of interest (C). Whereas the first two analyses removed linear trends from signal segments, the third analysis did not detrend segments. All three analyses found a significant negative correlation between age and $f_v$. However, the third analysis yielded the strongest correlation (see figure for r and p values), suggesting that removing linear trends from data also reduces the variance and is detrimental to computing $f_v$.*

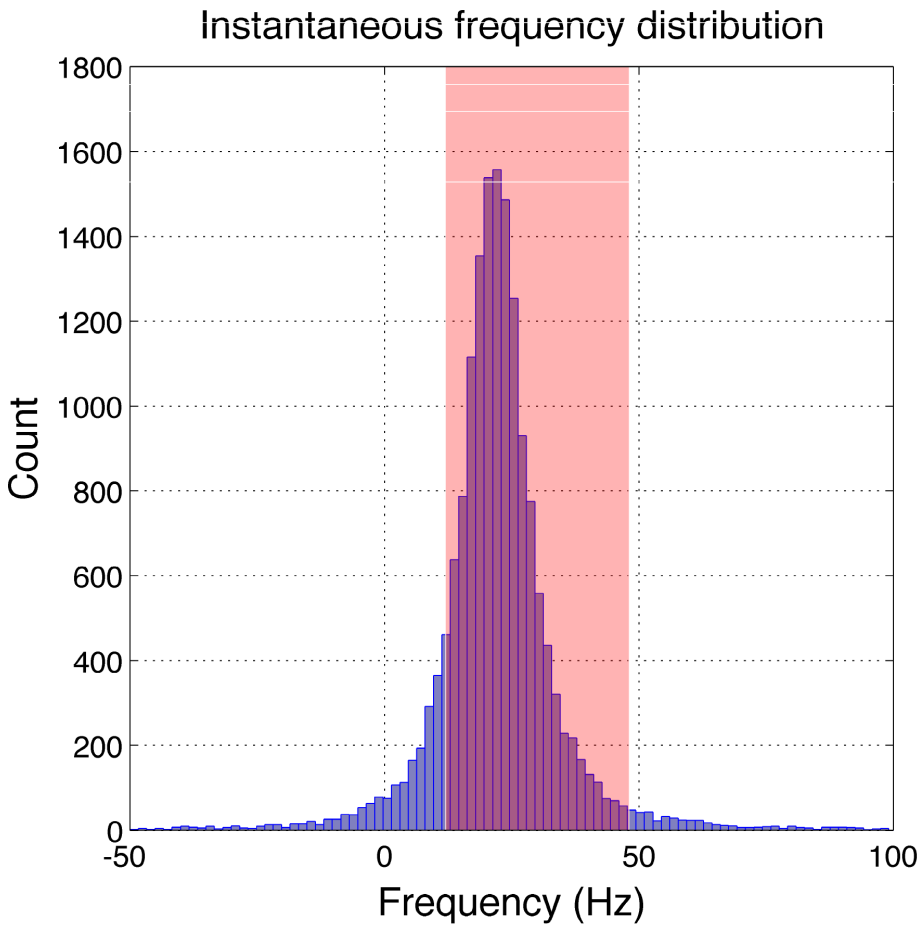


***Figure 2.10 Instantaneous frequency distribution from a typical dataset.*** *The instantaneous frequency $f_v$ was computed from a typical dataset. Mean values were not subtracted from $f_v$ values (m = 21.6 Hz, s = 15.2 Hz) to obviate the leptokurtic distribution of values (N = 1.66 × $10^4$, kurtosis = 23.9) about the center of the 12-48 Hz frequency band. Frequencies that lie within the frequency band are highlighted in red. Note that the distribution is off center from the FFT bandpass due to negative frequencies yielded by the Hilbert transform.*

Contrary to our hypothesis, we found that $f_v$ decreases with age, indicating that its inverse, frequency stability, increases with age. This result differs from the findings of prior studies which used different methods to measure brain variability. Two prior studies found that

brain variability positively correlated with age in event related potentials (ERPs) of infants and children and negatively correlated with behavioral variability in reaction time and facial recognition . Nonetheless, our findings can be interpreted by taking into account the fact that reciprocal connections between constituent neurons in cell assemblies are likely weak in early development, requiring several months to years of learning before synapses within the cell assembly are strongly potentiated. Long term potentiation (LTP) of cell assembly synapses increases the efficacy of constituent neurons to excite each other (Bliss and Collingridge 1993; Hughes 1958), resulting in a stronger, more stable assembly. Increased durations of stable synchrony within a cell assembly translate into lower frequency variance in the EEG signal.

Alternatively, it is also possible that transitions between metastable frequency states do not reflect synchronization and desynchronization of cell assemblies and that our finding of correlation between frequency stability and age is serendipitous, yet not spurious. Prior work has postulated that phase resets result from inhibitory bursting in thalamocortical circuits (Freeman et al, 2003; Thatcher et al, 2009b). In particular, orchestration and timing of phase resets by the thalamus may help explain the astonishing spatiotemporal correlation of cortical phase resets. Phase resets in the resting-state EEG of healthy adults show strong spatial correlation over temporal intervals as brief as 5 ms, with phase velocities as large as 40 m/s, considerably faster than serial synaptic corticocortical conduction velocities (Freeman et al. 2003).

While a similar cross-sectional study of development used PCA to measure dimensionality as a metric of EEG signal variability (McIntosh et al. 2008), we did not use PCA for this purpose, nor did we make any direct estimates of state space dimensionality. However,

the presence of chaotic transitions in recordings can nonetheless be used to infer a high-dimensional state space (Tsuda 2013). The dimensionality of a system betrays possible attractors thereof (closed subspaces of state space towards which trajectories evolve). For instance, systems with two or more dimensions are capable of periodic orbits (limit cycle attractors) and systems with three or more dimensions are capable of chaos (strange attractors, or extreme sensitivity to initial conditions). Metastability can be interpreted as saddle points in state space, which attract and repel trajectories in orthogonal directions, connected by heteroclinic channels (Fig. 2.11A). However, heteroclinic channels are unstable in low-dimensional systems. Alternatively, metastability may actually be chaotic itinerancy, the slowing of state space trajectories through quasi-attractors, or "ghosts" or recently destabilized attractors (Fig. 2.11B). Chaotic itinerancy, like heteroclinic cycles, implies a high dimensional state space (Tsuda 2013). The inferred presence of transitory dynamics in our data thus suggests a high-dimensional system with the potential for exotic chaotic behavior (Letellier and Rössler 2007; Rössler 1979).

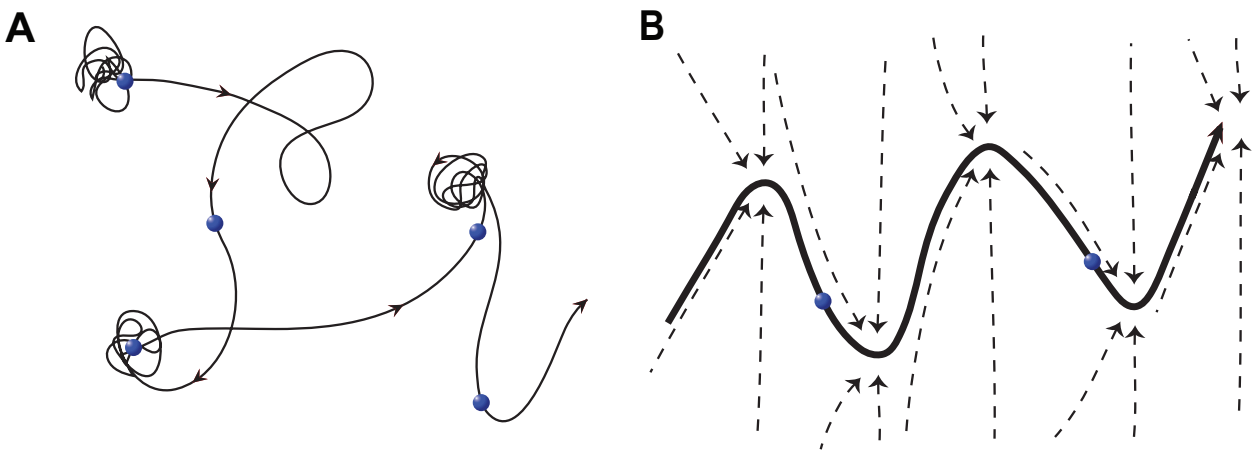


***Figure 2.11 Possible scenarios for the mechanisms underlying metastability.*** *The trajectory of the system through state space may be interpreted as chaotic itinerancy (A), in which the trajectory is slowed by attractor ruins, or "ghosts" of recently destabilized attractors. Alternatively, metastability may be the result of heteroclinic channels between metastable saddle points (B).*

### 2.4.1 – Mechanisms of phase resetting

To gain deeper insight into the physical phenomenon of phase resetting, it is useful to consider phase resets in the context of nonlinear dynamics (Table 2.1). As stated earlier, phase resets are state transitions between metastable cortical frequency states. State transitions occur in dynamical systems when a control parameter is tuned past a critical value and a loss of stability occurs. A familiar example is the liquid to gas state transition which occurs when water is heated past its boiling point. In this context, temperature is a control parameter and the boiling point is a critical value. Might feedforward thalamocortical inhibition serve as a control parameter for phase resets? This is consistent with the observation that phase resets occur at alpha (7.5 – 12.5 Hz) rates in healthy adults (Freeman et al. 2003) and evidence suggesting that the phase of thalamic alpha activity modulates the power of cortical gamma signals (Roux et al.

2013), which are carrier waves for phase resets (Freeman et al. 2003). Bursts of gamma aminobutyric acid (GABA)-mediated inhibition may attenuate the amplitude of the EEG signal, explaining previous findings of reduced signal amplitude coinciding with phase resets (Freeman et al. 2003). Such feedforward inhibition would disrupt bursts of synchronous firing in cortical pyramidal cells, which might subsequently transition to a new frequency of oscillations once disinhibited. Over the course of development, thalamocortical synapses onto inhibitory cortical interneurons may be lost during synaptic pruning (Bianchi et al. 2013; P. R. Huttenlocher 1979; P. R. Huttenlocher and Dabholkar 1997), explaining the increase in frequency stability with age observed in our recordings (Fig. 2.10). Over-pruning has already been hypothesized to trigger neurodevelopmental disorders such as schizophrenia (Feinberg 1982; Frohlich and van Horn 2014; Granger 1996; Kehrer et al. 2008; Olney and Farber 1997), and may also explain differences in phase locking duration observed in ASD (Thatcher et al. 2009), a disorder which is already associated with mutations in and abnormal expression levels of $GABA_A$ receptor genes (Fatemi et al. 2010, 2011; Kang and Barnes 2013; McCauley et al. 2004; Menold et al. 2001).

Although the timing and orchestration of phase resets might be explained in terms of subcortical mechanisms, the framework of nonlinear dynamics also allows for an explanation consistent with the theory that metastable states between phase resets represent the activation of cell assemblies. In nonequilibrium systems such as the brain, a critical point may serve as an attractor for the system, such that the system spontaneously undergoes state transitions without the tuning of a control parameter. This phenomenon, in which systems enjoy a wide repertoire of possible states by virtue of being poised near a critical point, is a hallmark of complexity known as self-organized criticality (SOC) (Bak P et al. 1987, 1988). For

example, one can imagine a sandpile which is built until its slope reaches a critical angle: adding additional sand to the pile will cause arbitrarily large avalanches ranging in size from a few grains of sand to a considerable portion of the pile. In this context, complexity cannot be explained in terms of the individual parts themselves, but rather in terms of feedback between a slow process (adding sand) which increases energy and a fast process (the avalanche) that dissipates energy. SOC is thus an attractive mechanism by which cell assemblies might spontaneously synchronize in the brain, with local synchrony propagating as a neuronal avalanche (Plenz and Thiagarajan 2007).

An important property of avalanches in SOC is scale-invariance or fractal organization (Bak P et al. 1987). Scale invariance is observed at almost all levels of the brain, generally in the form of pink noise, or $1/f$ noise, where spectral power is inversely proportional to frequency (He 2014; Plenz and Thiagarajan 2007). Examples include the temporal distributions of ion channel openings (Toib et al. 1998), spike trains (Teich et al. 1997), neurotransmitter exocytosis (Lowen et al. 1997), and amplitude fluctuations (Linkenkaer-Hansen et al. 2001) and power spectral density (Pritchard 1992) in EEG recordings. Spatially distributed brain data, such as the topology of functional brain networks, has also been shown to obey power laws (Sporns 2011). "Neuronal avalanches" have been widely reported in local field potential (LFP) recordings from *in vitro* cortical slices, taking the form of bursts of spatiotemporal activity following power law distributions (Beggs and Plenz 2003, 2004; Plenz and Thiagarajan 2007). In our study, the parameters of the empirical distribution associated with $|f_v|$ revealed power law scaling in the limit of large $|f_v|$, as illustrated by a log-log transform (Fig. 2.12)., suggesting that phase resets

are, in fact, critical fluctuations driven by SOC in the brain. Regardless of the mechanism, this finding adds another entry to the vast body of work describing scale-invariance in the brain.

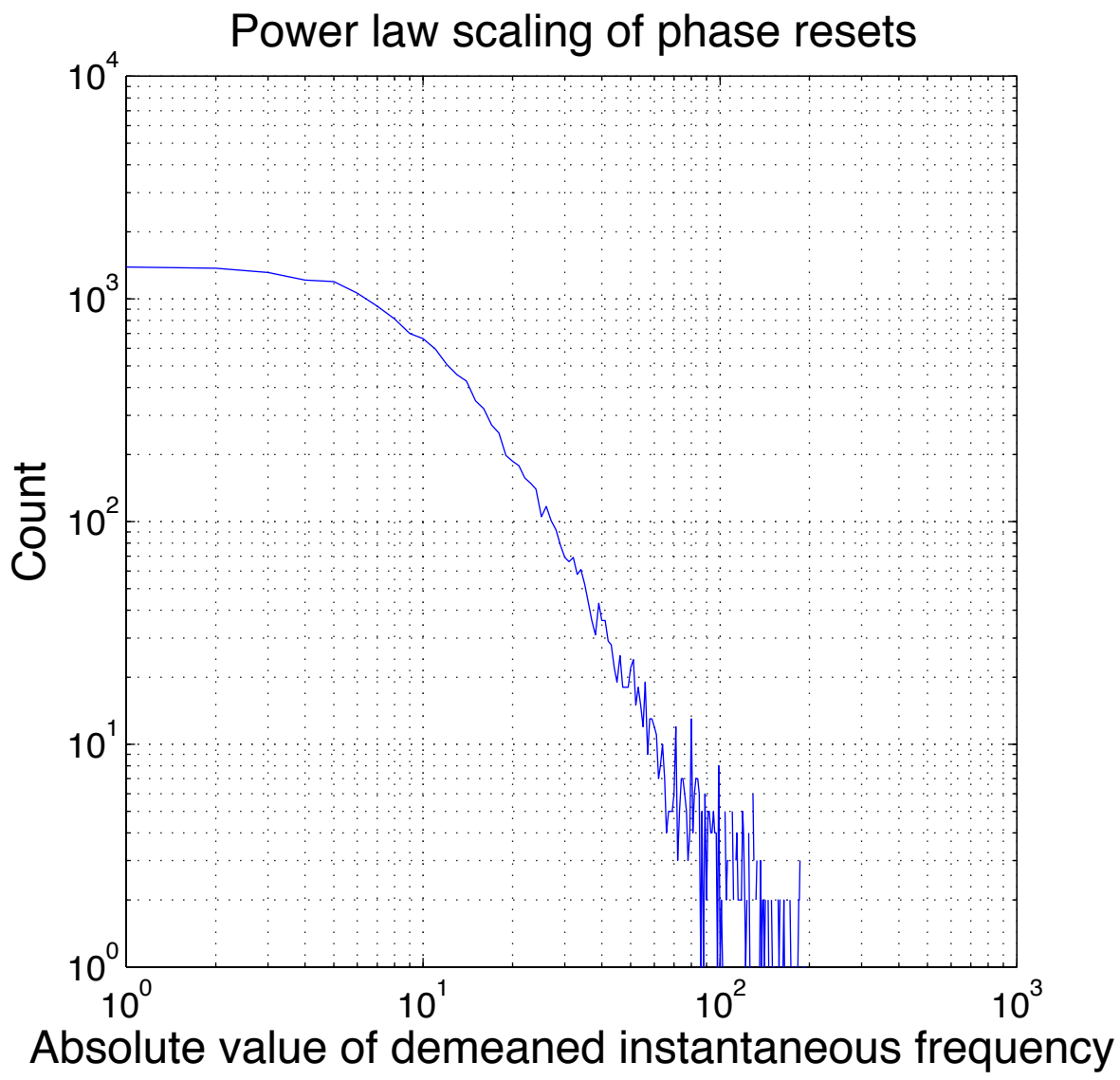


***Figure 2.12 Evidence of power law distribution for phase resets.*** *A linear region, indicative of power law scaling, is revealed by a log-log transform of the histogram of $|f_v|$. Power law relationships exist when one quantity varies as a power of the other. Such relationships are scale free, as scaling the first quantity*

*by a constant factor only causes a proportional increase in the second quantity. Power laws and scale invariance are features of self-organized criticality (SOC), in which a system operating near a critical point experiences arbitrarily large fluctuations.*

**Table 2.1 Interpretations of frequency metastability**

| | Cell assembly synchronization | Inhibitory thalamocortical bursting |
|---|---|---|
| Computational model | Self-organized criticality (SOC) | Tuning-dependent state transition |
| Physical metaphor | Avalanche (sandpile model) | Thermodynamic phase transition (e.g., water boiling into steam) |
| Neural mechanism | Synchronization of neural networks | Gamma-aminobutyric acid (GABA) mediated feedforward inhibition |
| Cause of developmental changes | Synaptic potentiation between constituent neurons | Synaptic pruning weakening inhibitory afferents |
| Evidence | -Brain is far from equilibrium system<br>-Phase resets are aperiodic<br>-Neuronal avalanches reported *in vitro*<br>-Critical state may enhance computational power of brain | -Explains anomalous phase velocities and spatiotemporal correlations of phase resets<br>-Role of $GABA_A$ receptors in generating high frequency EEG rhythms<br>-Possible relationship with thalamic alpha activity |
| Possible relevance to atypical development | -Cognitive inflexibility results from reduced ability of cell assemblies to form as neuronal avalanches | -$GABA_A$ receptor mutations associated with ASD: weakened thalamocortical inhibition |

Two principal limitations of our study should be considered. Firstly, our study was performed cross-sectionally and therefore does not support the same firm conclusions one might draw from a longitudinal study. Additionally, in comparing our study to prior studies of metastability and brain variability in development (Koenig et al. 2002; Lippé et al. 2009; McIntosh et al. 2008; Thatcher et al. 2009), we have simultaneously introduced a new method, a different age group, and, in some cases, a different paradigm. Not having controlled for all

variables separately, reasons for differences between our findings and the findings of other groups remain uncertain.

Our recruitment of typically developing children was part of a larger study of atypical development, and our group is currently applying this method to age-matched children with ASD. Other future work should be focused along similar lines by examining changes in frequency stability with age in atypical development and neurodevelopmental disorders with onset in early childhood, such as ASD and attention deficit hyperactivity disorder (ADHD). Future studies should also use a longitudinal design to validate conclusions regarding the relationship between frequency stability and age.

# Chapter 3: A quantitative electrophysiological biomarker of duplication 15q11.2-q13.1 syndrome

## 3.1 Introduction

Advances in genetic testing have accelerated the diagnosis of causative genetic syndromes in the context of neurodevelopmental disorders, in particular autism spectrum disorder (ASD), with the diagnostic yield of combined chromosomal microarray and whole exome sequencing of 3-20% (Gaugler et al. 2014; Schaefer and Mendelsohn 2013; Tammimies et al. 2015). In parallel, there has been an emerging interest in defining neurophysiological markers that may stratify children with ASD into biologically meaningful subgroups (Jeste et al. 2015). The convergence of discoveries in genetics and neurophysiology in ASD holds tremendous potential for the identification of biomarkers, grounded in genetic mechanisms, that can improve diagnosis, selection of treatment targets, and treatment monitoring in future clinical trials for genetically defined syndromes within the spectrum of neurodevelopmental disorders

This convergence of genetics with neurophysiology finds promise in the investigation of duplications of 15q11.2-q13.1 (or Dup15q syndrome), one of the most common copy number variants (CNVs) associated with ASD, accounting for 1-3% of cases (Cook Jr et al. 1997). Clinical features of Dup15q syndrome include hypotonia, global developmental delay, intellectual disability, social communication impairments, and often severe epilepsy including infantile spasms (Al Ageeli et al. 2014; DiStefano et al. 2016; Hogart et al. 2010; Urraca et al. 2013). Two duplication types exist: isodicentric duplications, which are characterized by two extra copies of

the 15q11.2-q13.1 region of maternal origin on a supernumerary chromosome, and interstitial duplications, which can be one or more extra copies of this region on the q arm of chromosome 15 (DiStefano et al. 2016).

The 15q11.2-q13.1 region contains many genes critical to neural function, including *UBE3A*, a ubiquitin-protein ligase important in synaptic function (Dindot et al. 2007; Greer et al. 2010; Smith et al. 2011), and three gamma aminobutyric acid type A receptor ($GABA_AR$) subunits genes, *GABRA5, GABRB3,* and *GABRG3*. Recently, two studies have qualitatively noted the presence of persistent beta frequency (12 – 30 Hz) activity in clinical electroencephalogram (EEG) recordings from children with Dup15q syndrome (Al Ageeli et al. 2014; Urraca et al. 2013). The clinical EEGs are quite distinctive, with spontaneous beta oscillations (SBOs) evident with visual inspection alone. These SBOs resemble the EEG effects of allosteric modulation of $GABA_ARs$ by benzodiazepine drugs, even though the children for whom this observation was reported were not taking these medications (Al Ageeli et al. 2014; Urraca et al. 2013). Since the SBOs in these studies occurred in both maternal and paternal duplication cases, it is possible that these SBOs could result from aberrant GABAergic transmission and not primarily from the maternally expressed *UBE3A* gene.

Herein, we sought to quantify EEG beta power in Dup15q syndrome to determine if it distinguished Dup15q syndrome from non-syndromic ASD and typical development. To accomplish this goal we obtained spontaneous EEG recordings from (1) children with Dup15q syndrome, (2) age-and-IQ matched children with non-syndromic ASD and (3) age matched typically developing (TD) children. We hypothesized that spontaneous beta power would differentiate children with Dup15q syndrome from these comparison groups. In a follow up

study we examined the variation in beta power within a larger Dup15q cohort by analyzing age, duplication type, and epilepsy status as predictors of SBO strength. Given the likelihood that SBOs are related to copy number variation and seizures in Dup15q syndrome, we hypothesized that both duplication type and epilepsy would relate to spontaneous beta power.

## 3.2 Subjects and Methods

### 3.2.1 Study 1: Comparison of Dup15q syndrome with ASD and TD

#### 3.2.1.a Participants

All data were acquired in accordance with the Institutional Review Board of the University of California, Los Angeles. This study was specifically approved by the Institutional Review Board. Parents of participants provided informed written consent prior to the start of study activities. EEG datasets analyzed for this study will be deposited in a public repository following publication of this manuscript. Participants were clinically referred through the Dup15q clinic at UCLA and the national Dup15q Alliance. Children were excluded from the study if treated with medications known to pharmacologically induce beta oscillations (benzodiazepines, benzodiazepine derivatives, or barbiturates). A total of 16 participants were recruited for the first study, 5 of whom were omitted due to treatment with exclusionary medications (*n*=2*)*, duplication type that did not include the canonical 15q11.2-q13.1 region (*n*=1), or insufficient length or quality of EEG recordings (*n*=2). The remaining sample included 11 participants (5 male), 16-144 months of age (median = 54 months). Details of the sample, including age, intelligence quotient (IQ), and duplication type can be viewed in Table 3.1; medication can be viewed in Table 3.2. A wide age range was included to ensure that a clinically representative sample was being studied, and age matching of the comparison groups ensured

that the group level comparisons would not be confounded by age differences. Both isodicentric (*n* = 8) and interstitial (*n* = 3) duplications were represented in this cohort, and 2 participants with isodicentric duplications had a diagnosis of epilepsy. Data from an ongoing study of electrophysiological biomarkers in ASD were utilized for the two comparison groups: (1) an age and IQ-matched cohort of children with non-syndromic ASD (*n* = 10) and (2) an age-matched group of TD children (*n* = 9). Preschool age children with ASD were recruited as part of a larger study investigating predictors of treatment outcome in preschoolers enrolled in a UCLA early intervention program. All children enter the program with a prior clinical diagnosis of ASD, made through the California State Regional Center, independent clinical psychologists, child psychiatrist, and/or developmental pediatricians. Diagnoses were confirmed by UCLA psychologists based on DSM-IV criteria. Non-syndromic ASD was defined by normal clinical chromosomal microarray testing, but most children had not undergone whole exome sequencing. Details of both comparison groups are available in Table 3.1 and Table 3.2.

Clinical assessment

Owing to the large range in age and developmental ability amongst participants in our study, several assessments were used to evaluate cognition, language, and motor skills. The following measures were used to match participants by cognitive function: the Mullen Scales of Early Learning (MSEL) (Mullen 1995), the Stanford Binet Intelligence Scales-Fifth Edition (SB5) (Roid 2003), the Differential Ability Scales Second Edition (DAS II) (Elliot CD 2007), Preschool Language Scales-Fifth Edition (PLS-5) (Zimmerman et al. 2011), and the Leiter International Performance Scales – Revised (Leiter-R) (Roid and Miller 2011).

### 3.2.1.b EEG recording

Spontaneous EEG was recorded at 500 Hz using high-density 129 channel geodesic nets with Ag/AgCl electrodes (Electrical Geodesics, Inc., Eugene, OR, USA) while participants watched non social silent videos of bouncing soap bubbles and other abstract images on a computer monitor for 2 to 6 minutes, depending on the child's level of compliance with the paradigm. No sedation was employed for electrode placement or EEG recording. EEG signals were amplified using a Net Amps 300 amplifier (Electrical Geodesics, Inc., Eugene, OR, USA) with a low pass analog filter cutoff frequency of 6 KHz. EEG signals were vertex-referenced at the time of recording and later re-referenced to average after preprocessing and artifact reduction.

Data processing

EEG recordings were band pass filtered at 1 – 50 Hz using a finite impulse response (FIR) filter with the EEGLAB toolbox (Delorme and Makeig 2004). Recordings were then segmented into 1000 ms segments for preprocessing. Noisy or loose channels were spherically interpolated using EEGLAB, and EEG recording segments with more than 11 interpolated channels were rejected. All remaining segments were manually inspected for non-stereotyped artifacts, e.g., electromyogram (EMG), and rejected based on qualitative inspection. Following manual artifact rejection, a combined principal component analysis (PCA) and independent component analysis (ICA) approach was used to eliminate stereotyped artifacts, e.g., ocular artifacts. PCA was performed prior to ICA to reduce each dataset to 24 dimensions, an important consideration for successful extraction of meaningful independent components (ICs) from EEG recordings (Onton et al. 2006). ICs corresponding to physiological artifact were subtracted from EEG

recordings. All EEG recordings were re-referenced to an average reference prior to power calculations.

EEG recordings from TD and ASD cohorts were acquired and processed according to the same protocol described above with the sole discrepancy that 8 ASD and 9 TD recordings were sampled at a lower frequency (250 Hz) than those with Dup15q syndrome. Accordingly, EEG signals from all groups were downsampled to 250 Hz prior to spectral analysis if originally sampled at 500 Hz to ensure that all power spectral densities (PSDs) are computed with the same frequency resolution.

**3.2.1.c Statistical analysis of spectral power**

To study spectral power, 9 regions of interest (ROI) were defined corresponding to the locations of channels F3, Fz, F4, C3, Cz , C4, P3, Pz, P4 in the international 10-20 montage, as per prior studies by our group (McEvoy et al. 2015). Each ROI consisted of 4 electrodes and was chosen to allow for maximum spatial coverage of the scalp (see Fig. 3.1A). For each electrode, PSDs were computed according to Welch's method (Welch 1967) using the pwelch function in MATLAB. This method divides the signal into sections of equal length with 50% overlap and uses a Hamming window to estimate a modified periodogram for each segment. Segments are overlapped by 50% owing to the fact that the Hamming window weighs the center of the data segment more strongly than the sidelobes, which are attenuated by 42.5 dB. Periodograms for all segments are then averaged to provide a final spectral estimate. Relative power was then calculated for specific frequency bands, and these relative power values were then averaged across a particular ROI. 2000 ms of signal sampled at this rate were zero-padded to created 512-point Hamming windows to compute PSDs with approximately 0.5 Hz frequency resolution.

The 2000 ms signal length was chosen as twice the period of the slowest oscillation examined (1 Hz delta activity). The following frequency bands were examined separately: delta (1 – 4 Hz), theta (4 – 8 Hz), alpha (8 – 12 Hz), beta1 (12 – 20 Hz), beta2 (20 – 30 Hz), and gamma (30 – 48 Hz). EEG power was calculated from PSDs as relative power, i.e., the proportion of total (1 – 48 Hz) spectral power accounted for by a given frequency band. Normalizing spectral power in this manner allows for meaningful comparisons between subjects with different overall levels of signal power.

Relative power values from 6 frequency bands and 9 ROIs were analyzed using repeated measures analysis of variance (ANOVA), with multiple testing corrected for using false discovery rates (FDR). The final model for each band included group (Dup15q, ASD, TD) and ROI main effects. Because no significant group-by-ROI interactions were found, interactions were removed from the final model. Since estimated variances for relative power in the Dup15q group was larger compared to ASD and TD groups, especially for beta power, separate group variances and within subject correlations were allowed for in the fitted repeated measures ANOVA models. Comparisons of spectral power were performed both with and without outliers (defined by being more than three standard deviations from the mean) in order to assess the extent to which comparisons might be biased by outliers.

### 3.2.2 Study 2: Subgroup analyses of EEG power within Dup15q syndrome

#### 3.2.2.a Participants

All data were acquired in accordance with the Institutional Review Board of the University of California, Los Angeles. This study was specifically approved by the Institutional Review Board of the University of California, Los Angeles. Parents of participants provided

informed written consent prior to the start of study activities. After this initial study, we expanded the cohort in order to examine the variability in beta power within Dup15q syndrome. Spontaneous EEG data were acquired from individuals at the 2015 National Dup15q Alliance conference in Orlando, Florida, with consenting procedures as described in the first study. EEG datasets analyzed for this study will be deposited in a public repository following publication of this manuscript.

**3.2.2.b EEG recording and processing**

EEG recording followed the protocol described in the initial cohort study. A total of 24 participants underwent EEG recordings at the Orlando site, with 9 participants omitted due to insufficient quality of EEG recordings or use of exclusionary medications. Mean beta power did not differ between testing sites using Welch two-sample *t*-tests (beta1 power: $p = 0.69$, $t = 0.41$; beta2 power: $p = 0.50$, $t = 0.68$). Therefore, the data acquired from the Orlando site were combined with the 11 participants in the initial Dup15q cohort and 1 additional adult tested at UCLA, resulting in a final sample of 27 participants, 16-384 months of age (median = 81.2 months). As with the first study, no sedation was employed for electrode placement. Table 4.1 provides details about this cohort. EEG data were processed according to the protocol described in the initial study.

**3.2.2.c Statistical analysis of spectral power**

To model the effects of age, duplication type, and epilepsy on beta power, several simple linear regression models were implemented using two outcome measures, beta1 power and beta2 power, averaged across all ROIs. Simple linear regressions were used, with each variable as a separate predictor of beta1 and beta2 power. Age was treated as a continuous

variable while duplication type and epilepsy were treated as binary variables. Prior to regression modeling, Welch two-sample *t*-tests were used to test for differences in mean beta power between testing sites. Having tested the null hypothesis that means of outcome measures do not differ between testing sites, three univariate regressions were performed for beta1 power and beta2 power using the aforementioned predictors.

## 3.3 Results

### 3.3.1 Study 1 – Comparison of Dup15q syndrome with ASD and TD

Results of behavioral testing, along with duplication type and epilepsy history, are summarized for all participants in Table 3.1. Participant medications are disclosed in Table 3.2. Qualitative analysis of bandpass filtered EEG traces from several participants with Dup15q syndrome revealed fast sinusoidal oscillations at beta frequencies apparent upon visual inspection. Fig. 3.1 shows beta activity from 9 scalp regions of interest (ROIs) in a 29-month old TD child (Fig. 3.1C), a 27-month-old child with nonsyndromic ASD (Fig. 3.1D), a 28-month-old child with Dup15q syndrome (Fig. 3.1E) and a 43-month old participant with both Dup15q syndrome and epilepsy (Fig. 3.1F). ROIs were selected for maximum scalp coverage and their correspondence to 10-20 montage channels (McEvoy et al. 2015). Visual inspection of topographic scalp plots for both beta1 (12-20 Hz) relative power and beta2 (20-30 Hz) relative power averaged across participants revealed a diffuse pattern of beta activity in Dup15q syndrome that appeared strongest over frontotemporal regions (Fig. 3.2), in stark contrast to both comparison groups. Frontotemporal distributions of beta power in Dup15q syndrome are best visualized by projection onto 3-dimensional head models (Fig. 3.2D).

**Table 3.1. Participant characteristics.** Older participants tested in Orlando did not undergo cognitive testing, as age-appropriate cognitive tests were not available. N/A = not available.

| Participant | Group | Age (months) | Site | Gender | Genetics | Epilepsy | VDQ | NVDQ |
|---|---|---|---|---|---|---|---|---|
| 1 | Dup15q | 99.9 | UCLA | female | isodicentric | no | 43 | 47 |
| 2 | Dup15q | 42.5 | UCLA | male | isodicentric | no | 12 | 32 |
| 3 | Dup15q | 44.5 | UCLA | male | isodicentric | no | 72 | 64 |
| 4 | Dup15q | 28.1 | UCLA | female | isodicentric | no | 39 | 46 |
| 5 | Dup15q | 42.8 | UCLA | female | isodicentric | yes | 6 | 4 |
| 6 | Dup15q | 55.9 | UCLA | female | interstitial | no | 105 | 100 |
| 7 | Dup15q | 230.1 | UCLA | female | interstitial | no | N/A | 56 |
| 8 | Dup15q | 54.2 | UCLA | male | interstitial | no | 8 | 24 |
| 9 | Dup15q | 57 | UCLA | male | isodicentric | no | 48 | 46 |
| 10 | Dup15q | 143.8 | UCLA | female | isodicentric | yes | 7 | 12 |
| 11 | Dup15q | 106.1 | UCLA | male | interstitial | no | 33 | 34 |
| 12 | Dup15q | 15.8 | UCLA | female | isodicentric | no | 48 | 79 |
| 13 | Dup15q | 93.2 | Orlando | male | isodicentric | yes | 39 | 37 |
| 14 | Dup15q | 108.2 | Orlando | male | interstitial | no | N/A | N/A |
| 15 | Dup15q | 147.3 | Orlando | female | isodicentric | yes | 14 | N/A |
| 16 | Dup15q | 110.5 | Orlando | male | isodicentric | no | 12 | 21 |
| 17 | Dup15q | 117.5 | Orlando | female | interstitial | no | 37 | 44 |
| 18 | Dup15q | 65.45 | Orlando | male | isodicentric | yes | 9 | 13 |
| 19 | Dup15q | 44.9 | Orlando | female | interstitial | no | 11 | 27 |
| 20 | Dup15q | 47 | Orlando | female | isodicentric | no | N/A | N/A |
| 21 | Dup15q | 81.2 | Orlando | male | isodicentric | yes | N/A | N/A |
| 22 | Dup15q | 48.7 | Orlando | male | isodicentric | no | N/A | N/A |
| 23 | Dup15q | 384 | Orlando | female | interstitial | yes | N/A | N/A |
| 24 | Dup15q | 161.6 | Orlando | male | interstitial | no | N/A | N/A |
| 25 | Dup15q | 29.4 | Orlando | male | isodicentric | no | 36 | 29 |
| 26 | Dup15q | 111.7 | Orlando | female | interstitial | no | 26 | 24 |
| 27 | Dup15q | 86 | Orlando | female | isodicentric | no | N/A | N/A |
| 28 | ASD | 61.2 | UCLA | Male | N/A | no | 51 | 48 |
| 29 | ASD | 26.6 | UCLA | Male | N/A | No | 19 | 45 |
| 30 | ASD | 39.3 | UCLA | Male | N/A | No | 33 | 46 |
| 31 | ASD | 63 | UCLA | Male | N/A | No | 43 | 41 |
| 32 | ASD | 28.8 | UCLA | Male | N/A | No | 28 | 52 |
| 33 | ASD | 53.2 | UCLA | Female | N/A | No | 56 | 51 |
| 34 | ASD | 48.6 | UCLA | Male | N/A | No | 17 | 49 |
| 35 | ASD | 32.3 | UCLA | Male | N/A | No | 25 | 43 |
| 36 | ASD | 58.5 | UCLA | Famale | N/A | No | 103 | 74 |
| 37 | ASD | 98.7 | UCLA | Male | N/A | no | 21 | 50 |
| 38 | TD | 57 | UCLA | Famale | N/A | no | 122 | 94 |
| 39 | TD | 54 | UCLA | Male | N/A | No | 98 | 97 |
| 40 | TD | 29 | UCLA | Male | N/A | No | 131 | 157 |
| 41 | TD | 55 | UCLA | Male | N/A | no | 140 | 107 |
| 42 | TD | 38.8 | UCLA | Famale | N/A | No | 145 | 149 |
| 43 | TD | 43.8 | UCLA | Male | N/A | No | 109 | 115 |
| 44 | TD | 40.8 | UCLA | Male | N/A | No | 141 | 113 |
| 45 | TD | 59.6 | UCLA | Female | N/A | No | 127 | 103 |
| 46 | TD | 59.6 | UCLA | Male | N/A | no | 112 | 117 |

**Table 3.2 Participant medications.** Families of some Dup15q syndrome participants were only asked to disclose antiepileptic medications.

| Participant | Group | Meds |
|---|---|---|
| 1 | Dup15q | risperidone |
| 2 | Dup15q | none |
| 3 | Dup15q | none |
| 4 | Dup15q | none |
| 5 | Dup15q | levetiracetam |
| 6 | Dup15q | none |
| 7 | Dup15q | zoloft |
| 8 | Dup15q | none |
| 9 | Dup15q | none |
| 10 | Dup15q | levetiracetam |
| 11 | Dup15q | no anticonvulsant |
| 12 | Dup15q | no anticonvulsant |
| 13 | Dup15q | rufinamide 1200 mg b.i.d., levetiracetam 2000 mg b.i.d., lacosamide 40 mg b.i.d., Epidiolex (canibidiol) 7 mL x2 |
| 14 | Dup15q | no anticonvulsant |
| 15 | Dup15q | lamotrigine 300 mg b.i.d. lacosamide 100mg b.i.d. Felbamate 1200mg/800mg/1000mg |
| 16 | Dup15q | no anticonvulsant |
| 17 | Dup15q | no anticonvulsant |
| 18 | Dup15q | levetiracetam 500mg AM 750mg PM lamotrigine 100 mg b.i.d. |
| 19 | Dup15q | no anticonvulsant |
| 20 | Dup15q | no anticonvulsant |
| 21 | Dup15q | Valproic acid 250mg b.i.d. oxcarbazepine 300mg b.i.d. |
| 22 | Dup15q | no anticonvulsant |
| 23 | Dup15q | Valproic acid |
| 24 | Dup15q | no anticonvulsant |
| 25 | Dup15q | no anticonvulsant |
| 26 | Dup15q | no anticonvulsant |
| 27 | Dup15q | no anticonvulsant |
| 28 | ASD | Focalin, risperdione |
| 29 | ASD | None |
| 30 | ASD | None |
| 31 | ASD | None |
| 32 | ASD | None |
| 33 | ASD | risperidone |
| 34 | ASD | None |
| 35 | ASD | None |
| 36 | ASD | Zoloft |
| 37 | ASD | Melatonin |
| 38 | TD | None |
| 39 | TD | None |
| 40 | TD | None |
| 41 | TD | None |
| 42 | TD | None |
| 43 | TD | None |
| 44 | TD | None |
| 45 | TD | None |
| 46 | TD | None |

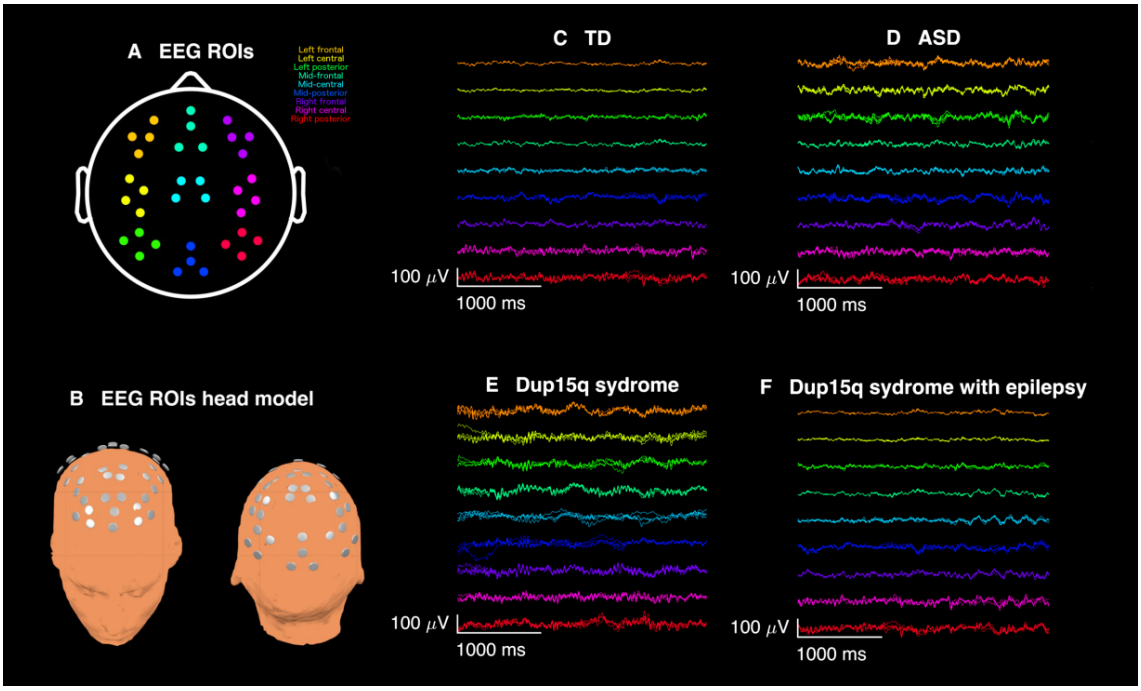


***Figure 3.1 Example EEG recordings in Dup15q syndrome****. Qualitative analysis of resting-state electroencephalogram (EEG) recordings from participants with Dup15q syndrome revealed overt beta frequency oscillations apparent upon visual inspection. (A) EEG recordings from 9 scalp regions of interest (ROIs) were analyzed: left frontal (orange), left central (yellow), left posterior (green), mid-frontal (aquamarine), mid-central (cyan), mid-posterior (blue), right frontal (purple), right central (pink), right posterior (red). (B) 3-dimenisonal head model showing ROI electrode locations. (C) 3 s of broadband EEG recordings from a representative 29-month-old TD child from 36 channels across 9 ROIs. (D) Same duration of EEG recorded from a 27-month-old child with nonsyndromic ASD. (E) EEG from a representative Dup15q syndome participant (age 28 months) reveals spontaneous beta oscillations (SBOs) in virtually all channels and all ROIs. The overt quality of SBOs likely allows for their easy detection in clinical EEG recordings. By contrast, (F) a 43-month-old participant with both Dup15q syndrome and epilepsy does not show nearly such distinct SBOs. It is possible that beta activity is reduced in children with both Dup15q syndrome and epilepsy.*

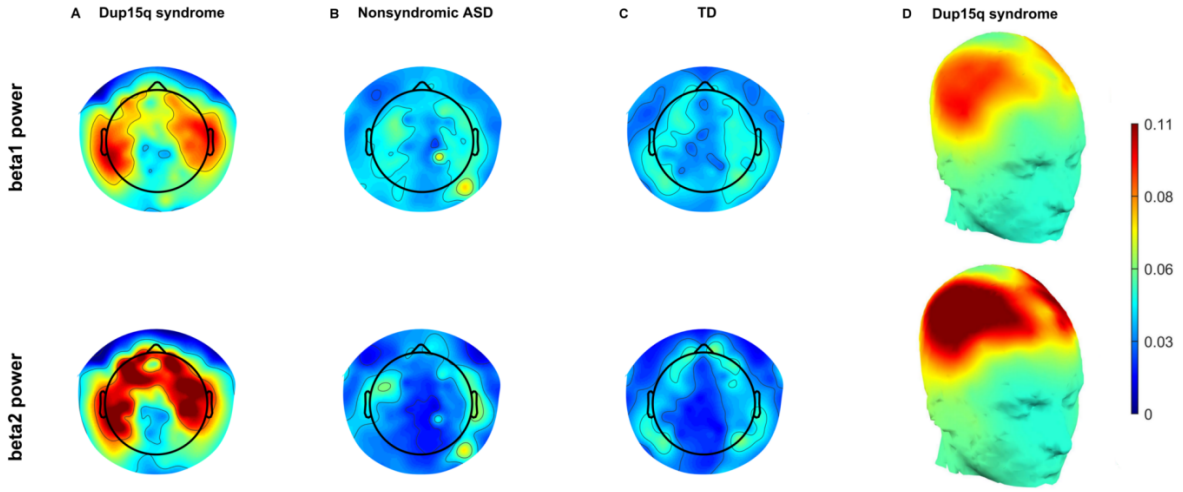


***Figure 3.2 Group averaged EEG topoplots****. Topographic scalp plots of relative beta1 (12–20 Hz) power (row 1) and relative beta2 (20–30 Hz) power (row 2) averaged across all participants. Three groups are compared, Dup15q syndrome group (A), nonsyndromic ASD group (B), and TD group (C). Qualitative inspection of these scalp plots reveals profound differences in relative power between Dup15q syndrome and comparison groups. This contrast is most pronounced in the beta2 band. Beta power in both subbands is most pronounced over frontotemporal scalp regions and attenuated over the midline. This is best visualized in the Dup15q syndrome cohort by projecting averaged power onto a generic 3-dimensional head model (D).*

Because no significant group-by-ROI interactions were found in modeling power in each frequency band, group means were averaged across regions, and comparisons were made between (1) the Dup15q cohort and the ASD cohort and (2) the Dup15q cohort and the TD cohort, resulting in a total of 12 frequency comparisons (2 pairwise comparisons for 6 frequency bands, see Table 3.3). Group comparisons were robust to the removal of outliers

greater than 3 standard deviations from the mean, and thus outliers were included in the final analysis.

**Table 3.3 Results from contrast analysis following repeated measures ANOVA**.

| Frequency | Comparison | Mean estimate | *t* statistic | p-value | FDR adj. |
|---|---|---|---|---|---|
| *Delta* | Dup15q - ASD | **-0.089** | **-2.51** | **0.013** | **0.025** |
| | Dup15q - TD | **-0.094** | **-2.67** | **0.0081** | **0.024** |
| *Theta* | Dup15q – ASD | 0.0072 | 0.23 | 0.82 | 0.82 |
| | Dup15q - TD | 0.024 | 0.79 | 0.43 | 0.47 |
| *Alpha* | Dup15q – ASD | -0.024 | 0.011 | 0.036 | 0.055 |
| | Dup15q - TD | -0.027 | 0.015 | 0.078 | 0.10 |
| *Beta1* | Dup15q – ASD | **0.026** | **2.57** | **0.011** | **0.025** |
| | Dup15q – TD | **0.026** | **2.75** | **0.0065** | **0.024** |
| *Beta2* | Dup15q – ASD | **0.066** | **4.15** | **<0.0001** | **0.0006** |
| | Dup15q – TD | **0.062** | **4.02** | **<0.0001** | **0.0006** |
| *Gamma* | Dup15q - ASD | **0.015** | **2.31** | **0.022** | **0.038** |
| | Dup15q - TD | 0.0078 | 1.18 | 0.24 | 0.29 |

Effect sizes were computed from raw data averaged across ROIs using Cohen's *d*. Large effect sizes were found in both beta1 power (Dup15q – ASD, $d$ = 1.08; Dup15q – TD, $d$ = 1.12) and beta2 power (Dup15q – ASD, $d$ = 1.73; Dup15q – TD, $d$ = 1.63). These are especially large effect sizes for studies of EEG power in neurodevelopmental disorder. The Dup15q cohort was

best distinguished from comparison groups in the beta2 band, in which participants exhibited significantly stronger spontaneous power than both the ASD ($p = 6 \times 10^{-4}$, FDR corrected) and TD ($p = 6 \times 10^{-4}$, FDR corrected) groups (see Table 3.3 and Fig. 3.3). Children with Dup15q syndrome also exhibited stronger spontaneous beta1 power (Fig. 3.3) than both the ASD group ($p = 0.0252$, FDR corrected) and the TD group ($p = 0.02$, FDR corrected). Two other significant findings included weaker spontaneous delta power in Dup15q syndrome compared to both the ASD group ($p = 0.03$, FDR corrected; $d = -1.07$) and the TD group ($p = 0.02$, FDR corrected; $d = -1.13$) and higher spontaneous gamma power in Dup15q syndrome compared to the ASD group ($p = 0.04$, FDR corrected; $d = 0.97$). Spontaneous gamma power was not significantly different between children with Dup15q syndrome and the TD group.

These data suggest that a pattern of high beta power and low delta power distinguishes Dup15q syndrome from both children with nonsyndromic ASD and TD children, with the largest effect size found in the beta2 band. High gamma power may also distinguish Dup15q syndrome from nonsyndromic ASD. We next asked if gamma power is related to beta2 power, possibly as an extension of the same broadband electrophysiological activity, by adding EEG recordings from Study 2 to examine a larger Dup15q syndrome cohort ($n = 27$). In fact, beta2 power and gamma power were significantly correlated in every cohort (Dup15q syndrome, $r = 0.43$, $p = 0.024$; non-syndromic ASD, $r = 0.78$, $p = 0.0080$; TD, $r = 0.88$, $p = 0.0017$), suggesting that gamma power and beta2 power reflect the same electrophysiological process. Given the reciprocal pattern of high beta power and low delta power in Dup15q syndrome, we then asked a similar question about how these two frequency bands might be related. We observed that delta power and beta power are significantly related only in the Dup15q cohort (beta1, $r = -$

0.63, $p = 5 \times 10^{-3}$; beta2, $r$ = -0.47, $p$ = 0.013) and are thus possibly codependent features of the same EEG signature. This relationship between delta power and beta power was not significant in either comparison group, but appeared as a trend in the ASD cohort (beta1, $r$ = -0.62, $p$ = 0.056; beta2, $r$ = -0.62, $p$ = 0.056).

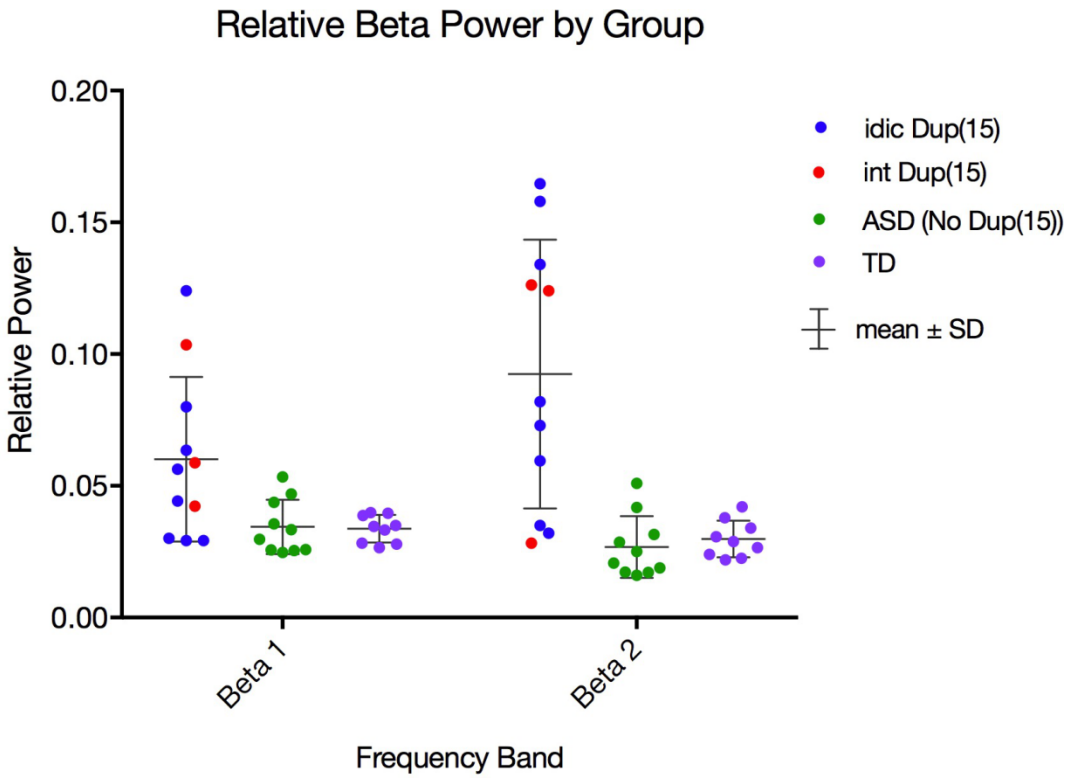


***Figure 3.3 Distributions of relative beta1 and beta2 power for all groups****. Dot plots of relative beta1 (12–20 Hz) power (A) and beta2 (20–30 Hz) power (B) averaged across all ROIs in the Dup15q syndrome group (left), nonsyndromic ASD group (center), and TD group (right). Participants with interstitial duplications [int Dup(15)] are colored red, while participants with isodicentric duplications [idic Dup(15)] are colored blue. Comparison group participants with nonsyndromic ASD are colored green, while children in the TD comparison group are colored purple. The Dup15q cohort features greater mean and standard deviation (mean ± S.D.) in beta1 power (0.060 ± 0.031) and beta2 power (0.092 ± 0.051) in*

*relation to comparison groups [beta1 power: 0.034 ± 0.010 (ASD), 0.034 ± 0.0052 (TD); beta2 power: 0.027 ± 0.012 (ASD), 0.030 ± 0.0070 (TD)].*

While spectral power measures are integrated across frequency bins, they do not capture peaks and valleys in the frequency domain. To capture such spectral features, grand averaged PSDs were visualized in Fig. 3.4A by computing the mean across ROIs and all participants. A clear spectral peak in beta band can be seen for the Dup15q syndrome cohort in Fig. 3.4A. Fig. 3.4B shows the presence of beta spectral peaks in PSDs averaged across ROIs for individual participants with Dup15q syndrome. After removing the 1/*f* trends (dotted lines) that account for most variance in EEG PSDs (Fig. 3.4C), the peak frequency for participants with Dup15q syndrome (~23 Hz) was higher than that of both the ASD (~8 Hz) and TD (~9 Hz) comparison groups (Fig. 3.4D).

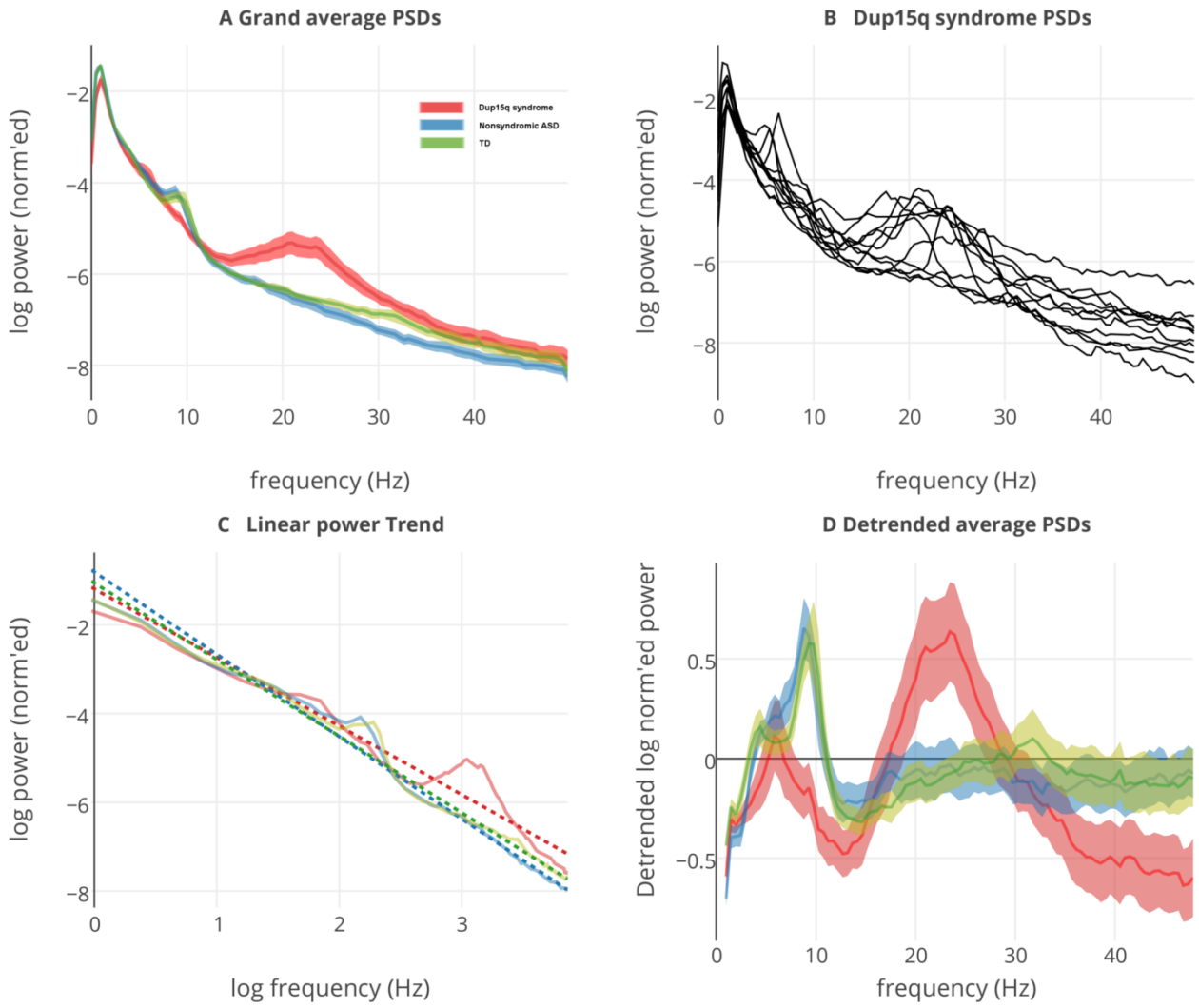


***Figure 3.4 Grand averaged power spectral densities from all groups.*** *(A) Power spectral densities (PSDs) averaged across all regions of interest (ROIs) and participants for the Dup15q syndrome group (red), nonsyndromic ASD group (blue), and TD group (green). Before averaging, participant PSDs are normalized such that the area under the curve equals 1 to emphasize relative power. Translucent highlights represent standard error of the mean (SEM) computed across participants. An enormous peak from 12–30 Hz reveals the presence of powerful spontaneous beta oscillations (SBOs) in the Dup15q cohort. PSDs are normalized to represent relative power. (B) Individual PSDs, averaged across ROIs, from participants with Dup15q syndrome. (C) Group averaged linear trends (dotted lines) fitted from log-log*

*transformed PSDs. Linear trends represent the 1/f distribution inherent in the EEG. (D) Group averaged PSDs with linear trends removed to emphasize deviations from the 1/f trend. Dup15q syndrome shows the largest deviation, with a peak frequency (~23 Hz) in the beta band. Both comparison groups feature peak frequencies in the alpha band.*

### 3.3.2 Study 2 – Within group analysis

Of the regression models tested, only epilepsy diagnosis statistically predicted beta2 power, with stronger beta2 power in participants with Dup15q syndrome who did not have epilepsy ($p$ = 0.03, $R^2$ = 0.17; Fig. 3.5). Qualitative evidence for this finding can be seen in averaged scalp plots of beta power in individuals with Dup15q with and without epilepsy (Fig. 3.5B, 5D). Neither age nor duplication type significantly predicted beta power within the Dup15q cohort. Because between group differences were also found in delta power and gamma power, we asked if these variables could also predict epilepsy status. Neither delta power nor gamma power significantly predicted epilepsy status in Dup15q syndrome, although a trend level finding is observed for gamma power ($p$ = 0.076, $R^2$ = 0.12).

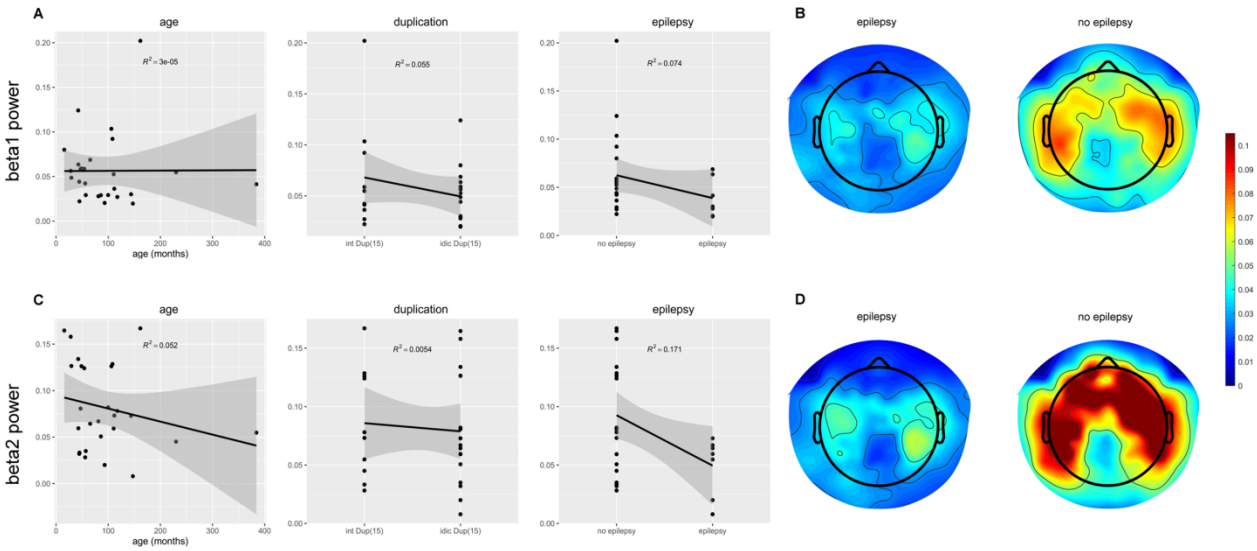


***Figure 3.5 Age, duplication type, and epilepsy as predictors of beta1 and beta2 power.*** *(A) Scatter plots of age, duplication type, and epilepsy against relative beta1 (12–20 Hz) power. Duplication type and epilepsy are treated as binary variables. Interstitial duplications and no epilepsy are represented as 0; Isodicentric duplications and epilepsy are represented as 1. Highlighted area around regression line represents the 95% confidence region. (B) Topographic scalp plots of beta1 power averaged across participants with epilepsy (left) and without epilepsy (right). (C) Scatter plots of age, duplication type, and epilepsy against relative beta2 (20–30 Hz) power. (D) Topographic scalp plots of beta2 power averaged across participants with epilepsy (left) and without epilepsy (right). The relationship between epilepsy and beta2 power is statistically significant ($R^2$ = 0.17, p = 0.032).*

## 3.4 Discussion

Dup15q syndrome is highly penetrant for intellectual disability, epilepsy, and ASD. Several clinical reports have described a distinctive feature on clinical EEG that may represent an electrophysiological biomarker of this syndrome in the form of increased beta oscillations. We found that EEG beta power (SBOs) most strongly distinguished children with Dup15q

syndrome from both (1) age/IQ-matched children with nonsyndromic ASD and (2) age-matched TD children. Changes in the EEG beta band were qualitatively obvious upon visual inspection of data as SBOs. These SBOs, as measured by power in the beta1 and beta2 bands, correlate with epilepsy diagnosis but not age or duplication type. Although our clinically referred sample included a small cohort with a relatively large age range, the robustness of this EEG signature in both this cohort and the larger sample examined in the second study is evident by the large effect sizes ($|d| > 1$).

The promise of biomarkers

There has been a tremendous interest in the field of neurodevelopmental disorders in the identification of quantitative measures of brain function that may relate to specific genetic etiologies, as these "biomarkers" can help provide clues into the neurobiological sequelae of a genetic variation (linking genes to brain) and shed light on the impact of aberrant brain function on behavior (linking brain to behavior). A quantitative measure of neural function in a genetically defined subgroup may provide a more refined assay of subtle individual differences that can inform predictors of outcome, particularly in the context of interventions that target the specific mechanism underlying the measure. In other words, one may see a change in a biomarker with treatment that precedes any overt behavioral change but that suggests engagement of the biological target and, therefore, hope for clinical improvement.

For both practical and scientific reasons, EEG is a particularly robust method to measure neural function in developmental disorders. Not only does it have excellent motion tolerance, its temporal resolution allows it to resolve neurophysiological oscillations and dynamics on a millisecond scale. Power Spectral Densities (PSDs) from EEG recordings follow a characteristic

1/*f* distribution, so named because spectral power is inversely proportional to frequency. 1/*f* distributions are ubiquitous in the brain and are a likely signature of balance between neural excitation and inhibition (E/I balance) (Poil et al. 2012; Voytek et al. 2015).

### 3.4.1 Presumed mechanisms of spontaneous oscillations in Dup15q syndrome

Enhanced SBOs and diminished delta oscillations observed in Dup15q syndrome represent deviations from the 1/*f* distribution (Figure 4C). Because E/I balance is believed to be necessary for varied and complex electrophysiological signals (Poil et al. 2012; Voytek et al. 2015), deviations from the 1/*f* distribution likely represent a disruption of balanced neurotransmission. In Dup15q syndrome, a disruption of E/I balance could be created by $GABA_AR$ subunit gene overexpression. SBOs observed in Dup15q syndrome (Al Ageeli et al. 2014; Urraca et al. 2013) strongly resemble those induced by positive allosteric modulators (PAMs) of $GABA_ARs$ such as benzodiazepines and barbiturates (Domino et al. 1989; Feshchenko et al. 1997; van Lier et al. 2004). Benzodiazepines, barbiturates, and other $GABA_AR$ PAMs increase the net chloride flux through the $GABA_AR$'s ion pore (Löscher and Rogawski 2012; Nutt and Malizia 2001). Barbiturates (Löscher and Rogawski 2012; Macdonald and Twyman 1991) and at least one benzodiazepine compound, zolpidem (Fain 1999; I Mody et al. 1994) have been shown to increase the time constant of $GABA_ARs$ by lengthening the duration of hyperpolarizing chloride currents through the receptor's ion pore. Beta activity resulting from $GABA_AR$ modulation or other dysfunction may actually represent slowed gamma activity, as the $GABA_AR$ time constant is known to control the frequency of gamma oscillations (Buzsáki 2006). In the healthy brain, inhibitory interneurons with reciprocal connections fire synchronously to inhibit pyramidal cells, silencing themselves in the process. Pyramidal cells recover from inhibition to

enjoy a period of excitability before being silenced again by interneurons, beginning the gamma cycle anew (Buzsáki 2006; Buzsáki and Wang 2012). Lengthening the time constant of $GABA_A$Rs through altered $GABA_A$R gene expression would lengthen the period of the gamma cycle to that characteristic of beta oscillations. Together, high-frequency beta and gamma oscillations are hypothesized to play a critical role in temporal binding of local circuits during cognitive tasks.

In addition to elevated beta power, spectral anomalies were also observed in the delta and gamma bands of EEG recordings from participants with Dup15q syndrome. It is possible that reduced delta power observed in Dup15q syndrome may be linked to enhanced beta power in a reciprocal manner. A significant negative correlation was observed between delta power and both beta1 power and beta2 power only in the Dup15q syndrome cohort. Angelman syndrome, most commonly caused by maternal deletion of the 15q11-q13 region, including *UBE3A*, features enhanced delta oscillations in clinical EEG recordings (Laan and Vein 2005; Robinson et al. 2015; Sidorov et al. 2017), suggesting a reciprocal relationship between deletion and duplication of the $GABA_A$R subunits. Furthermore, loss of *UBE3A* has been associated with enhanced delta oscillations (Judson et al. 2016) and suppression of ventral striatal GABA co-release in mouse models of Angelman syndrome (Berrios et al. 2016), underscoring the relationship between the ubiquitin ligase and GABAergic transmission.

Evidence from pharmacological studies also suggests that reduced delta power in Dup15q syndrome may be directly related to $GABA_A$R subunit gene overexpression rather than *UBE3A per se*. For instance, the benzodiazepine compounds diazepam and zolpidem decrease cortical EEG delta power in awake, behaving rats (Nickel and Szelenyi 1989; van Lier et al. 2004). Similarly, midazolam has been shown to reduce EEG delta power during sleep in rats

(Lancel et al. 1994). In humans with generalized anxiety disorder, the benzodiazepine clorazepate has been shown to reduce delta power in scalp EEG recordings (Buchsbaum et al. 1985). All studies considered so far also associated increased beta power with benzodiazepine challenge. The foregoing evidence from both rodents and humans suggests that $GABA_AR$ potentiation and EEG delta power are inversely related.

Finally, we suggest that our finding of stronger gamma oscillations in Dup15q syndrome as compared with nonsyndromic ASD may reflect a common mechanism for beta2 and gamma oscillations involving feedback inhibition between pyramidal cells and interneurons. This hypothesis is supported by the fact that beta2 power and gamma power were strongly correlated in all three cohorts. Nonetheless, the effect size observed in beta2 ($d$ = 1.73) was greater than that of gamma ($d$ = 0.97), suggesting that SBOs are a clearer biomarker of Dup15q syndrome than gamma oscillations.

**3.4.2 SBOs as markers of gene expression?**

Although we did not measure *UBE3A* and GABA receptor gene expression from participants in our study, these data support the need for future investigations that can directly examine the relationship between EEG power and mRNA transcript levels from *GABRA5, GABRB3, GABRG3*, and *UBE3A,* all genes which are duplicated in Dup15q syndrome. In particular, there already exists evidence from pharmacological studies of $GABA_AR$ PAMs (i.e., benzodiazepines) (Domino et al. 1989; Feshchenko et al. 1997; van Lier et al. 2004), as well as correlations between motor evoked beta power and resting GABA levels (Gaetz et al. 2011), suggesting an important relationship between beta activity and GABAergic transmission. As with beta power in our study, Scoles et al. found greater mean and variance in neural *GABRB3*

expression in a small cohort (*n* = 8) of postmortem tissue samples from individuals with Dup15q syndrome (isodicentric duplications) compared to nonsyndromic ASD and TD tissue samples (Scoles et al. 2011). The close resemblance between the distribution of *GABRB3* expression in the Scoles et al. study and the distribution of beta power in our study can be visualized in Fig. 4B of Scoles et al. (Scoles et al. 2011)(*cf*. Fig. 3.3, this paper). Slight overlap in distributions of beta power between the Dup15q syndrome cohort and the ASD comparison group could potentially reflect point mutations of $GABA_AR$ subunit genes in some children in the ASD comparison group. Finally, many studies of benzodiazepine $GABA_AR$ PAMs have shown reductions of in delta power in a variety of contexts (Buchsbaum et al. 1985; Lancel et al. 1994; Nickel and Szelenyi 1989; Poyares et al. 2004; van Lier et al. 2004; Wisor et al. 2002), suggesting that reduced delta power in the wakeful spontaneous EEG of Dup15q syndrome participants could also be explained by $GABA_AR$ abnormalities such as altered subunit expression. Further work in humans and animal models will be necessary to test this hypothesis.

Another possible cause of reduced EEG delta power in Dup15q syndrome is duplications of *UBE3A*, the causative gene of Angelman syndrome. Patients with Angelman syndrome do not express *UBE3A* in neural tissue and show elevated EEG delta power (Berrios et al. 2016; Robinson et al. 2015; Sidorov et al. 2017), the opposite electrophysiological phenotype as Dup15q syndrome. For this reason, it is plausible that an inverse relationship exists between EEG delta power and *UBE3A* expression levels. It is also possible that *UBE3A* overexpression influences beta power, perhaps an indirect effect mediated through the GABAergic system. For instance, a recent study in a *UBE3A*-null mouse model found that loss of *UBE3A* can impair co-release of subcortical GABA, thus demonstrating their intrinsic functional relationship (Berrios

et al. 2016)(Berrios et al. 2016). However, considering that SBOs have been reported in individuals with paternal Dup15q syndrome (Al Ageeli et al. 2014; Urraca et al. 2013), the paternally imprinted *UBE3A* alone cannot explain SBOs in Dup15q syndrome.

### 3.4.3 SBOs and epilepsy risk

We identified an inverse relationship between SBOs, particularly beta2 power, and epilepsy in Dup15q syndrome in the larger cohort analysis. At first glance, this result could be interpreted as SBOs being markers of enhanced GABAergic tone (as found in GABAergic medications such as the benzodiazepines), thus providing neural protection against seizures in this population. However, interpretation of this relationship requires caution, as likely there are modifying factors such as background EEG, antiepileptics, and developmental level of individuals with epilepsy that may influence this relationship (Pillai and Sperling 2006). In particular, with our small sample, we could not fully disentangle the relationship between age and epilepsy. To better understand the relationship between age, duplication type, epilepsy status, and beta2 power, we visualized all four variables in Fig. 3.6. Log-transformed age (abscissa) is plotted against beta2 power (ordinate), with interstitial duplications represented by diamonds and isodicentric duplications represented by circles. Children are color coded by epilepsy status (pink for epilepsy, blue for no epilepsy). As seen in this figure, those participants with the highest beta2 power included our youngest children without epilepsy. Of note, while it is difficult to separate the role of epilepsy *per se* from the impact of medications on EEG, anticonvulsant medications typically increase beta activity rather than decrease such activity (Veauthier et al. 2009). Although no subjects in this study were treated with benzodiazepine or barbiturate medication, most children with Dup15q syndrome with epilepsy were treated with

levetiracetam, which has been shown to increase (rather than decrease) relative beta power in epilepsy patients (Veauthier et al. 2009).

We must emphasize that the relationship between GABAergic activity and epilepsy is complex as is, most likely, the relationship between beta oscillations and epilepsy. It may seem paradoxical that a syndrome associated with overexpression of GABA receptor genes could also confer such a high risk for epilepsy. In general, synaptic, i.e. phasic, inhibition is mediated by $\alpha 1$ or $\alpha 2$ containing GABA receptors that also have a γ2 subunit producing an increase in chloride conductance favoring hyperpolarization. The extrasynaptic GABA receptors, usually $\alpha 4$ or $\alpha 6$ combined with δ (no gamma) are sensitive to small changes in ambient GABA, and they produce sustained lowering of the membrane potential (Istvan Mody 2001). Excessive GABAergic activity can produce two effects that are both potentially epileptogenic. First, the spike-wave bursts in the thalamo-cortical network are initiated by hyperpolarization, since the lowered membrane potential is the trigger for the low-threshold calcium currents (Crunelli and Leresche 2002). Secondly, prolongation of inhibition can promote synchronization of such networks, which can occur with enhancement of tonic inhibition (Errington et al. 2011). Thus spike-wave stupor can be treated with intravenous benzodiazepines which act only at synaptic receptors. On the other hand, generalized spike-wave paroxysms become more frequent and longer in duration when ambient GABA is increased by other medications.

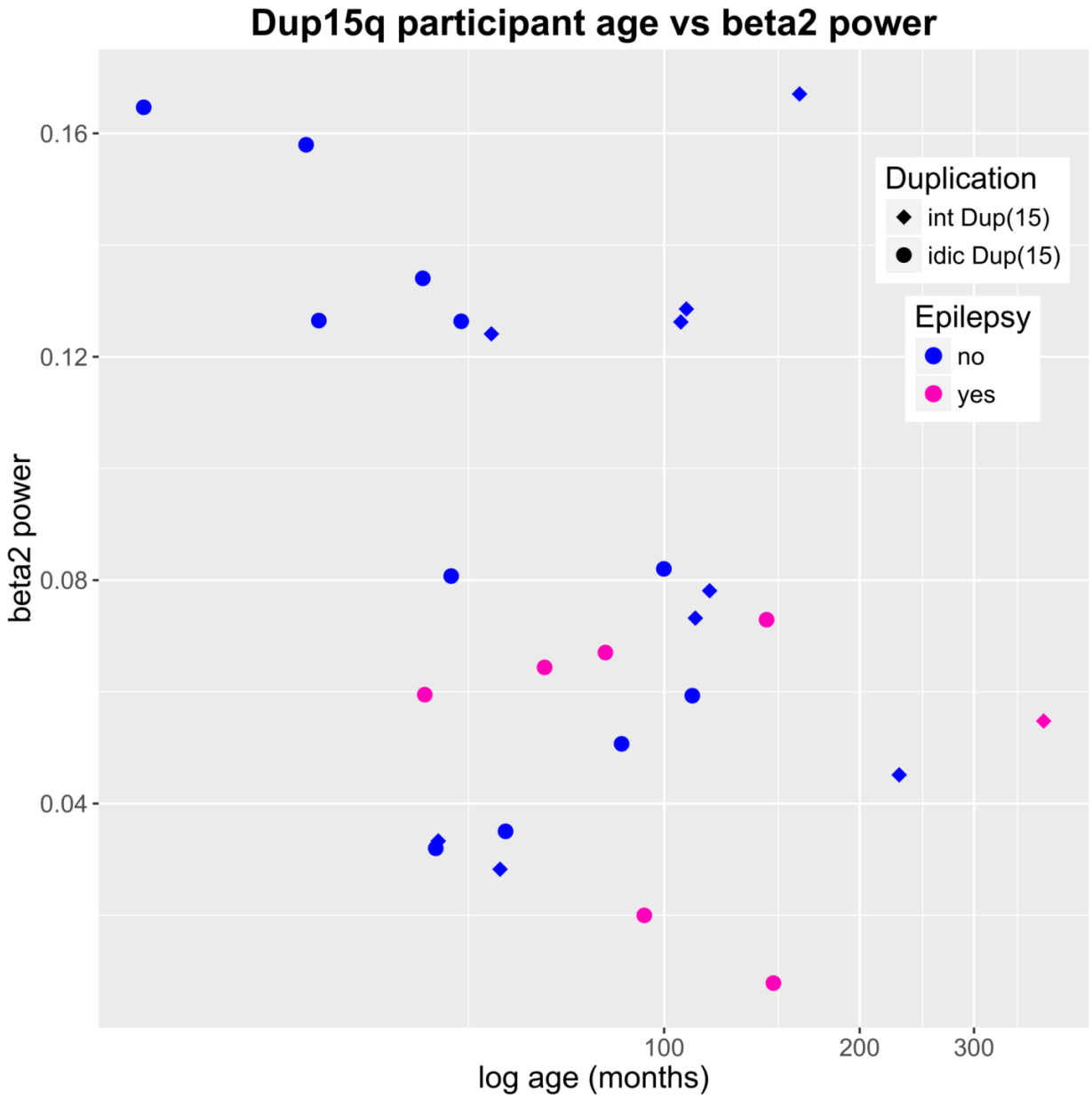


***Figure 3.6. Dup15q syndrome participants by age, beta2 power, duplication type, and epilepsy status.*** *A scatter plot of age versus beta2 power in Dup15q syndrome reveals a cluster of very young participants with very high beta2 power (top left corner). None of these participants have epilepsy. All participants with epilepsy feature beta2 power < 0.08. Note that the abscissa has been log-transformed to accommodate a large number of young participants and a much smaller number of older participants.*

### 3.4.4 Limitations and future directions

The relatively small sample size, albeit representative of the full clinical spectrum of this rare disorder, does limit further subgroup analyses and examination of clinical correlates of this biomarker. The sample size also precludes the development of a multi-variable prediction model of these elevated beta oscillations. The association with epilepsy, in particular, warrants further investigation through two approaches. First, through longitudinal studies we can examine changes in EEG power after the onset of epilepsy and, by doing so, elucidate whether beta oscillations represent a protective biomarker for the development of seizures.

However, these findings have laid the foundation for a larger scale study of the functional and clinical implications of electrophysiological biomarkers in this syndrome. Through a multi-site, coordinated effort with the National Dup15q Alliance, we will expand our sample size to ask the following questions: First, do changes in state modulate beta power, in particular during cognitive or perceptual tasks, or during sleep? One might hypothesize that persistent beta power in sleep could disrupt sleep architecture enough to impact cognition and behavior in these children with neurodevelopmental disabilities. Moreover, a lack of modulation of EEG oscillations during cognitive tasks could directly hinder learning. We will directly examine the relationship between beta power and changes in beta power with more quantitative measures of cognition and autism severity. Second, what are the exact genetic underpinnings of this biomarker? We will examine electrophysiological markers in several pre-clinical models of Dup15q syndrome (full genetic duplication compared to *UBE3A* overexpression mouse). Translational studies linking gene expression and SBOs in individuals with Dup15q syndrome will elucidate the specific role of *UBE3A*, *GABRA5*, *GABRB3*, and

*GABRG3* gene expression on this biomarker and help further understand the genetic effects on transcript levels that lead to the pathogenesis of Dup15q syndrome.

**3.5 Conclusions**

The field of ASD research has sorely lacked quantifiable biomarkers that may help parse the neurobiological heterogeneity of this spectrum of disorders. Moreover, as genetic testing in ASD and related neurodevelopmental disorders becomes clinical gold standard, an increasing number of children are diagnosed with genetic variants that not only will elucidate causal mechanisms but also therapeutic targets (Jeste and Geschwind 2016). The identification of these targets necessitates quantifiable biomarkers that relate directly to genetic mechanisms. Studies in Dup15q syndrome provide a promising path towards this mission, as the elucidation and quantification of an electrophysiological biomarker could improve diagnosis and prognostication, as well as measurement of target engagement and outcomes in clinical trials, a model that can inform similar investigations in the quickly expanding number of high-risk genetic syndromes associated with neurodevelopmental disorders.

# Chapter 4: Neuronal *UBE3A* overexpression is not necessary for the Dup15q syndrome beta EEG phenotype

## 4.1 Background

Duplications and triplications of 15q11.2-q13.1 (Dup15q syndrome) are highly penetrant for intellectual disability, autism spectrum disorder (ASD), delayed development, and epilepsy (DiStefano et al. 2016; Finucane et al. 2016; Hogart et al. 2010; Urraca et al. 2013). Dup15q syndrome is often considered the most common copy number variation in ASD (Abrahams and Geschwind 2008). Several genes in this region impact early brain development, namely synaptic function and inhibitory neurotransmission (Miao et al. 2013; Smith et al. 2011a; Tanaka et al. 2012). The relative contributions of these genes to Dup15q syndrome pathology are poorly understood. However, allele specific expression in neurons (maternal or paternal imprinting) may allow their contributions to be elucidated by examining maternal and paternal duplications separately.

The parent of origin modulates the Dup15q syndrome clinical phenotype. Children with maternal duplications present with a more severe clinical phenotype and greater risk of ASD (Cook Jr et al. 1997). This is likely due to paternal imprinting of *UBE3A* in neurons (Albrecht et al. 1997; Yamasaki et al. 2003), a gene linked to ASD (Guffanti et al. 2011; Nurmi et al. 2001) that encodes a ubiquitin protein ligase and regulates synaptic development (Dindot et al. 2007; Greer et al. 2010; Miao et al. 2013; Smith et al. 2011). Two 15q duplication types exist: interstitial and isodicentric duplications (Finucane et al. 2016). Interstitial duplications manifest as extra copies of 15q11.2-q13.1 found within chromosome 15 and are generally cases partial trisomy. Isodicentric duplications are extra copies of 15q11.2-q13.1 ligated end-to-end as an

extranumarary chromosome. These are cases of partial tetrasomy which confer a more severe clinical phenotype (Finucane et al. 2016).

To guide targeted treatments of Dup15q syndrome and other forms of ASD, biomarkers are needed that reflect a molecular or circuit level treatment response (Jeste et al. 2015). Such mechanism-based biomarkers may serve as surrogate endpoints in clinical trials whose short durations preclude observation of long-term behavioral changes. Dup15q syndrome is characterized by an unusual electroencephalogram (EEG) signature that likely reflects molecular pathology (Al Ageeli et al. 2014; Urraca et al. 2013). Recently, our group quantified this EEG signature as spontaneous beta (12-30 Hz) oscillations in children with Dup15q syndrome, none of whom were taking benzodiazepines or other medications known to induce beta activity (Frohlich et al. 2016). The Dup15q EEG signature is thus a promising biomarker that may quantify disease pathophysiology or index drug target engagement in the development of Dup15q syndrome treatments.

Proper use of the Dup15q syndrome biomarker will crucially depend on understanding which aspect of Dup15q syndrome pathology the biomarker reflects. Several 15q genes have been linked to the disease pathology, including the paternally imprinted gene *UBE3A* and a cluster of non-imprinted gamma-aminobutyric acid type-A ($GABA_A$) receptor β3, α5, and γ3 subunit genes (Finucane et al. 2016). *UBE3A* is the causative gene of Angelman syndrome (Kishino et al. 1997), another 15q disorder typically caused by deletion of this region on the maternal allele (Dagli et al. 2011) and characterized by delayed development, seizures, and EEG anomalies. Because *UBE3A* is only expressed from the maternal allele of most human neurons (Albrecht et al. 1997; Yamasaki et al. 2003), *UBE3A* is unlikely to be responsible for a paternal

Dup15q syndrome phenotype (Urraca et al. 2013). Phenotypes common to both paternal and maternal duplications are best explained by biallelically expressed, nonimprinted genes. The most likely non-imprinted candidate genes within the duplication are a cluster of GABA receptor subunits including *GABRB3*, *GABRA5*, *and GABRG3*. These $GABA_A$ receptor genes encode the β3, α5, and γ3 subunits, respectively, and have been linked to epilepsy and ASD in both patients and animal models (Chen et al. 2014; Cook Jr et al. 1998; DeLorey et al. 1998; Mesbah-Oskui et al. 2017; Møller et al. 2017; Zurek et al. 2016). A potential role for the β3/α5/γ3 gene cluster in the Dup15q syndrome EEG phenotype is emphasized by a similarity between the Dup15q syndrome beta EEG phenotype (Frohlich et al. 2016) and the well-documented phenomenon of beta oscillations induced by $GABA_A$-modulating compounds (e.g., benzodiazepines) in the human EEG (Domino et al. 1989).

To infer the extent to which dysregulation of *UBE3A* or the β3-α5-γ3 subunit gene cluster is necessary or sufficient for the beta EEG phenotype, we performed two studies. To test the hypothesis that GABAergic dysfunction is sufficient to produce the beta EEG phenotype, we compared this phenotype in Dup15q syndrome to beta oscillations pharmacologically induced by the $GABA_A$ modulator midazolam in healthy adults. Next, to test the hypothesis that *UBE3A* dysregulation is necessary for the beta EEG phenotype, we compared two cases of paternal Dup15q syndrome to a reference cohort of children with Dup15q syndrome. Our findings bring the field of neurodevelopmental disorders closer to much needed EEG biomarkers that guide drug development and clinical trials, e.g., by indexing a treatment response or drug target engagement.

## 4.2 Methods

### 4.2.1 Recruitment and EEG acquisition

To test our predictions outlined in the introduction, we analyzed spontaneous EEG recordings from 1) a reference cohort of n = 28 children with Dup15q syndrome, 2) a control cohort of n = 14 children with typical development, 3) n = 2 children with paternal duplications of 15q11-q13, and 4) n = 12 healthy adult volunteers challenged with 5 mg of midazolam. Recruitment and data acquisition are detailed for each below.

### 4.2.2 Dup15q syndrome reference cohort

Because Dup15q syndrome is a rare disease with a 1 in 10,000 prevalence rate (Moeschler et al. 2002), we utilized national family conferences to increase our sample size in accordance with the University of California, Los Angeles (UCLA) Institutional Review Board (IRB). To further increase our sample, we recruited children of all ages and developmental abilities. All Dup15q syndrome reference cohort data were acquired through UCLA in accordance with the IRB. Parents of participants provided informed written consent prior to the start of study activities. Our reference cohort drew from a large sample of awake-state spontaneous EEG recordings collected from n = 71 participants with Dup15q syndrome as part of an ongoing study that included EEG and behavioral assessments. This sample featured all comers from a broad age range encompassing children from three different sites: (1) UCLA, (2) the 2015 National Dup15q Alliance conference in Orlando, Florida, and (3) the 2017 National Dup15q Alliance conference in Redondo Beach, California. See Table 4.1 for details of the reference cohort, including sample sizes by site.

For this study, we considered only children (age < 18 years) with full 15q11-q13 duplications (duplications of only BP1- BP2 were excluded). Several participants gave data at multiple visits. In these instances, we processed EEG data from the earliest visit with usable data. To eliminate confounding factors such as epilepsy and antiepileptic medications that act on the GABAergic system, we carefully selected a subsample of children with no history of seizures and no antiepileptic medications of any type. After eliminating n = 40 participants due to medication, seizures, or data quality, n = 2 further participants were excluded for the following reasons: 1) sleep during EEG recording, and 2) fewer than 20 valid time windows for the lowest frequency analyzed. An additional (n = 1) participant with paternal Dup15q syndrome was removed from the reference cohort and examined separately. Our final reference cohort retained n = 28 participants.

High density (HD) EEG data were acquired at a sampling rate of 500 Hz using 129 channel vertex-referenced EGI geodesic nets with Ag/AgCl electrodes (Electrical Geodesics, Inc., Eugene, OR, USA). Full details of the data acquisition are found in a previous publication (Frohlich et al. 2016).

| | Interstitial | Isodicentric | Total |
|---|---|---|---|
| **Dup15q total reference sample** | 14 | 14 | 28 |
| **UCLA sample** | 3 | 6 | 9 |
| **Orlando sample** | 4 | 2 | 6 |
| **Redondo sample** | 7 | 6 | 13 |
| **Dup15q age (months, mean ± SD)** | 79.6 ± 41.1 | 60.9 ± 37.8 | 70.3 ± 39.9 |
| **Dup15q DQ (mean ± SD)** | 48.8 ± 26.1 | 37.8 ± 16.0 | 43.5 ± 22.1 |
| **Dup15q missing DQ** | 1 | 2 | 3 |
| **TD sample** | N/A | N/A | 14 |
| **TD age (months, mean ± SD)** | N/A | N/A | 55.0 ± 28.5 |
| **TD DQ (mean ± SD)** | N/A | N/A | 118 ± 15.5 |

***Table 4.1 Dup15q syndrome reference cohort****. Sample sizes are reported by EEG site: UCLA (Center for Autism Research and Treatment), Orlando (2015 National Dup15q Alliance conference), and Redondo (2017 National Dup15q Alliance conference). Cognitive ability is reported as developmental quotient derived (DQ) from age appropriate developmental scales. Calculations of mean and standard deviation (SD) for DQ scores ignore missing data reported in rows 'Missing DQ' row.*

### 4.2.3 TD control group

To confirm high beta power in the Dup15q syndrome reference cohort, we examined awake-state spontaneous EEG data from TD children (n = 14) recruited through UCLA. This control group spanned a broad age range (55.0 ± 28.5 months, mean ± SD; min = 16 months; max = 111 months) and did not significantly differ in age from the Dup15q syndrome reference cohort ($p = 0.16$, $t = 1.42$). All TD children had DQ > 100 (118 ± 15.5, mean ± SD). All EEG data were recorded at UCLA. Recruitment, parental consent, and EEG protocol were identical to that described above for Dup15q syndrome.

### 4.2.4 Paternal Dup15q syndrome case studies

Paternal Dup15q syndrome is both less common that maternal Dup15q syndrome and features a milder clinical phenotype (Isles et al. 2016; Urraca et al. 2013), impeding detection and recruitment. For this reason, we focused on investigation on just two children with paternal duplications. Both paternal duplication subjects have been previously described in a study of individuals with interstitial Dup15q (Urraca et al. 2013). Thus, they are referred to here by their IDs from the previous publication. The first participant (801-005) was a boy aged 13 years (161 months) with paternally derived interstitial Dup15q syndrome recruited through UCLA at a

Dup15q Alliance family conference. Awake-state spontaneous EEG data were recorded using the high density EGI system and protocol described above. The second participant (801-015) was a girl aged 8 years (96 months) with paternally derived interstitial Dup15q syndrome recruited through University of Tennessee Health Science Center (UTHSC). Neither participant had a history of seizures, though both participants had a diagnosis of attention deficit hyperactivity disorder (ADHD). See Table 4.1 for clinical phenotype and duplication size of both participants. Awake-state spontaneous EEG data were collected from 801-015 at LeBonheur Children's Hospital (LCH) in Memphis, Tennessee in a multi-hour, nonconsecutive recording (sampling rate f = 512 Hz) using a 21-channel clinical system. We extracted 10 minutes of data from the longest segment of consecutive data in the recording and excluded ear channels (A1 and A2), retaining 19 channels corresponding to the 10-20 montage. Data were referenced to average prior to importing. Because the number of EEG channels differed between recording systems used for each participant, EEG data from the participant with the greater number of EEG channels (801-005) were spatially interpolated to a 19-channel montage congruent with the other participant's EEG.

| ID | Dup type | Dup size | Age | Gender | Seizure | ASD | ADHD | Full DQ | EEG |
|---|---|---|---|---|---|---|---|---|---|
| ***801-005*** | Interstitial | 5.7 Mb | 161 months | M | No | No | Yes | 67 | research |
| ***801-015*** | Interstitial | 5.0 Mb | 96 months | F | No | No | Yes | 77 | clinical |

***Table 4.2 Phenotype, duplication, and EEG details of participants with paternal Dup15q syndrome.*** Participant 801-005 was a 13-year-old boy with paternal Dup15q syndrome. Participant 801-015 was an 8-year-old girl with paternal Dup15q syndrome. Both participants had interstitial duplications and met

criteria for ADHD. Neither participant had seizures or met criteria for ASD. Participants had similar DQs, though 801-005, but not 801-015, had a DQ measured below the threshold for intellectual disability.

### 4.2.5 Midazolam pharmaco-EEG

To assess the similarity of the beta EEG phenotype in Dup15q syndrome to beta oscillations pharmacologically induced with a $GABA_A$ positive allosteric modulator (PAM), we examined pharmaco-EEG from n = 12 healthy adult controls challenged with the benzodiazepine compound midazolam. Midazolam is a nonselective $GABA_A$ PAM that binds to the $GABA_A$ receptor so as to increase the conductance of the receptor when the channel is opened by GABA. We chose adults due to ethical considerations that preclude similar pharmacological experimentation in children. The study protocol was approved by the National Research Ethics Service (NRES) committee.

A baseline EEG was recorded at the start of the study at the same time of day that the drug would be administered at a later date. A sub-sedative dose of midazolam was administered orally (5 mg) on day 2 of the study, and pharmaco-EEG was recorded 1 hour following drug challenge (4 minutes eye closed resting, 4 minutes eyes open resting). On both days, EEG data were acquired at sampling rate of 256 Hz (alpha trace digital EEG EPV-32, Neuro Medical, Arnheim, Netherlands; recording reference POz). We averaged spectral power across eyes open and eyes closed data within each condition (baseline and post drug) following a wavelet convolution frequency transform (signal processing details are described below).

### 4.2.6 EEG preprocessing

Raw data were imported to MATLAB (The MathWorks, Inc., Torrance, California) for data processing. We processed all data using customized scripts and in-house tools. For all HD EEG datasets, we excluded 46 "skirt channels" that are particularly sensitive to noise and muscle artifact (see Fig. 4.1). This left 83 channels for processing and analysis. For EEG collected with other systems, we imported 19 channels corresponding to the 10-20 montage for processing and analysis.

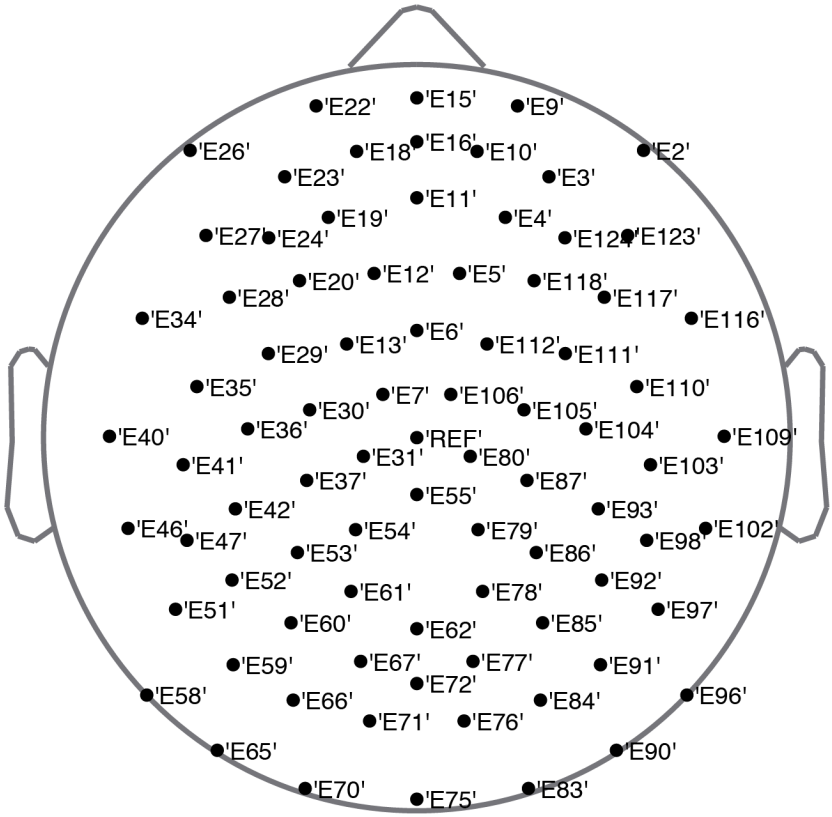


***Figure 4.1 HD EEG channels used in analysis.*** *For all EEG collected through UCLA using 129 channel EGI geodesic nets ("HD EEG"), we excluded 46 "skirt channels" (defined as channels with EGI polar coordinate r > 0.5) near the periphery of the EEG net that are particularly sensitive to noise and muscle artifact. The remaining 83 channels retained for analysis are shown above and labeled with their EGI*

*channel number.*

Data were bandpass filtered 1 – 45 Hz (FIR, filter order: 2 x sampling rate) and artifact reduced using a combination of manual artifact selection and independent component analysis (ICA). Manual artifact selection identified technical artifacts and gross physiological artifacts for exclusion. Noisy channels were also marked for interpolation at this stage, and datasets for which the number of noisy channels exceeded the square root of the total number of imported channels were excluded from analysis. A minimum of 60 s of clean data were analyzed for each participant. ICA was performed with the FastICA algorithm (Hyvarinen 1999a; Jung et al. 2000). Components corresponding to stereotyped physiological artifacts (e.g., blinks, saccades, neck movement) were subtracted from EEG data. Following artifact reduction, bad channels were spline-interpolated. Data were averaged referenced prior to the wavelet convolution. In contexts where HD EEG were compared directly to 19-channel EEG, we spatially interpolated HD EEG to 19 channels correspond to the 10-20 montage coordinates prior to the wavelet convolution. See Table 4.3 for number of bad channels, artifact components, and length of good data for each cohort and paternal duplication case.

| | **Clean data** | **Bad channels** | **Total channels** | **Artifact ICs** | **Total ICs** |
|---|---|---|---|---|---|
| **Reference cohort** | 208 ± 100 s | 1.64 ± 2.09 | 83 | 32.4 ± 12.4 | 82 |
| **TD controls** | 128 ± 31.9 s | 0.86 ± 1.17 | 83 | 22.6 ± 8.75 | 82 |
| **Paternal dup 801-005** | 483 s | 0 | 19 | 34 | 82 |
| **Paternal dup 801-015** | 581 s | 0 | 19 | 2 | 18 |
| **Healthy adult cohort** | 221 ± 26.7 s | 0 ± 0 | 19 | 4.9 ± 1.94 | 18 |

***Table 4.3 Details of data processing.*** *Second of clean data, number of bad channels, and number of artifact components are given as mean ± SD for datasets analyzed from the reference cohort, TD controls, and healthy adult cohort; the total number of each category is also reported for both paternal duplication cases. Each dataset analyzed had a minimum of 60 s of clean data. Datasets for which the number of bad channels exceeded the square root of the total number of channels were discarded and not analyzed. Numbers for the healthy adult cohort are reported as mean and standard deviation per participant, and drug condition.*

### 4.2.7 Frequency transform and analysis

Data were frequency transformed by convolution with Morlet wavelets (Tallon-Baudry et al. 1997). A total of 54 Morlet wavelet kernels were used with logarithmically spaced frequencies from 2 - 45 Hz (8 wavelets per octave) and with a spectral smoothing of 1/3 octave. After convulsion, elements of the time-frequency representation corresponding to excluded data were removed. Datasets were discarded if their time-frequency representation contained fewer than 20 valid (i.e., non-excluded) time windows for the 2 Hz wavelet convolution. We estimated spectral power by averaging power values of successive 3/4-overlapping temporal windows of continuous clean data in time-frequency representations. This gave a single estimation of spectral power at each of either 83 (HD EEG) or 19 (10-20 system) channels and 54 frequency bins.

Frequency output was smoothed in half-octave bins. Power at each frequency bin was then normalized per $\log_2$(Hz) (i.e., octave) to yield power spectral densities (PSDs). We computed PSDs using $\log_2$(Hz) and plotted PSDs in a logarithmic space to account for the

logarithmic nature of electrophysiological signals (Buzsáki and Draguhn 2004). Our analysis used absolute power because relative power measurements are vulnerable to normalization artifacts. For example, large theta oscillations present in several of our participants artifactually reduce beta band power when relative power is computed. In instances where channel-averaged power was reported, we first averaged across channels before log-scaling PSDs and then averaging across participants.

For generating figures and to precisely report peak frequencies, we used a spline-interpolation to derive a higher frequency resolution (100 frequency bins per octave). Peak frequencies are reported as the local maximum in the beta band (14 – 30 Hz, lower frequencies are excluded to avoid spectral leakage from the alpha band). In instances of multiple beta peaks, only the largest peak is captured by the local maximum. Topographic scalp plots were generated using EEGLAB (Delorme and Makeig 2004) for HD EEG and Fieldtrip (Oostenveld et al. 2011) for 19-channel EEG. Power differences were tested with t-tests using the Satterthwaite approximation to derive corrected degrees of freedom. To compare PSDs from paternal Dup15q syndrome cases to our reference cohort, we used simple linear regression to account for age differences. We modeled PSDs for all participants in the reference cohort using $\log_2$(age), where the log transform accounts for larger developmental gains at younger ages. We then reconstructed PSDs for each reference cohort participant using the $\log_2$(age) of the paternal Dup15q syndrome participant and adding back model residuals for each participant.

**4.3 Results**

### 4.3.1 Dup15q syndrome reference cohort

We first compared PSDs, averaged across channels and participants, from the TD cohort and Dup15q syndrome reference cohort. Both groups displayed spectral peaks in different bands (Fig. 2A). The Dup15q syndrome reference cohort displayed a prominent group-level peak in the beta band (peak frequency: f = 23.1 Hz) and the TD cohort displayed a prominent group-level peak in the alpha band (peak frequency: f = 8.94 Hz). Dup15q syndrome peak beta power did not differ between sites (one-way ANOVA, F(2,25) = 0.19, p = 0.83, spline-interpolated peak frequency). To verify the presence of higher beta power in Dup15q syndrome, we performed a one-tailed test of beta power at the Dup15q syndrome spline-interpolated peak frequency. Beta power at this frequency was higher in Dup15q syndrome ($p = 2.4 \times 10^{-4}$; t = 3.83), well in line with a previous quantification of the Dup15q syndrome beta EEG phenotype (Frohlich et al. 2016). Next, in light of clinical reports of reduced alpha power in Dup15q syndrome (Battaglia 2008; Bruining et al. 2015), we performed a one-tailed test of alpha power at the TD cohort spline-interpolated peak frequency. Alpha power at this frequency was higher in the TD cohort ($p = 6.8 \times 10^{-3}$; t = -2.60, a new finding not previously observed within the limits of our previous study's statistical power (Frohlich et al. 2016). The Dup15q syndrome reference cohort scalp topography (Fig. 2B) features enhanced power at the spline-interpolated peak frequency (f = 23.1 Hz) compared to the TD cohort (Fig. 2C) at all channels (effect size: d' = 0.860 ± 0.303, mean ± SD across channels). The largest effect sizes (d > 1) were located in frontocentral scalp regions (Fig. 2D).

To test for a gene dosage effect within Dup15q syndrome, we next visualized PSDs separately for participants with interstitial and isodicentric duplications (Fig. 3A). Using a one-

tailed test of greater power in isodicentric duplications, we found no significant difference in beta power between duplication types at the Dup15q syndrome reference cohort spline-interpolated peak frequency ($f = 23.1$ Hz, $p = 0.14$, $t = 1.12$). To further investigate the spectral relationship between duplication types, we performed two-tailed tests at each of 54 frequency bins. We detected no significant differences in power, even before correcting for multiple comparisons across frequency bins ($p > 0.05$, all frequency bins). We did, however, observe considerably larger variance in interstitial Dup15q syndrome at most frequency bins. Both duplication types featured prominent group-level oscillatory peaks in the beta band (interstitial peak frequency $f = 22.9$ Hz; isodicentric peak frequency $f = 23.3$ Hz). We also observed similar patterns of scalp topography for both duplication types at 23.1 Hz (Fig. 3B,C). Although we were unable to detect significant differences in power, we did note small but positive effect sizes in every channel (Fig 3D) when we subtracted mean interstitial power from mean isodicentric power at $f = 23.1$ Hz.

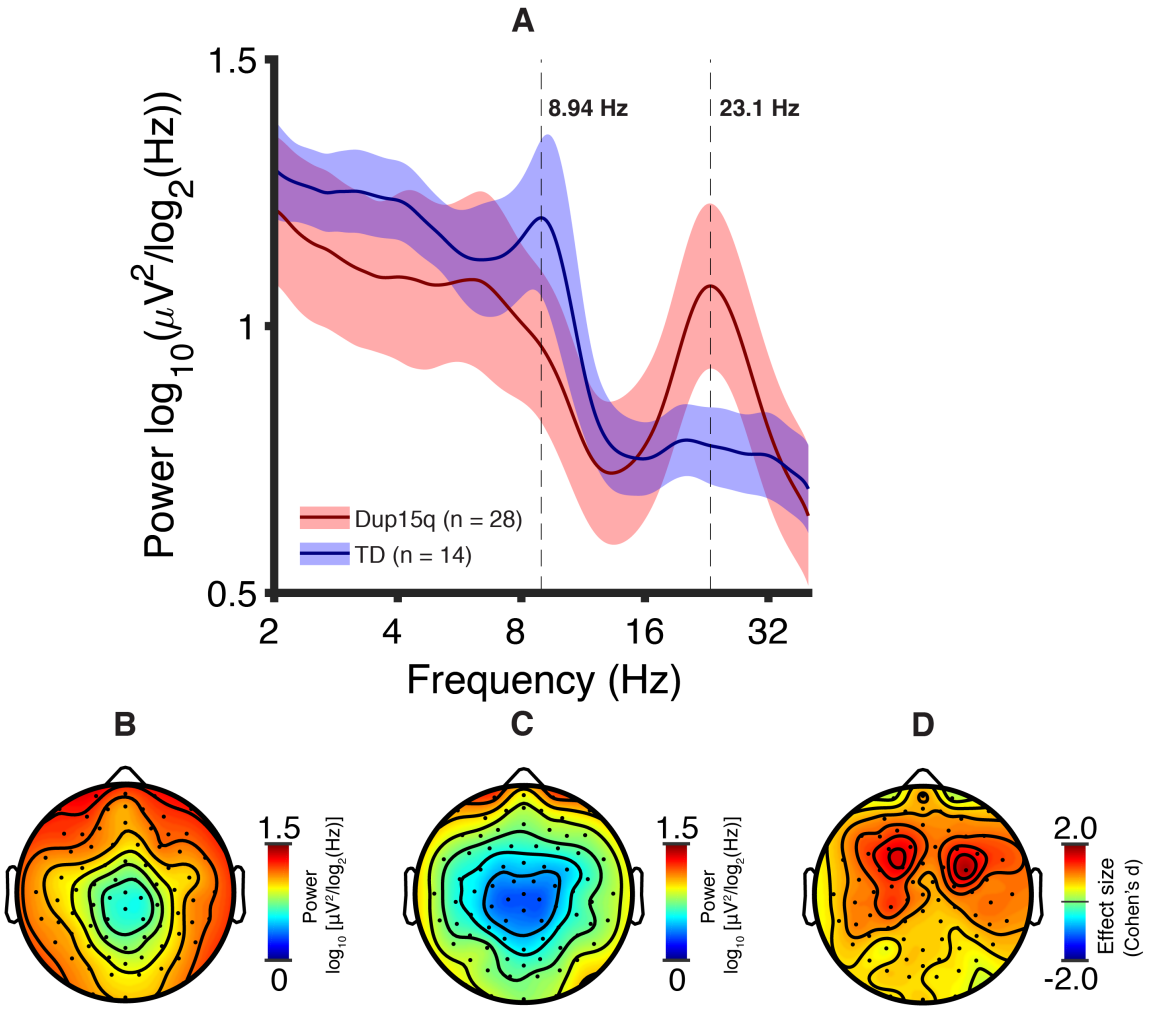


***Figure 4.2 Dup15q syndrome versus TD***. *(A) Spectral profiles of children with Dup15q syndrome (red) and TD children (blue). PSDs are averaged across channels and participants; colored highlights represent 95% confidence interval of the mean. Power is significantly higher in Dup15q syndrome at the Dup15q syndrome beta peak frequency, f = 23.1 Hz ($p = 2.4 \times 10^{-4}$; t = 3.83). Power is significantly higher in the TD cohort at the TD cohort alpha peak frequency, f = 8.94 Hz ($p = 6.8 \times 10^{-3}$; t = -2.60). (B) Dup15q syndrome topographic scalp power (mean across participants at f = 23.1 Hz). (C) TD topographic scalp power (mean across participants at f = 23.1 Hz). (D) Dup15q syndrome versus TD power difference effect sizes (Cohen's d) at f = 23.1 Hz. Mean effect size across channels, d = 0.86 (min, d = 0.30; max, d = 1.8).*

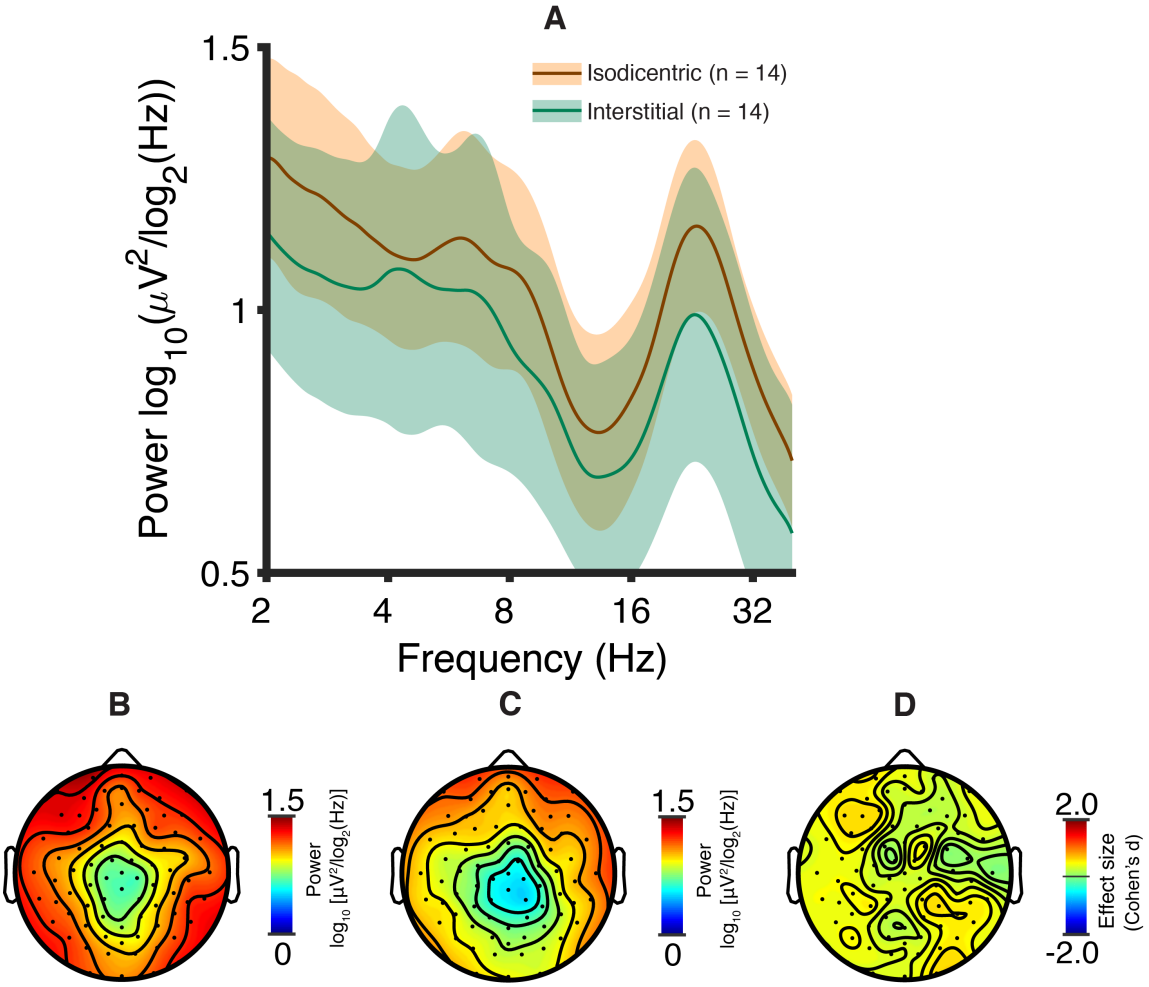


***Figure 4.3 Dup15q syndrome by duplication type***. *(A) Spectral profiles of isodicentric (orange) and interstitial (green) duplication. PSDs are averaged across channels and participants; colored highlights represent 95% confidence interval of the mean. Both duplication types show prominent spectral peaks in the beta band (group-level averages: isodicentric, f = 23.3 Hz; interstitial, f = 22.9 Hz). Power does not differ between duplication types (p > 0.05, all frequencies). (B) Mean topographic scalp power of reference cohort participants with isodicentric duplications at f = 23.1 Hz (i.e., the Dup15q syndrome spline-interpolated peak frequency). (C) Mean topographic scalp power of all reference cohort participants with interstitial duplications at f = 23.1 Hz. (D) Isodicentric versus interstitial power*

*difference effect sizes (Cohen's d) at f = 23.1 Hz. Mean effect size across channel, d = 0.37 (min, d = 0.0039; max, d = 0.60).*

### 4.3.2 The Dup15q syndrome beta EEG phenotype resembles the effects of midazolam in healthy adults

Next, we compared EEG from the reference cohort with healthy adults challenged with the $GABA_A$ PAM midazolam (5 mg oral administration). Participants showed spectral peaks in the alpha band and beta band both before and after midazolam administration (Fig. 4.4A). The midazolam condition showed the highest beta power in central scalp regions at the Dup15q syndrome peak frequency (f = 23.1 Hz, Fig. 4.4B), whereas the baseline condition showed higher beta power in peripheral scalp regions at the same frequency (Fig. 4.4C). Most channels displayed positive changes in beta power, with the largest change occurring at channel Cz (76% increase, Fig. 4.5A). The average power change across all channels was greatest at peaked at 16.1 Hz and plateaued until approximately the Dup15q syndrome peak frequency (23.1 Hz, Fig. 4.5B). We then performed paired samples t-tests across all channels at the Dup15q syndrome peak frequency. Three channels, Fz, Cz, and Pz, displayed a significant increase in power after correcting for multiple comparisons using the false discovery rate (FDR, $p < 0.05$ corrected, Fig. 4.5C). Effect sizes of $d' > 1$ were also observed at channels that survived the FDR correction (Fig. 4.4D). The average power change for these channels displayed a peak frequency at 23.0 Hz (30% increase, Fig. 4.5D), very close to the Dup15q syndrome peak frequency (f = 23. 1 Hz). While examining the channels that yielded the largest power change at 23.1 Hz biases our results towards a larger power change at this frequency, it does not bias our results towards a

peak power change at this frequency. Thus, our finding of very similar peak frequencies for Dup15q syndrome and midazolam drug challenge is interesting and unexpected, suggesting an isomorphism between the Dup15q syndrome beta EEG phenotype and midazolam pharmaco-EEG.

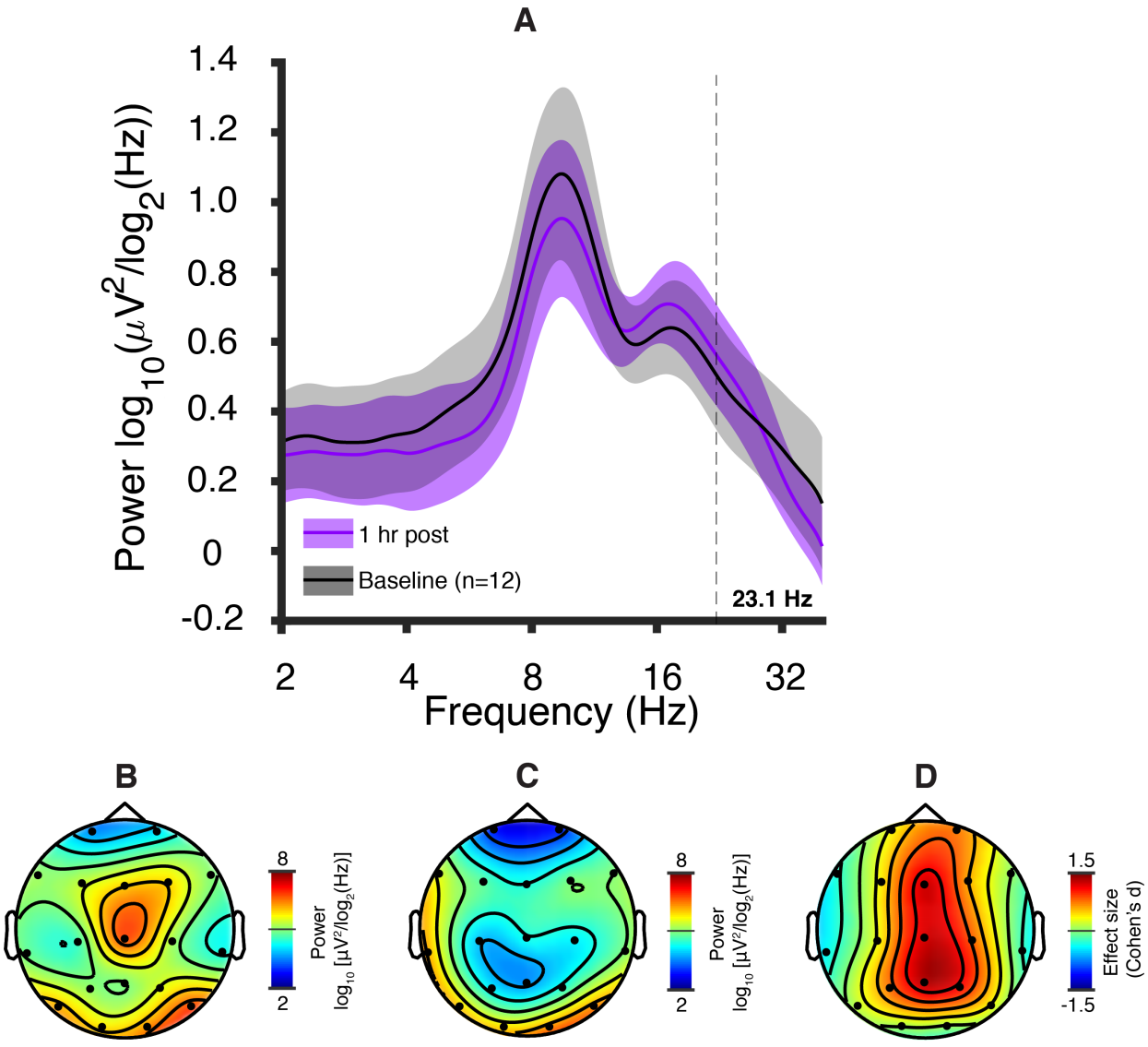


***Figure 4.4 Midazolam pharmaco-EEG at baseline and 1 hour post administration (5 mg oral).*** *(A) PSDs averaged across participants for the baseline (black) and 1 hour post administration (purple) conditions. Colored highlights represent 95% confidence intervals of the mean. Both conditions show spectral peaks*

*in the alpha and beta bands; the alpha peak appears diminished and the beta peak appears enhanced by midazolam challenge. (B) Topographic scalp power 1 hour post administration at the Dup15q syndrome peak frequency (23.1 Hz). (C) Topographic scalp power from the baseline condition at the Dup15q syndrome peak frequency (23.1 Hz). (D) Effect sizes (Cohen's d) of midazolam induced power change at 23.1 Hz. The largest power changes occur at central channels Fz, Cz, and Pz (Cf. Fig 4.5C).*

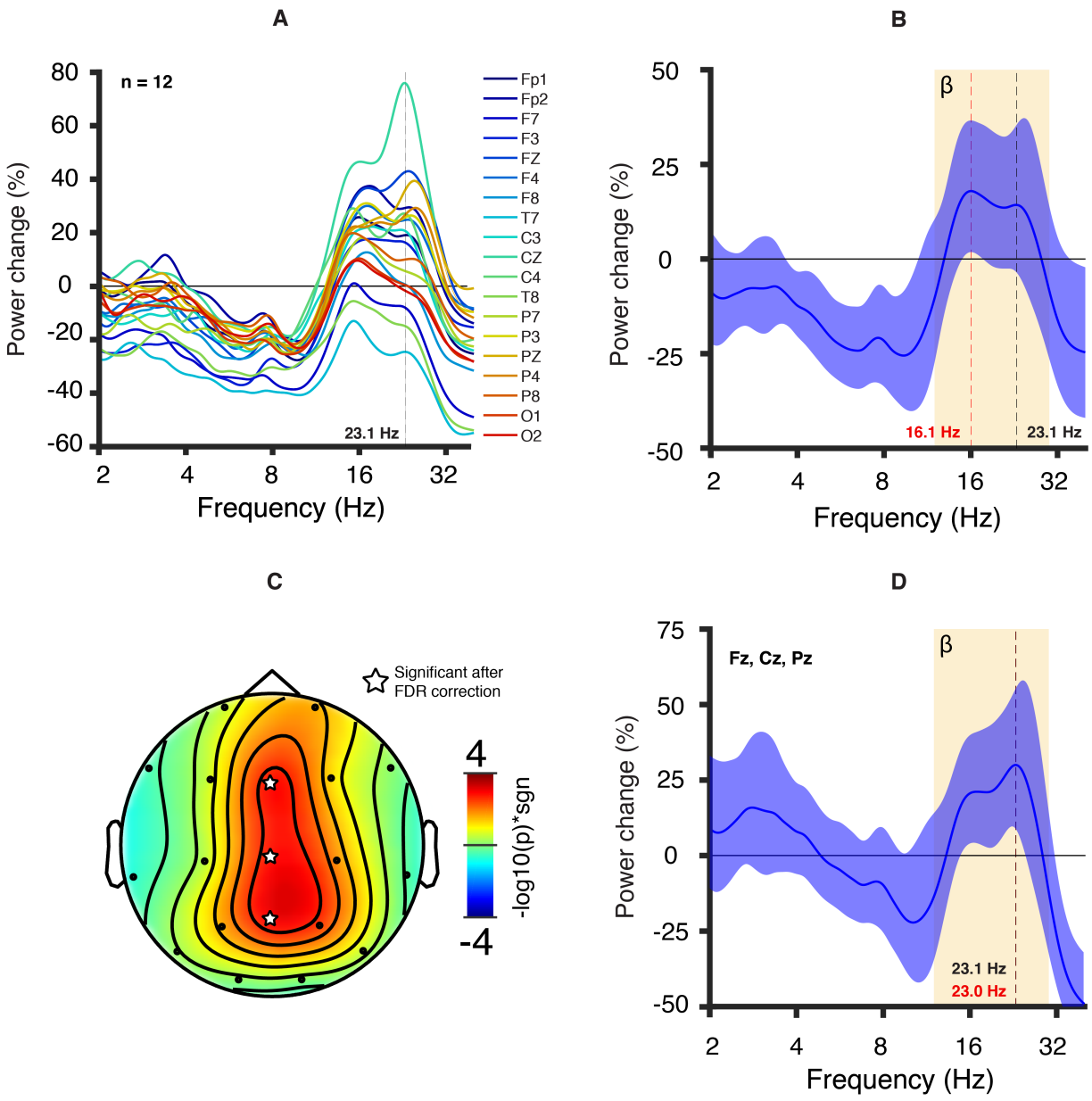


***Figure 4.5 Pharmaco-EEG from healthy adult participants challenged with midazolam.*** *Healthy adult volunteers (n=12) were challenged orally with 5 mg midazolam. (A) Average power change in all channels 1 hour following drug administration referenced to baseline (absolute power averaged across participants). Most channels displayed an increase in power in the beta band, with some channels displaying peaks in both low beta ("beta1", 12-20 Hz) and high beta ("beta2", 20-30 Hz). (B) Channel-averaged power change. The colored highlight represents the 95% confidence interval of the*

*mean. The average power change appears to largely plateau between the peak power change (16.1 Hz, red vertical line) and the Dup15q syndrome peak frequency (23.1 Hz, black vertical line). (C) Scalp topography of the -log$_{10}$(p-value) multiplied by the sign of the t-statistic from a two-tailed t-test at 23.1 Hz. Three central channels (Fz, Cz, and Pz, indicated with a star symbol) survive an FDR correction for multiple channels (p-value threshold = 3 x 10$^{-3}$). (D) Power change averaged across central channels. We visualized the average power change for those channels that survived the FDR correction at 23.1 Hz. The colored highlight represents the 95% confidence interval of the mean. The power change peaks at 23.0 Hz (red vertical line), very close to the Dup15q syndrome peak frequency (23.1 Hz, black vertical line; Cf. Fig. 4.2A).*

### 4.3.3 The beta EEG phenotype is observed in paternal Dup15q syndrome

Results from each participant with paternal Dup15q syndrome are described below separately. In both cases, we find that the quantitative beta EEG phenotype is observable in paternal Dup15q syndrome.

#### 4.3.3.a Paternal Dup15q participant 801-005

Data from this participant was acquired using HD EEG and was thus spatial interpolated for correspondence with the 10-20 montage. We observed highly prominent peaks in the beta band for PSDs derived from all 19 channels (Fig. 4.6A, peak frequency: f = 19.8 ± 1.90 Hz, mean ± SD). We then examined the channel averaged PSD in the context of the Dup15q reference cohort. Because of the broad age range of the reference cohort, we used a simple linear regression model to account for age differences (see Methods). Paternal duplication beta power was elevated above the Dup15q reference cohort 95% confidence interval of the mean for all beta frequencies (Fig. 4.6B). The channel-averaged paternal duplication PSD showed a

beta peak at f = 20.4 Hz, while the reference cohort displayed a group-level beta peak at f = 23.3 Hz. Similar results are yielded using only reference cohort participants with interstitial duplications (Fig. 4.7A). Beta power (reference cohort peak frequency) for this paternal duplication participant lies near the upper end of the reference cohort distribution (Fig. 4.6C, f = 23.3 Hz).

After examining PSDs, we examined the topographic power distribution at the reference cohort peak frequency (reconstructed power). The scalp topography derived from 801-005 exhibited higher power at all channels (Fig. 4.8A) as compared with the reference cohort mean scalp topography (Fig. 4.8B). Scalp topography derived from only interstitial duplications in the reference cohort (Fig. 4.8C) appeared similar to that of the overall reference cohort. All three scalp distributions featured the highest power at frontal electrodes, also in line with previous findings by Frohlich and colleagues (Frohlich et al. 2016).

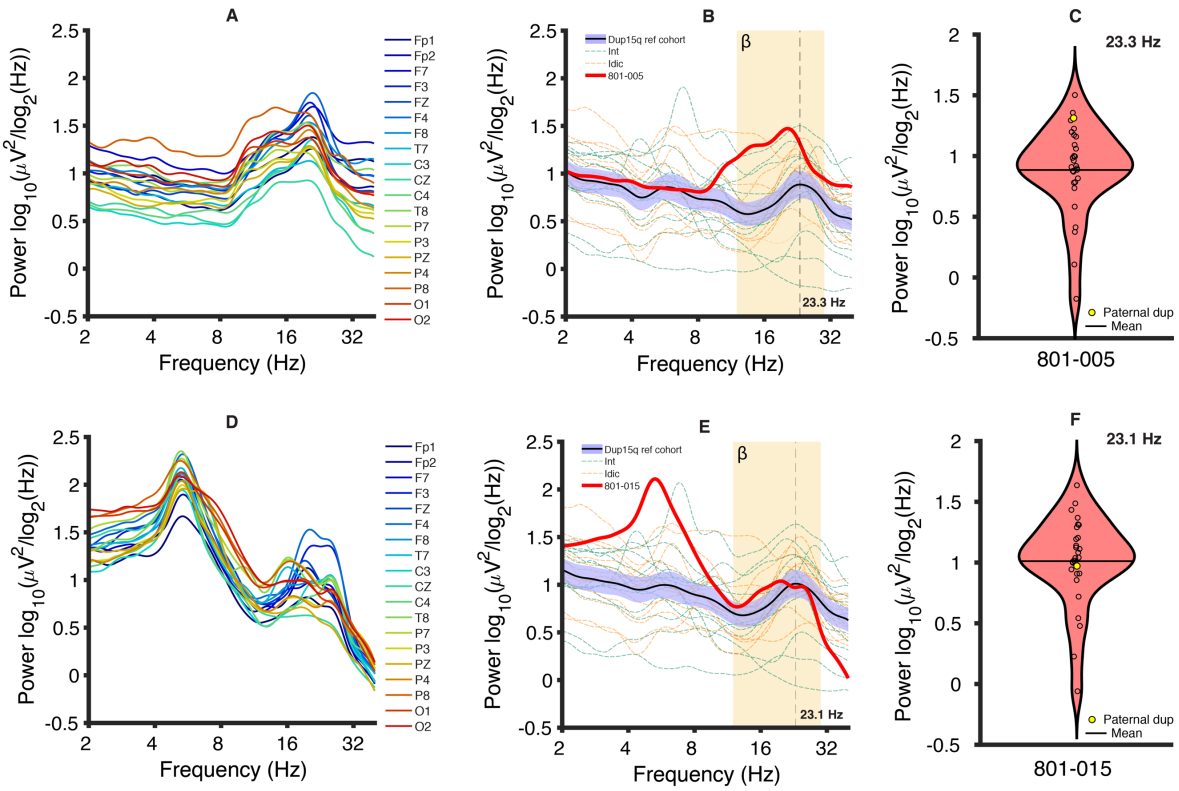


***Figure 4.6 Paternal Dup15q syndrome PSDs.*** *(A) PSDs derived from all 19 channels (spatially interpolated from HD EEG) show prominent beta peaks in a 13-year-old boy with a paternal duplication (ID: 801-005). (B) Reference cohort PSDs were reconstructed using a simple linear regression model, plugging in the log age of 801-005 (161 months). Channel-averaged PSD derived from 801-005 shows higher beta power at all frequency bins than the Dup15q reference cohort 95% confidence interval of the mean. The channel-averaged peak beta frequency is lower in 801-005 (f = 20.4 Hz) as compared with the reference cohort (f = 23.3 Hz). (C) Violin plot of power at the reference cohort peak frequency (f = 23.3 Hz, reconstructed power), with 801-005 indicated in yellow near the top of the distribution. (D) PSDs derived from all 19 channels (clinical EEG) show prominent beta peaks in an 8-year-old girl with a paternal duplication (ID: 801-015). (E) Reference cohort PSDs were reconstructed using a simple linear regression model, plugging in the log age of 801-015 (96 months). Channel-averaged PSD derived from 801-015 shows beta power largely in the range of the Dup15q reference cohort 95% confidence interval*

*of the mean. The channel-averaged peak beta frequency is lower in 801-015 (f = 19.7 Hz) as compared with the reference cohort (f = 23.1 Hz). (F) Violin plot of power at the reference cohort peak frequency (f = 23.1 Hz, reconstructed power), with 801-015 indicated in yellow near the mean of the distribution.*

#### 4.3.3.b Paternal Dup15q participant 801-015

Data from this participant was acquired using 19-channel clinical EEG (10-20 montage). We observed broadly elevated power across the beta band in PSDs derived from all of 19 channels. Individual channels showed considerable variability in beta peak frequency (Fig. 4.6D, peak frequency: f = 19.3 ± 2.95 Hz, mean ± SD) and even peaks at multiple frequencies within the beta band (here we have reported the frequencies of the largest peaks). These factors cause smearing in the channel-averaged PSD, giving it a less prominent peak in the beta band than 801-005. Thus, the spectral profile of this paternal Dup15q syndrome case appears different than that of 801-015 while still exhibiting the beta EEG phenotype. The highest beta power was observed in channels F3 and F4. We also observed highly prominent theta peaks for all channels in the 4 – 8 Hz frequency range (peak frequency: f = 5.29 Hz ± 0.05 Hz, mean ± SD).

As with 801-005, we compared beta power from 801-015 with our Dup15q syndrome reference cohort using reconstructed power. Paternal duplication beta power was higher than the Dup15q reference cohort 95% confidence interval of the mean from 13.8 – 19.5 Hz and lower than the same confidence interval at frequencies above 27.9 Hz (Fig. 4.6E). The paternal duplication PSD showed a beta peak at f = 19.7 Hz, similar to the peak frequency observed for 801-005 (f = 20.4 Hz), while the reference cohort displayed a group-level beta peak at f = 23.1 Hz. Reference cohort participants with interstitial duplications also showed a group level peak

frequency at 23.1 Hz (Fig. 4.7B). Beta power (reference cohort peak frequency) for this paternal duplication participant lies slightly below the mean of the reference cohort distribution (Fig. 4.6F, f = 23.1 Hz).

The scalp topography (power at the Dup15 reference cohort peak frequency) derived from 801-015 exhibited higher power at several channels (F3, Fz, F4, T7, Fp1, Fz, Fp2, P7; see Fig. 4.8D) as compared with the reference cohort mean scalp topography (Fig. 4.8E). Scalp topography was similar between the overall Dup15q syndrome reference cohort and participants with interstitial duplications (Fig. 4.8F). 801-015 exhibited a bifrontal maximum in scalp power at the reference cohort peak frequency; this is similar to the scalp topography seen in 801-005.

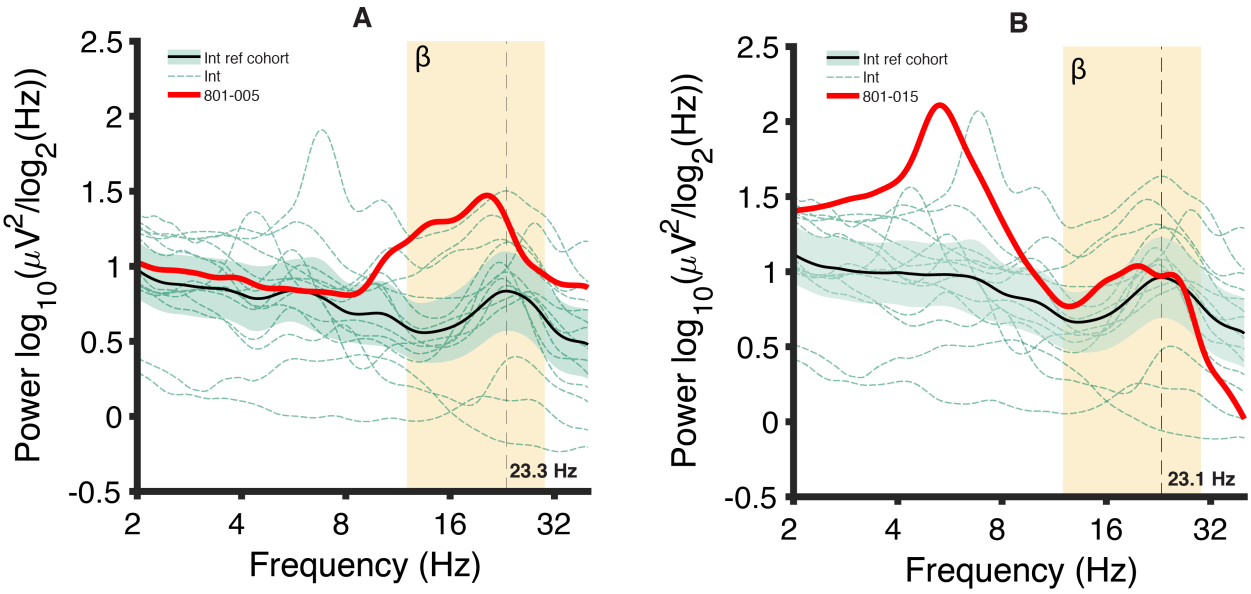


***Figure 4.7 Paternal Dup15q syndrome PSDs compared with the interstitial Dup15q syndrome reference cohort.*** *(A) Channel-averaged PSD derived from 801-005 compared with the interstitial reference cohort. 801-005 shows higher power at most beta frequencies than the interstitial reference cohort 95% confidence interval of the mean. (B) Channel-averaged PSD derived from 801-015 compared with the*

*interstitial reference cohort. 801-015 shows beta power almost entirely in the range of the interstitial reference cohort 95% confidence interval of the mean.*

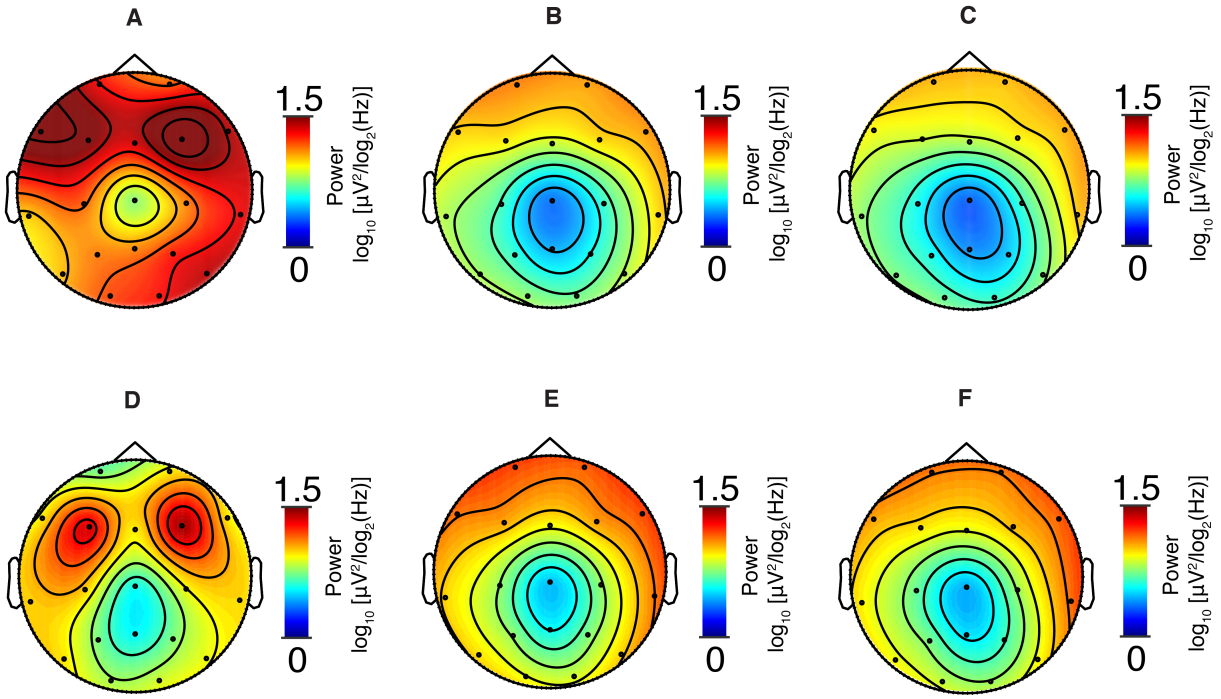


***Figure 4.8 Paternal Dup15q syndrome scalp topography.*** *(A) 801-005 beta power scalp topography measured at f = 23.3 Hz (reference cohort reconstructed power peak frequency). (B) Dup15q syndrome reference cohort beta power scalp topography measured at the group level peak frequency f = 23.3 Hz (reconstructed power from 801-005 regression model). (C) Interstitial reference cohort beta power scalp topography measured at the group level peak frequency f = 23.3 Hz (reconstructed power from 801-005 regression model). (D) 801-015 beta power scalp topography measured at 23.1 Hz (reference cohort reconstructed power peak frequency). (E) Dup15q syndrome reference cohort beta power scalp*

*topography measured at the group level peak frequency f= 23.1 Hz (reconstructed power from 801-015 regression model). (C) Interstitial reference cohort beta power scalp topography measured at the group level peak frequency f= 23.1 Hz (reconstructed power from 801-015 regression model).*

## 4.4 Discussion

In this study, we investigated the possibility that GABAergic modulation simulates the Dup15q syndrome beta EEG phenotype in healthy adults. We also inferred that *UBE3A* dysregulation is not necessary for producing the same phenotype in Dup15q syndrome. By identifying a likely GABAergic mechanism underlying this phenotype, our work facilitates the application of this biomarker to clinical trials for Dup15q syndrome as a surrogate endpoint or marker of disease pathology or target engagement. Furthermore, our work informs future studies that may attempt to rescue the beta EEG phenotype in animal models of Dup15q syndrome.

### 4.4.1 $GABA_A$ receptor modulation simulates the beta EEG phenotype in healthy adults

Clinical and scientific observations dating back several years (Frohlich et al. 2016; Urraca et al. 2013) have noted that the Dup15q syndrome beta EEG phenotype has the same appearance as beta activity pharmacologically induced by benzodiazepines and other $GABA_A$ PAMs. Our study is the first to compare the spectral profile of healthy adults challenged with a benzodiazepine compound, midazolam, to the spectral profile of Dup15q syndrome. These spectral profiles both include large increases in beta band power. Notably, several channels in the midazolam study show nearly the same peak power change (f = 23.0 Hz) as the Dup15q syndrome peak frequency (23.1 Hz). Midazolam likely simulates the Dup15q syndrome beta

EEG phenotype in healthy adult by modeling effects of $GABA_A$ β3/α5/γ3 subunit dysregulation. However, a lack of significant findings from Dup15q syndrome postmortem brain tissue studies (Parikshak et al. 2016; Scoles et al. 2011) precludes us from stating that these subunits are actually overexpressed in Dup15q syndrome. Although the topographic power distributions for Dup15q syndrome (Fig. 4.2B) and midazolam drug challenge (Fig. 4.4B) appear quite different, this is likely due to the fact that midazolam is a nonselective $GABA_A$ PAM, whereas the β3/α5/γ3 subunits may possess anatomically distinct expression profiles (McGinnity et al. 2017). Furthermore, the small proportion of channels (3 out of 19) the survived an FDR correction may be explained by both our small sample (n = 12) and the fact that midazolam was administered at a sub-sedative dose (5 mg). Nonetheless, our proof of principle model demonstrates that GABAergic dysfunction *per se* is sufficient to produce the beta EEG phenotype.

Based on the midazolam model, we concluded that the beta EEG phenotype likely reflects GABAergic dysfunction in Dup15q syndrome. However, this interpretation must be reconciled with our finding that beta power does not differ between duplication types. Unexpectedly, we found no differences in beta power between interstitial and isodicentric EEG (with the latter group generally showing higher copy number than the former). Our negative finding may imply an asymptotic relationship between gene dosage and the beta EEG phenotype.

### 4.4.2 *UBE3A* dysregulation is not necessary for the Dup15q syndrome EEG phenotype

Our data from two cases of paternal Dup15q syndrome demonstrate that the beta EEG phenotype is observable even in duplications of the paternal allele from which *UBE3A* is

silenced in neurons. This suggests that *UBE3A* dysregulation is not necessary for the beta EEG phenotype. Both paternal Dup15q syndrome cases were of different ages studied with different EEG systems, thus suggesting that beta oscillations in paternal Dup15q syndrome are not specific to one particular developmental age group, nor an artifact of a particular EEG system.

Our finding delineates a smaller role for *UBE3A* in influencing the overall Dup15q syndrome phenotype than previously assumed. Given its causative role in Angelman syndrome (Buiting et al. 2016; Kishino et al. 1997) and its connection to nonsyndromic ASD (Guffanti et al. 2011; Nurmi et al. 2001), *UBE3A* likely underlies many features of Dup15q syndrome pathology. Our finding that *UBE3A* is not necessary for the beta EEG phenotype in Dup15q syndrome thus brings us towards a new and broader understanding of Dup15q syndrome pathophysiology. Combining our findings from paternal Dup15q syndrome with those from our investigation of midazolam in healthy adults, we conclude that the $GABA_A$ β3-α5-γ3 subunit gene cluster plays an important role in Dup15q syndrome cortical dynamics; these abnormal dynamics may in turn underlie features of the Dup15q syndrome clinical phenotype, including intellectual disability and epilepsy. Accordingly, the beta EEG phenotype may be conceptualized as an intermediate phenotype bridging gene expression and behavior. As such, it may be used as a biomarker in clinical trials for Dup15q syndrome that target $GABA_A$ receptors.

### 4.4.3 Towards quantitative biomarkers of neurodevelopmental disorders for drug development and clinical trials

Advances in genetic sequencing and testing have yielded an increasing proportion of ASD cases (3-20%) with a readily identifiable genetic cause (Gaugler et al. 2014; Schaefer and Mendelsohn 2013; Tammimies et al. 2015). Duplications of 15q are the most common copy

number variation identified in ASD, accounting for 1-3% of cases (Cook Jr et al. 1997; Moreno-De-Luca et al. 2013). Given that our study provides additional evidence that altered GABAergic signaling is as a likely mechanism of the beta EEG phenotype in Dup15q syndrome, this phenotype may be used as a quantitative biomarker that reflects GABAergic dysfunction in Dup15q syndrome. For instance, the biomarker may be used to index disease pathology, drug target engagement, and treatment response in clinical trials for Dup15q syndrome. Many clinical features of Dup15q syndrome are associated with altered excitatory/inhibitory balance, including intellectual disability (Souchet et al. 2014, 2015), ASD (E. Lee et al. 2017; Rubenstein and Merzenich 2003), and seizures (Fritschy 2008; Stief et al. 2007). This motivates a clear readout of GABAergic tone in Dup15q syndrome. Towards this end, the molecular efficacy of drug treatments designed to correct excitatory/inhibitory balance in Dup15q syndrome could be assessed using the beta biomarker. Circuit changes that proceed behavioral changes could also be measured using the beta biomarker, thus allowing investigators to evaluate the success of short trials that preclude observation of long-term behavioral changes. To further assess the utility of this biomarker as a surrogate endpoint, future work will explore the relationship between the beta EEG phenotype and clinical phenotypes in Dup15q syndrome.

In fact, the beta EEG phenotype may also be used as a biomarker in indications beyond Dup15q syndrome. Nonsyndromic ASD etiology is attributed to the sum of many mutations, each with mild penetrance. Because the β3/α5/γ3 gene cluster encompassed by duplications of 15q is also associated with nonsyndromic ASD (Buxbaum et al. 2002; Cook Jr et al. 1997; McCauley et al. 2004; Menold et al. 2001), it is plausible that many such cases of “idiopathic” ASD include contributing variants in these $GABA_A$ receptor genes. Thus, markers of GABAergic

pathology in Dup15q syndrome could also have wider applicability to cases of nonsyndromic ASD rooted partially in GABAergic dysfunction. We expect ASD patients with point mutations in $GABA_A$ receptor genes (e.g., as identified by whole exome sequencing) to exhibit a mild beta EEG phenotype which may be quantified and refined as a translational biomarker. Future work should test this prediction in a large nonsyndromic ASD cohort genotyped with whole exome sequencing.

**4.5 Limitations and future directions**

Our comparison of the Dup15q syndrome beta EEG phenotype to pharmaco-EEG from healthy adults challenged with midazolam is limited by several factors. 1) The healthy adult participants do not overlap in age with the Dup15q syndrome reference cohort, which is comprised entirely of children. 2) EEG data were acquired using different systems. These incongruencies between cohorts preclude a direct statistical comparison. 3) Furthermore, our conclusions are not formal inferences and do not prove that the mechanism underlying the Dup15q syndrome beta EEG phenotype is GABAergic. 4) Finally, postmortem brain studies, limited by small samples, have yet to demonstrate a significant overexpression of the β3/α5/γ3 gene cluster in Dup15q syndrome (Parikshak et al. 2016; Scoles et al. 2011).

Nonetheless, our data support the hypothesis that dysfunction of the β3/α5/γ3 gene cluster drives this phenotype in Dup15q syndrome. While we have demonstrated a likely GABAergic mechanism for the beta EEG phenotype, the relationship between this EEG phenotype and clinical traits remains unknown. A forthcoming study by our group will explore relationships between clinical phenotypes and EEG phenotypes in Dup15q syndrome, thus evaluating whether the beta EEG phenotypes is a useful surrogate endpoint in clinical trials.

We also acknowledge two limitations in the comparison of two paternal Dup15q syndrome cases to the Dup15q syndrome reference cohort. 1) We observed a somewhat more persuasive spectral profile in one case (801-005) than the other (801-015). We acknowledge that PSDs derived from both children appeared different, yet both nonetheless demonstrated the Dup15q syndrome beta EEG phenotype. Furthermore, the channel-averaged PSD derived from 801-015 features a smudged beta peak owing to high across channel variance in peak frequency. 2) Although *UBE3A* is paternally silenced in neurons, it is expressed biallelically in astrocytes (Judson et al. 2014). This consideration may challenge the validity of paternal Dup15q syndrome as a *UBE3A*-normal control group. Nonetheless, the milder clinical phenotype of paternal Dup15q syndrome strongly suggests minimal *UBE3A*-related pathology in paternal duplications.

While this study has demonstrated that *UBE3A* dysregulation is not necessary for the beta EEG phenotype, yet it may be sufficient in this regard. A forthcoming study by our group will test this possibility using EEG recordings from individuals with Prader Willi Syndrome (PWS), another 15q disorder. PWS is characterized by delayed development, hyperphagia, and obesity, and often caused by maternal uniparental disomy (UPD) of chromosome 15 (Cassidy and Driscoll 2009), which should cause overexpression of *UBE3A* in neurons. Because maternal UPD cases of PWS are expected to show elevated *UBE3A* expression without $GABA_A$ receptor gene duplication, this population is an ideal control group for evaluating the sufficiency of *UBE3A* for producing the beta EEG phenotype.

Finally, future studies in patient derived iPSC cultures or Dup15q syndrome animal models should individually knockdown *GABRB3*, *GABRA5*, and *GABRG3*. Abolishing a Dup15q-

like electrophysiological phenotype in these models through gene knockdown would demonstrate that one or more of these genes are necessary for the phenotype. Finally, we advocate for future studies exploring an expectedly milder beta EEG phenotype in cases of nonsyndromic ASD. Such a phenotype may also serve as a biomarker in drug development and clinical trials for ASD.

**4.6 Conclusions**

Quantitative biomarkers, rooted in mechanism and thus positioned to guide clinical trials, are greatly needed in neurodevelopmental disorders such as ASD. Here, we gained valuable insights into the mechanism of an EEG biomarker of Dup15q syndrome. This biomarker cannot be easily explained by elevated UBE3A levels *per se* but can be simulated by GABAergic modulation in healthy adults, suggesting that the phenotype is a readout of increased $GABA_A$ activity or sensitivity to GABA in Dup15q syndrome. Our work is an important step towards rooting the Dup15q syndrome biomarker in a molecular mechanism and facilitating its application in clinical trials.

# Chapter 5: Electrophysiological Phenotype in Angelman Syndrome Differs Between Genotypes

## 5.1 Introduction

Angelman syndrome (AS) is a rare genetic neurodevelopmental disorder with a prevalence of 1 in 10,000 – 24,000 births . Clinical traits of AS include global developmental delay, intellectual disability, epilepsy, sleep difficulties, and some phenotypic overlap with autism (Bird 2014; Thibert et al. 2013; Trillingsgaard and Østergaard 2004; Williams 1995). Furthermore, AS shows a strongly abnormal EEG (Boyd et al. 1988; Laan and Vein 2005; Sidorov et al. 2017; Williams 2005). AS is due to the loss of a functional maternal copy of the gene *UBE3A* on chromosome 15 (Buiting et al. 2016; Chamberlain and Lalande 2010; Kishino et al. 1997). This gene encodes a ubiquitin-protein ligase (Dindot et al. 2007; Greer et al. 2010; Smith et al. 2011) and is generally expressed only from the maternal allele in neurons but not in other cell types (Albrecht et al. 1997; Chamberlain and Lalande 2010; Yamasaki et al. 2003), though local instances of biallelic neuronal expression have been observed (Jones et al. 2016).

The downstream pathophysiological consequences of *UBE3A* dysfunction are poorly understood, but there is evidence that UBE3A is crucial to synaptic function and specifically impacts GABA signaling (DeLorey et al. 1998; Egawa et al. 2012; Judson et al. 2016). The GABA system, the main source of inhibitory signaling in the brain (Roberts 2007), is critically involved in shaping neuronal dynamics, including oscillatory processes that can be measured with EEG (Steriade and Timofeev 2003; X.-J. Wang 2010; Womelsdorf et al. 2014). Accordingly, the strongly abnormal EEG observed in AS, characterized by excess high amplitude, low frequency

activity (Boyd et al. 1988; Laan and Vein 2005; Sidorov et al. 2017; Williams 2005), may provide a systems level window into *UBE3A*-related AS pathophysiology.

The etiology of AS can be divided into two broad groups (Fig. 5.1). The first group, non-deletion AS, mainly affects the function of *UBE3A*, which is the only 15q11-q13 gene with a consistent pattern of paternal imprinting in most neurons (Buiting et al. 2016; DuBose et al. 2010; Hogart et al. 2008). Non-deletion AS includes *UBE3A* mutations, paternal uniparental disomy (UPD) and imprinting defects, and comprises 25-30% of all AS cases (Buiting et al. 2016; Clayton-Smith and Laan 2003). The second group, deletion AS, is defined by deletions of chromosome 15q11-q13. This encompasses *UBE3A* as well as about 11 – 15 other protein-coding genes, numerous small nucleolar RNA (snoRNA) genes, and non-coding regions of potential functional significance. Deletion AS accounts for the majority (about 70%) of AS cases (Buiting et al. 2016). Herein, we use "genotype" to refer to the two etiological groups defined above.

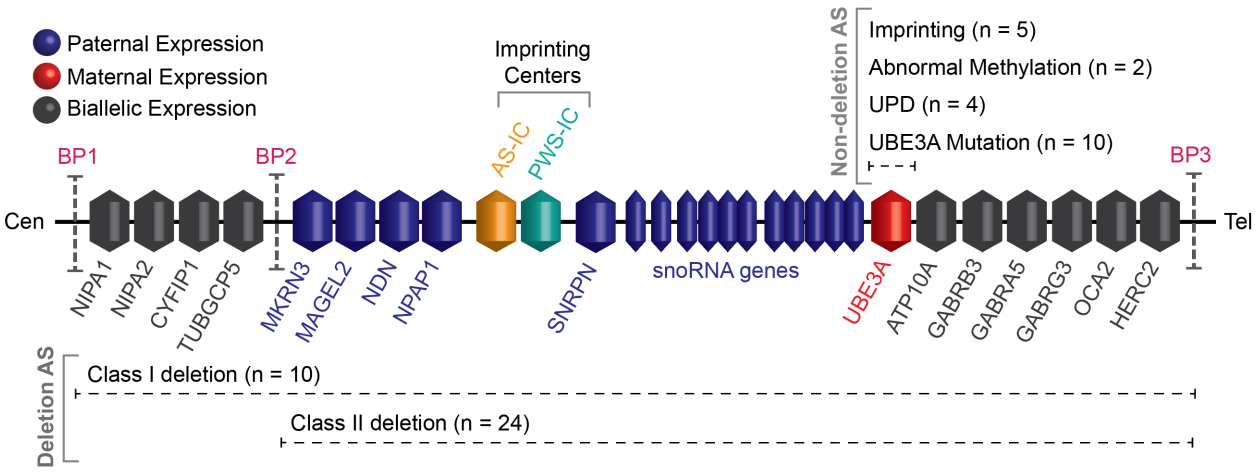


***Figure 5.1 Schematic of 15q11-q13 and AS mechanisms.*** *The maternally expressed (i.e., paternally*

*imprinted) gene UBE3A is shown in red, paternally expressed (i.e., maternally imprinted) genes are shown in blue. Genes shown in black are non-imprinted (i.e., biallelically expressed); "n" indicates the number of participants for different genotypes. UBE3A mutations (n = 10), paternal UPD (n = 4), imprinting defects (n = 5; could either be deletion within the imprinting center or an abnormal epigenetic imprint), and abnormal DNA methylation that are not deletions (could be either UPD or imprinting defects, n = 2) primarily affect UBE3A. These etiologies comprise the non-deletion genotype (n = 21) in our study. Deletions of 15q11-q13 are typically between canonical break point (BPs) labeled in the diagram above. Class I is a ~6 Mb deletion from BP 1 to BP3 (n = 10) that includes four additional genes near the centromere as compared with class II (~5 Mb) deletions, which span BP2 to BP3 (n = 24). Together with atypical (n = 2) and unknown (n = 1) deletion classes, class I and class II deletions comprise the deletion genotype (n = 37) examined in our study. Both deletions classes encompass the $GABA_AR$ β3-α5-γ3 subunit gene cluster (i.e., GABRB3, GABRA5, and GABRG3), which is central to the interpretation of our results.*

Individuals with deletions have a more severe clinical presentation than those with non-deletion Angelman syndrome genotypes (Gentile et al. 2010; Lossie et al. 2001; Minassian et al. 1998; Moncla et al. 1999), suggesting that genes other than *UBE3A* modulate the disease. Indeed, at least three distinct lines of evidence suggest an important role for GABA type-A receptor ($GABA_AR$) subunit genes (*GABRA5*, *GABRB3*, and *GABRG3*) in modulating the AS phenotype. (1) Mice with disruptions of *Gabrb3* recapitulate AS-like phenotypes (including seizures and EEG abnormalities) (DeLorey et al. 1998). (2) Deletion AS shows both altered cortical expression of the three $GABA_AR$ subunit genes (Roden et al. 2010) and reduced cortical $GABA_AR$ density (Holopainen et al. 2001). Furthermore, deletion AS yields grossly abnormal

somatosensory evoked responses that likely relate to GABAergic dysfunctions (Egawa et al. 2008). (3) Dup15q syndrome, a neurodevelopmental disorder characterized by intellectual disability, epilepsy, and duplications of 15q11.2-q13.1 (the "genetic converse" of deletion AS), has a strong EEG phenotype characterized by excessive beta oscillations (Frohlich et al. 2016). These oscillations closely resemble the EEG signature of $GABA_A$ enhancing drugs (e.g., benzodiazepines) (Greenblatt et al. 1989), thereby implicating *GABRA5*, *GABRB3*, and *GABRG3* in the Dup15q syndrome pathology and phenotype.

Thus, while the disruption of *UBE3A* alone seems to impact GABAergic signaling (DeLorey et al. 1998; Egawa et al. 2012; Judson et al. 2016), the deletion of the $GABA_AR$ β3-α5-γ3 subunit gene cluster may modulate the disease pathology in deletion AS and, furthermore, underlie the more severe phenotype. Differences in EEG between deletion and non-deletion AS may provide valuable insights into contributions of *UBE3A* and the $GABA_AR$ β3-α5-γ3 subunit gene cluster. However, such differences have not yet been quantitatively investigated.

Understanding the AS EEG phenotype also has important practical implications for the development of AS treatments. The genetics of AS provides a clear basis for drug targets that are actively pursued. For successful clinical development, biomarkers that quantify the disease pathophysiology and indicate a treatment response are of critical importance (Jeste et al. 2015). EEG has been suggested as a promising quantitative, robust, and translatable biomarker for AS (Sidorov et al. 2017). Highly targeted AS treatments (e.g., antisense oligonucleotides) acting specifically on *UBE3A* expression (Bishop 2017; Matsuura et al. 1997; Meng et al. 2015) require biomarkers to demonstrate target engagement and treatment effects. To this end, it is

important to understand if an EEG biomarker reflects *UBE3A*-related pathologies or pathologies related to other genes commonly deleted in AS.

With this motivation, we investigated differences in EEG power spectra between deletion and non-deletion AS. Considering the foregoing evidence, we tested two specific hypotheses concerning deletion AS compared to non-deletion AS: (1) stronger power in the delta frequency band and (2) weaker power in the beta frequency band, i.e., the opposite of the phenotype observed at 23 Hz in Dup15q syndrome by Frohlich and colleagues (Frohlich et al. 2016). We then explored a broad range of EEG frequencies in a data-driven manner.

## 5.2 Methods and Materials

### 5.2.1 Data Collection

EEG recordings were obtained from patients with AS through the AS Natural History Study (ClinicalTrials.gov identifier: NCT00296764) between 2006 and 2014 recorded at two sites: 1) Rady Children's Hospital San Diego (RCHSD) (50 datasets from 30 unique participants) and 2) Boston Children's Hospital (BCH) (47 datasets from 34 unique participants). Consent was obtained from participating families according to the Declaration of Helsinki and was approved by the institutional review boards of BCH and RCHSD. A subset of AS data from RSCHD were previously analyzed by Sidorov and colleagues as part of a separate study (Sidorov et al. 2017). EEG recordings from a control group of children with typical development (TD) were also obtained through BCH (56 participants, single recordings). All TD participants were children who had tested negative for neurological or developmental concerns. Groups were not age matched; however, this was accounted appropriately using a linear mixed model (LMM, see below).

EEG data were acquired in a clinical setting using an international 10-20 EEG montage (19 channels), some of which included auxiliary channels such as electrooculogram (EOG) and electrocardiogram (ECG). All data were acquired using BioLogic and Xltek systems (Natus Medical Incorporated, Pleasanton, California; sampling rates: 200 Hz, 256 Hz, and 512 Hz). Some EEGs included segments in which the participant was encouraged to sleep, as well as light flash stimuli and hyperventilation intended to trigger epileptiform activity; these sections of data were excluded from analyses. Most data were collected from children. To minimize effects related to age extremes, we excluded seven infants and adults by restricting the analyses to participants with ages between 12 – 216 months (1 - 18 years). 144 datasets entered preprocessing.

### 5.2.2 Preprocessing

Both the pediatric population and the loosely controlled clinical setting present challenges in the form of (1) many physiological and technical artifacts and (2) changes in the participant's state. A careful preprocessing is therefore essential to perform quantitative analyses. To this end, EEG data were bandpass filtered 0.5 – 45 Hz (FIR, filter order: 2 x sampling rate). Then, portions of unusable EEG data containing gross artifacts, including muscle bursts and technical artifacts, were identified by visual inspection and excluded from analysis. Furthermore, bad channels (i.e., flat or subject to frequent technical artifacts) were identified and excluded (number of bad channels per participant: 0.75 ± 0.82, mean ± std; range 0 – 3). For 10 datasets, the overall EEG data quality was considered insufficient for quantitative analysis. The artifact rejection was guided by inspection of EEG traces, physiological signals from auxiliary channels (EOG, electromyogram or EMG, proxy for EMG derived from >45 Hz

power), and data annotations provided by the EEG technician during acquisition indicating the participant's behavioral state. Sections of data that included sleep, drowsiness, light flashes, and instructed hyperventilation were marked for exclusion. Additionally, all remaining data were manually screened for sleep-related EEG features and corresponding sections were excluded if present. Then, independent component analysis (ICA) was applied to remove remaining artifacts including eye blinks, saccades, ballistocardiogram, and muscle activity (FastICA algorithm (Hyvarinen 1999b; Jung et al. 2000)); number of removed artefactual ICs: 5.26 ± 2.1, mean ± std; range: 0 – 9). Finally, rejected channels were interpolated and data were re-referenced to average.

The final dataset analyzed included 127 recordings from 106 participants. Three deletion AS participants (two atypical, one unknown deletion size) were excluded from the AS genotype comparison to allow for testing of differences between deletion class I and class II. The individual dataset length ranged from 2.82 – 41.3 minutes in length (15.9 ± 8.36 minutes, mean ± std), corresponding to 30 – 1003 frequency transform windows for the lowest frequency analyzed (see Frequency Transform; 259 ± 188 windows, mean ± std; 7 additional participants were excluded who had too little analyzable data, threshold: 25 analysis windows for lowest frequency analyzed, see Frequency Transform). See Table 5.1 for a summary of retained data by genotype and testing site.

| | Deletion AS | | | | | Non-deletion AS | | | | | TD |
|---|---|---|---|---|---|---|---|---|---|---|---|
| | **Class I** | **Class II** | **Atypical** | **Unknown** | **Sum** | **Mutation** | **UDP** | **Impr.** | **Methyl.** | **Sum** | **TD** |
| BCH | 2 (2) | 10 (13) | 2 (2) | 1 (1) | 15(18) | 6 (7) | 3 (3) | 4 (8) | 1 (1) | 14 (19) | 48 (48) |
| RCHSD | 8 (11) | 14 (20) | - | - | 22(31) | 4 (6) | 1 (1) | 1 (2) | 1 (2) | 7(11) | - |
| Sum | 10 (13) | 24 (33) | 2 (2) | 1 (1) | **37** (49) | 10 (13) | 4 (4) | 5 (10) | 2 (3) | **21** (30) | **48** (48) |

***Table 5.1 AS dataset overview.*** *The final dataset analyzed included 127 recordings from 106 participants. This table breaks down participants by genotypes and recording center. The number of datasets analyzed is provided in parenthesis. This deviates from the number of participants for the AS group since longitudinal data was acquired for some participants. UPD means maternal uniparental disomy; Impr. means imprinting defect; Methyl. means abnormal DNA methylation that is not related to a deletion (i.e. UPD or imprinting defect).*

### 5.2.3 Frequency Transform

Power spectral estimates were derived for logarithmically scaled frequencies with a spectral smoothing of 1/3 octave ($f/\sigma_f = 8.7$) using Morlet Wavelets (Tallon-Baudry et al. 1997). This frequency transform accounts for the logarithmic nature of electrophysiological signals (Buzsáki and Draguhn 2004). Center frequencies were spaced logarithmically according to the exponentiation of the base 2 with exponents ranging from 0 (1 Hz) to 5 (32 Hz) in steps of 1/8. Power spectral estimates were derived as average power values of successive 3/4-overlapping temporal windows of continuous clean data. Absolute power values were then scaled and log-transformed to have units $10*\log_{10}(\mu V^2/\log_2(Hz))$. Consequently, differences between signals have units dB. Note, the power spectral density is based on $\log_2(Hz)$ not Hz to account for the

logarithmic nature of electrophysiological signals (Buzsáki and Draguhn 2004). For analyses of relative power, data were expressed in units of $1/\log_2(\text{Hz})$.

### 5.2.4 Peak frequencies

To extract peak frequencies, we averaged power spectra across electrodes. Peak labeling was performed both automatically (using the local maximum) and manual (by visual inspection) within pre-defined frequency ranges (delta: 1.5 – 4 Hz; theta 4 – 8 Hz) for each visit of each participant with useable data. In instances where automatically and manually labeled peak frequencies agreed within 5%, the automatic peak label was used; otherwise, the manual peak label was used. As an alternative measure for peak location, we used the "center of mass" within the aforementioned pre-defined frequency ranges, derived as the expected value of the frequency within a frequency range.

### 5.2.5 Statistical analyses

For statistical analysis we used a Linear Mixed Model (LMM) (West et al. 2014). The advantage of LMMs is the ability to model correlated data from longitudinal measurements by construction. We used the following LMM and variants with less fixed factors:

$$P \sim 1 + GENOTYPE + AGE + GENOTYPE:AGE + (1|PARTICIPANT)$$

Where P is log-transformed power in a given frequency band, AGE is the $\log_2$-transformed and mean-centered age, and GENOTYPE contains categorical variables [AS, TD], [deletion, non-deletion], or [deletion class I, deletion class II]. We use log-transformed age to account for

developmental changes generally occurring decelerated with increase in age, i.e. faster at younger ages.

We then used two approaches to derive p-values and confidence intervals. First, to derive 95% confidence intervals for illustration, and to test specific hypotheses, we used t-tests within LMM while using the Satterthwaite approximation to derive corrected degrees of freedom. Second, we used log-likelihood ratio tests between nested models to test for relevance of factors (e.g. GENOTYPE or AGE). For all analyses where log-likelihood ratio tests were performed, we used the maximum likelihood (ML) method to fit the model; otherwise, we used the restricted maximum likelihood (REML) method. To account for multiple comparison correction when performing analyses across all frequencies, we additionally applied a random permutation approach (Nichols and Holmes 2002). More specifically, for each of 10,000 resamples, the GENOTYPE label for subjects (e.g. AS, TD) was randomly permuted; we then derived p-values for each frequency and retained only the smallest p-value across all frequencies for each resample to build a null-hypothesis distribution that accounts for multiple testing.

For illustration and to precisely determine peak frequencies, we used spline-interpolation to derive a higher frequency resolution. All data analyses were performed in MATLAB (The MathWorks, Inc., Torrance, California) using custom scripts, FastICA for independent component analyses (http://www.cis.hut.fi/projects/ica/fastica/, (Hyvarinen 1999a)), and the FieldTrip toolbox to create topographic plots (Oostenveld et al. 2011).

## 5.3 Results

We obtained clinical EEG data from children (1 to 18 years of age) with AS and TD controls. After preprocessing and quality control, we retained 49 datasets from 37 individuals with deletion AS, 30 datasets from 21 individuals with non-deletion AS, and single-visit datasets from 48 TD controls (Fig. 5.1). Age (deletion AS: 55.3 ± 35.9, non-deletion AS, 87.7 ± 40.1, TD controls: 105 ± 59.6, mean ± std in months, age averaged across multiple visits) significantly differed between AS genotypes ($p = 1.66 \times 10^{-4}$) and between AS and TD cohorts ($p = 2.5 \times 10^{-3}$), and was thus accounted for in the subsequent analyses.

### 5.3.1 Spectral power differs between AS and TD controls

We first investigated differences in EEG spectral power between AS (combined deletion and non-deletion genotypes) and TD controls. For each visit of each participant, we derived spectral power estimates (1 to 32 Hz) – averaged across electrodes – and fitted LMMs for each frequency separately (see methods). To test for differences between participants with AS and TD controls, we compared the model to a nested model lacking diagnosis (AS, TD) information. Importantly, the models accounted for age. We found that spectral power differed between AS and TD controls for all frequencies (genotype information AS vs TD significantly contributed to the model fit; random permutation test; $p < 0.05$, corrected for all frequencies).

To understand the directionality of the difference in spectral power between AS and TD controls, we fixed the age in the model to the mean 1 log age (5.4 years) and investigated group differences in spectral power. We found higher power for AS compared to TD controls across all frequencies analyzed (Fig. 5.2A, Fig. 5.3A). The largest difference manifested in a prominent peak in the delta frequency range (peak frequency = 2.8 Hz, peak frequency at higher spatial

resolution derived by spline interpolation = 2.89 Hz, Cohen's d = 1.22, power difference AS vs TD: 11.08 dB or 1182%). Excess power in the delta frequency is a global phenomenon that is visible at all electrodes, but the effect size is largest at temporal electrodes (Fig. 5.2B,C, Fig. 5.3B). Notably, testing total power (i.e. integrating power over all frequencies) yields a similar effect size (Table 5.2).

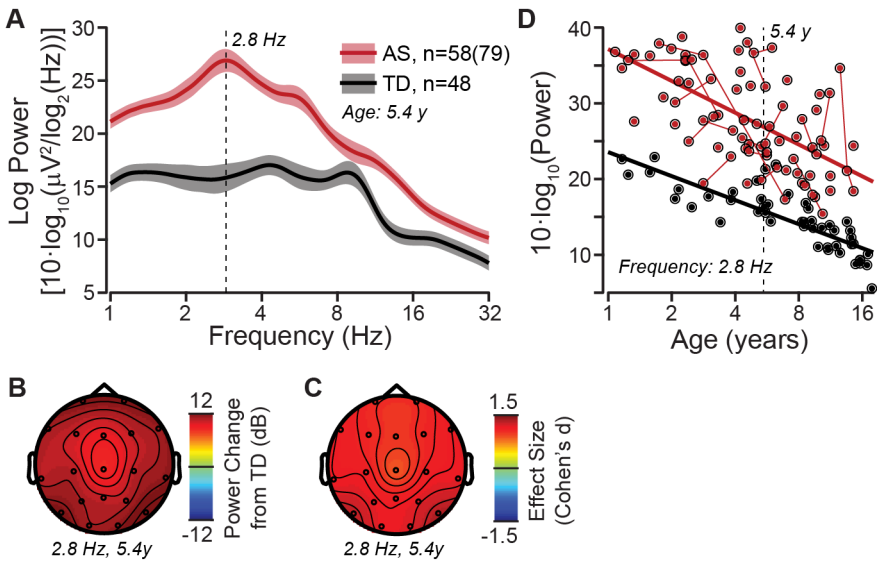


***Figure 5.2 Spectral power differences between AS and TD controls.*** *(A) Grand average power spectral density derived from the LMM, with age set to the mean log age of 5.4 years (average across all visits and electrodes). AS: red, TD controls: black. The colored bands show 95% confidence intervals. (B,C) Scalp topography of power change in dB and effect size (Cohen's d) between AS and TD controls derived from the LMM for 2.8 Hz (i.e., AS delta peak frequency) and the mean log age of 5.4 years. (D) Developmental trajectory of channel averaged delta power (2.8 Hz) derived from the LMM. Longitudinal visits are connected by solid lines.*

| Name | Estimate | SE | t-stat | DF | p-value | Lower | Upper |
|---|---|---|---|---|---|---|---|
| **Intercept** | 22.39 | 0.50 | 45.18 | 117.87 | $<10^{-14}$ | 21.41 | 23.37 |
| **AS** | 7.49 | 0.65 | 11.58 | 110.02 | $<10^{-14}$ | 6.21 | 8.77 |
| **LogAge** | -2.60 | 0.44 | -5.94 | 117.87 | $<10^{-14}$ | -3.47 | -1.73 |
| **AS:LogAge** | -0.57 | 0.60 | -0.96 | 116.66 | 0.3393 | -1.75 | 0.61 |

***Table 5.2 AS vs TD, LMM coefficients for total power analysis (1 – 32 Hz).*** *Fixed effects parameter for LMM POWER ~ 1 + GENOTYPE + AGE + GENOTYPE:AGE + (1|PARTICIPANT) with GENOTYPE being AS or TD and POWER being the 10·log10(TotalPower) where TotalPower is the integral over the frequency range from 1 to 32 Hz in units $\mu V^2$. SE is the standard error of the mean, DF is the degrees of freedom estimated using the Satterwaite approximation, Lower and Upper and provide the lower and upper end for 95% confidence intervals.*

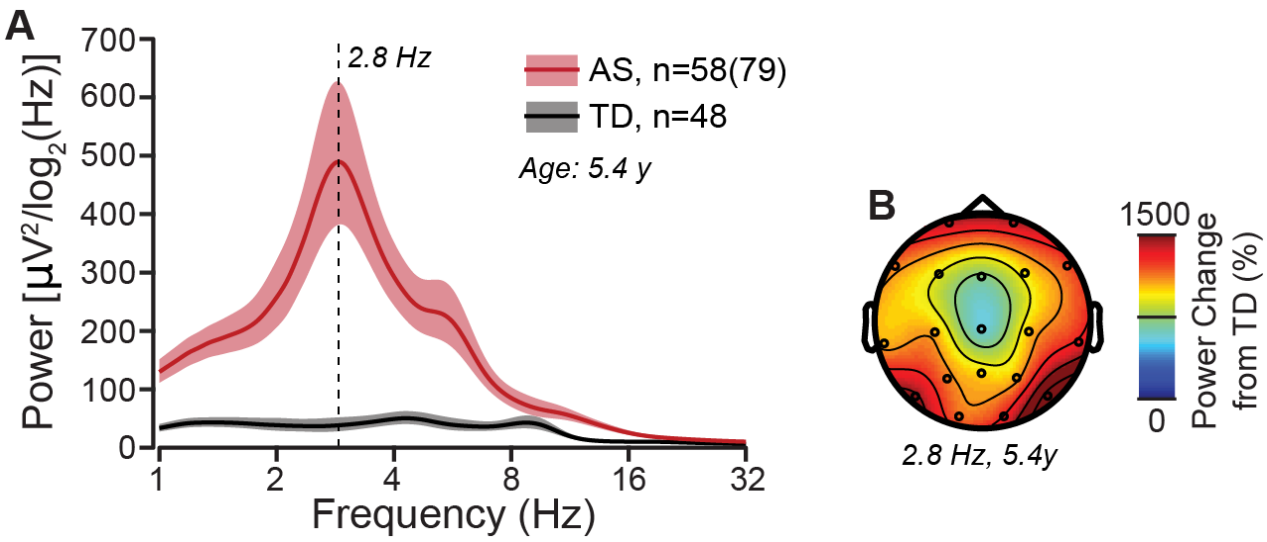


***Figure 5.3 Spectral power differences between AS and TD controls, continued.*** *(A) Grand averaged power spectral density derived from the LMM with age set to mean log age of 5.4 years (average across all visits and electrodes). Same as Figure 2A but with power instead of log-power scaling. AS: red, TD controls: black. The colored bands show 95% confidence intervals. (B) Scalp topography of power change*

*in % change from TD controls derived from the LMM for 2.8 Hz (i.e., AS delta peak frequency) and the mean log age of 5.4 years.*

We next investigated the developmental trajectory of AS delta power in terms of both power and peak frequency. Power at theAS delta peak frequency (2.8 Hz) exhibited a significant decline with age in both groups (Fig. 5.2D, LMM parameters in Table 5.3). The slopes did not significantly differ between AS and TD controls (Difference: -1.03 dB/oct, p = 0.202). Clear delta peaks could be identified in 70 EEG recordings from 54 of 58 participants with AS (Fig. 5.4A). The delta peak frequency was not associated with age (LMM, log-likelihood ratio test of model with and without age, p=0.492). Center of mass, an alternative metric for quantifying the dominant frequency, also showed no relationship with age (frequency range: 1.5 – 4 Hz, p=0.832). Thus, although the overall power changes during development for both groups, the AS delta EEG phenotype (i.e. the difference between TD controls and the AS peak frequency) varies little across age.

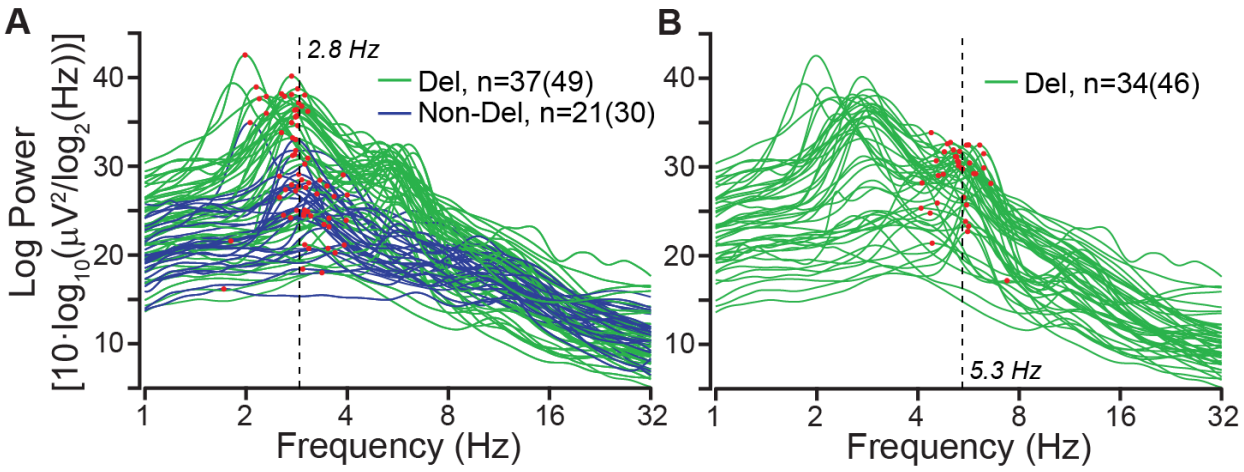

***Figure 5.4 Individually labeled delta and theta peaks.*** *Individually labeled spectral peaks on channel averaged power spectral densities from AS participants (labeling was performed separately for each visit in longitudinal data). Spectral peaks were manually labeled in the delta and theta frequency bands. If manually selected frequency values differed from an automatic approach using the local maximum by less than 5%, the automatic peak label was used instead. (A) Individually labeled delta (1.5 – 4 Hz) peaks indicated by red dots on spectra from participants with the AS deletion genotype (green) and the AS non-deletion phenotype (blue). We identified delta peaks in 70 of 79 recordings from 54 of 58 participants. (B) Individually labeled theta (4- 8 Hz) peaks indicated by red dots on spectra from participants with the AS deletion genotype (green) with atypical and unknown deletions excluded. We identified theta peaks in 37 of 46 recordings from 28 of 34 participants with deletion AS (only class I and class II are considered).*

| Name | Estimate | SE | t-stat | DF | p-value | Lower | Upper |
|---|---|---|---|---|---|---|---|
| **Intercept** | 15.80 | 0.67 | 23.65 | 120.82 | $<10^{-14}$ | 14.48 | 17.13 |
| **AS** | 11.08 | 0.87 | 12.82 | 112.97 | $<10^{-14}$ | 9.37 | 12.79 |
| **LogAge** | -3.17 | 0.59 | -5.37 | 120.82 | $<10^{-14}$ | -4.34 | -2.00 |
| **AS:LogAge** | -1.03 | 0.80 | -1.28 | 117.51 | 0.2021 | -2.61 | 0.56 |

***Table 5.3 AS vs TD, LMM coefficients for delta peak power (2.8 Hz).*** *Fixed effects parameter for LMM POWER ~ 1 + GENOTYPE + AGE + GENOTYPE:AGE + (1|PARTICIPANT) with GENOTYPE being AS or TD and POWER being the power spectral density at 2.8 Hz in units $10 \cdot log10(\mu V^2/log_2(Hz))$. SE is the standard error of the mean, DF is the degrees of freedom estimated using the Satterwaite approximation, Lower and Upper and provide the lower and upper end for 95% confidence intervals.*

Excess power in the delta frequency range is in line with previous reports of excess relative power in AS compared to TD controls (Sidorov et al. 2017). Our results show that power is increased across all frequencies analyzed (1-32 Hz) and exhibits the strongest difference in

the delta frequency range. Consequently, the effect size is larger for absolute as compared to relative power (Absolute power: Cohen's d = 1.22, relative power: Cohen's d = 0.67, at delta peak frequency, 2.8 Hz; see Fig. 5.5 for the analysis of relative power).

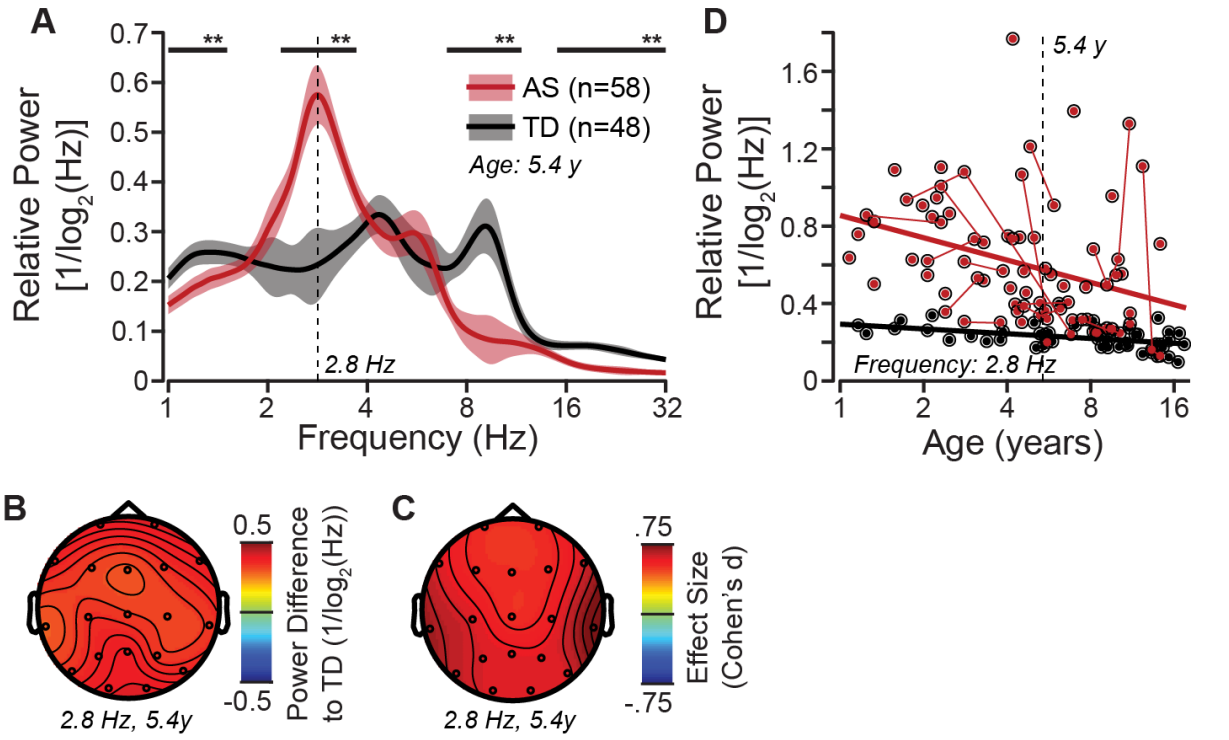


***Figure 5.5 Spectral differences of relative power between AS and TD controls.*** *(A) Grand averaged power spectral density for relative power derived from the LMM with age set to the mean log age of 5.4 years (average across all electrodes). AS: red, TD controls: black. The colored bands show 95% confidence intervals. The black bars indicate frequency ranges with significant group differences (corrected for multiple testing across frequencies). (B,C) Scalp topography of relative power difference and effect size (Cohen's d) between AS and TD controls derived from the LMM for 2.8 Hz (i.e., AS delta peak frequency) and the mean log age of 5.4 years. (D) Developmental trajectory of channel averaged relative delta power (2.8 Hz) derived from the LMM. Longitudinal visits are connected by solid lines. Developmental*

*trajectory: TD: -0.02 1/oct, 95% confidence interval: -0.09 to 0.04; p = 0.459; AS: -0.17 1/oct, 95% confidence interval: -0.17 to -0.06; p = 1.88 x $10^{-4}$). The slopes did differ significantly between AS and TD controls: -0.09 1/oct (95% confidence interval: -0.18 to 0.00; p = 0.042).*

### 5.3.2 Spectral power differs between AS genotypes

To investigate phenotypic differences in EEG spectral power between AS subtypes, we split the AS group into deletion AS (*n* = 34, participants with class I or class II deletion) and non-deletion AS (*n* = 21) subgroups. First, we tested the two specific hypotheses as outlined in the introduction. A 1-tailed test for higher delta power in AS deletion genotypes (hypothesis 1) at the AS group level peak frequency (2.8 Hz) revealed 2.973 dB higher power compared to the AS non-deletion genotype at mean log age of 4.7 years (corresponding to 198.3% power relative to non-deletion AS; Fig. 5.6A; $p$ = 2.49 x $10^{-2}$, LMM parameters in Table 5.4). The power differences decline with age and were greatest over temporal scalp regions (Fig. 5.6B,C). A 1-tailed test for lower beta power in AS deletion genotypes at the Dup15q syndrome peak frequency (hypothesis 2; 23 Hz (Frohlich et al. 2016)) revealed -1.691 dB lower power compared to non-deletion AS at mean log age of 4.7 years (corresponding to 67.7% relative to non-deletion AS; Fig. 5.7A; p = 7.66 x $10^{-3}$, LMM parameter in Table 5.5). Power differences at 23 Hz were greatest over central scalp regions (Fig. 4B,C). Thus, the AS deletion genotype exhibits stronger delta power but weaker beta power than the non-deletion AS genotype. The latter observation in the AS deletion genotypes resembles an inversion of the Dup15q syndrome EEG signature (Frohlich et al. 2016).

| Name | Estimate | SE | t-stat | DF | p-value | Lower | Upper |
|---|---|---|---|---|---|---|---|
| **Intercept** | 25.37 | 1.20 | 21.34 | 50.45 | $<10^{-14}$ | 22.98 | 27.75 |
| **DEL_AS** | 2.97 | 1.49 | 2.01 | 50.34 | 0.0498 | 0.00 | 5.94 |
| **LogAge** | -1.86 | 1.30 | -1.44 | 59.13 | 0.1544 | -4.44 | 0.72 |
| **DEL_AS:LogAge** | -2.69 | 1.56 | -1.75 | 60.21 | 0.0861 | -5.78 | 0.39 |

***Table 5.4 Deletion vs Non-deletion AS, LMM coefficients for delta peak power (2.8 Hz).*** *Fixed effects parameter for LMM POWER ~ 1 + GENOTYPE + AGE + GENOTYPE:AGE + (1|PARTICIPANT) with GENOTYPE being deletion AS or non-deletion AS and POWER being the power spectral density at 2.8 Hz in units 10·log10($\mu V^2/log_2(Hz)$). SE is the standard error of the mean, DF is the degrees of freedom estimated using the Satterwaite approximation, Lower and Upper and provide the lower and upper end for 95% confidence intervals.*

| Name | Estimate | SE | t-stat | DF | p-value | Lower | Upper |
|---|---|---|---|---|---|---|---|
| **Intercept** | 12.95 | 0.55 | 23.88 | 47.77 | $<10^{-14}$ | 11.86 | 14.04 |
| **DEL_AS** | -1.67 | 0.68 | -2.48 | 47.82 | 0.0168 | -3.03 | -0.32 |
| **LogAge** | -1.33 | 0.58 | -2.31 | 58.43 | 0.0242 | -2.48 | -0.18 |
| **DEL_AS:LogAge** | 0.13 | 0.69 | 0.19 | 61.48 | 0.8517 | -1.24 | 1.50 |

***Table 5.5 Deletion vs Non-deletion AS, LMM coefficients for beta peak power (23 Hz).*** *Fixed effects parameter for LMM POWER ~ 1 + GENOTYPE + AGE + GENOTYPE:AGE + (1|PARTICIPANT) with GENOTYPE being deletion AS or non-deletion AS and POWER being the power spectral density at 23 Hz in units 10·log10($\mu V^2/log_2(Hz)$). SE is the standard error of the mean, DF is the degrees of freedom estimated using the Satterwaite approximation, Lower and Upper and provide the lower and upper end for 95% confidence intervals.*

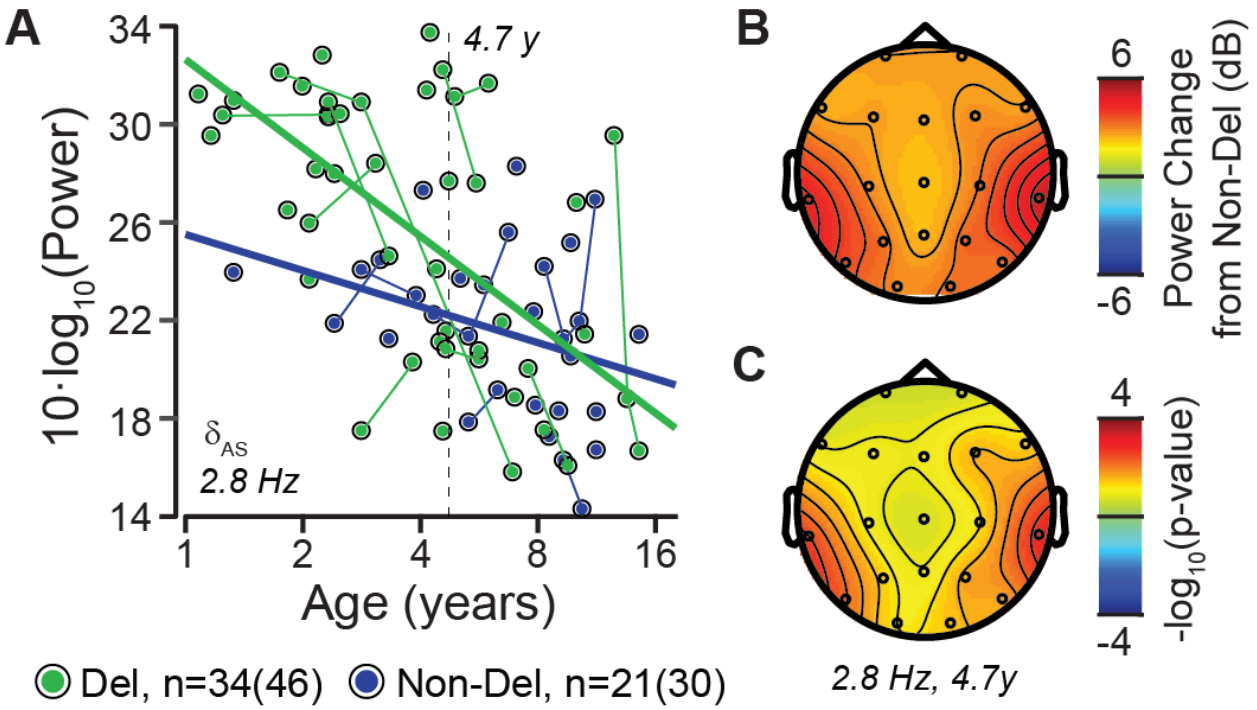


***Figure 5.6 Spectral power in delta frequency band differs between AS genotypes.*** *(A) Developmental trajectory of electrode averaged delta power (2.8 Hz) derived from the LMM (average across all electrodes). Deletion AS: green, Non-deletion AS: blue. Longitudinal visits are connected by solid lines. (B,C) Scalp topography of power change in dB and p-values for t-tests between deletion AS and non-deletion AS derived from the LMM for 2.8 Hz and the mean log age of 4.7 years.*

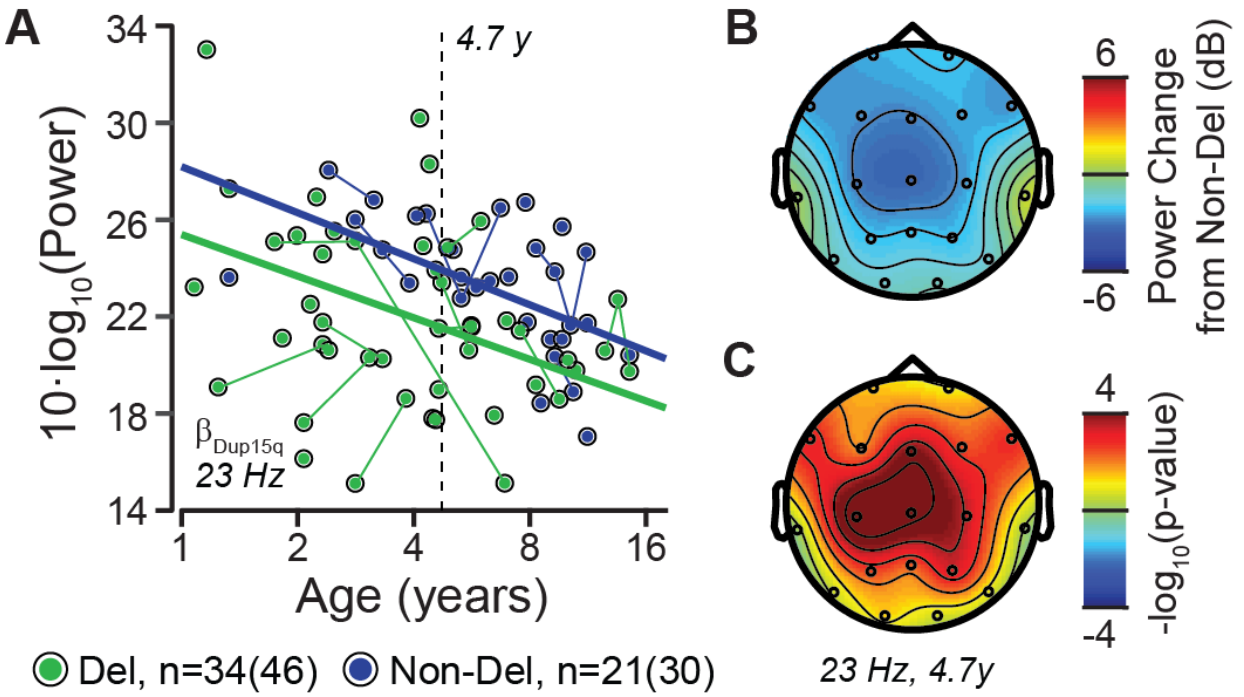


***Figure 5.7 Spectral power in beta frequency band differs between AS genotypes.*** *(A) Developmental trajectory of electrode averaged beta power (23 Hz according to hypothesis 2, i.e. peak frequency derived from Dup15q syndrome EEG phenotype, (Frohlich et al. 2016)) derived from the LMM (average across all electrodes). Deletion AS: green, Non-deletion AS: blue. Longitudinal visits are connected by solid lines. (B,C) Scalp topography of power change in dB and p-values for t-tests between deletion AS and non-deletion AS derived from the LMM for 23 Hz and the mean log age of 4.7 years*

Next, we switched to an exploratory analysis and tested for AS genotype differences in an unbiased and data-driven manner across the full frequency range (1 – 32 Hz). This analysis revealed highly significant excess theta power of 5.20 dB centered at 5.3 Hz (5.43 Hz from increased spectral resolution using spline interpolation) for deletion AS compared to non-deletion AS (corresponding to 331% of the non-deletion AS value; Fig. 5.8A,B, Fig. 5.9A-C; $p < 0.01$, LMM-based random permutation test corrected for multiple comparisons across

frequencies and accounting for age, LMM parameter for 5.3 Hz in Table 5.6). A local maximum exists in theta for the grouped averaged deletion AS power spectral density but not for that obtained from non-deletion AS. Power differences in 5.3 Hz power were greatest over centro-temporal regions (Fig. 5.8E-G). In sum, this suggests that the EEG phenotype of deletion AS is characterized by an oscillation in the theta frequency range that is absent in non-deletion AS.

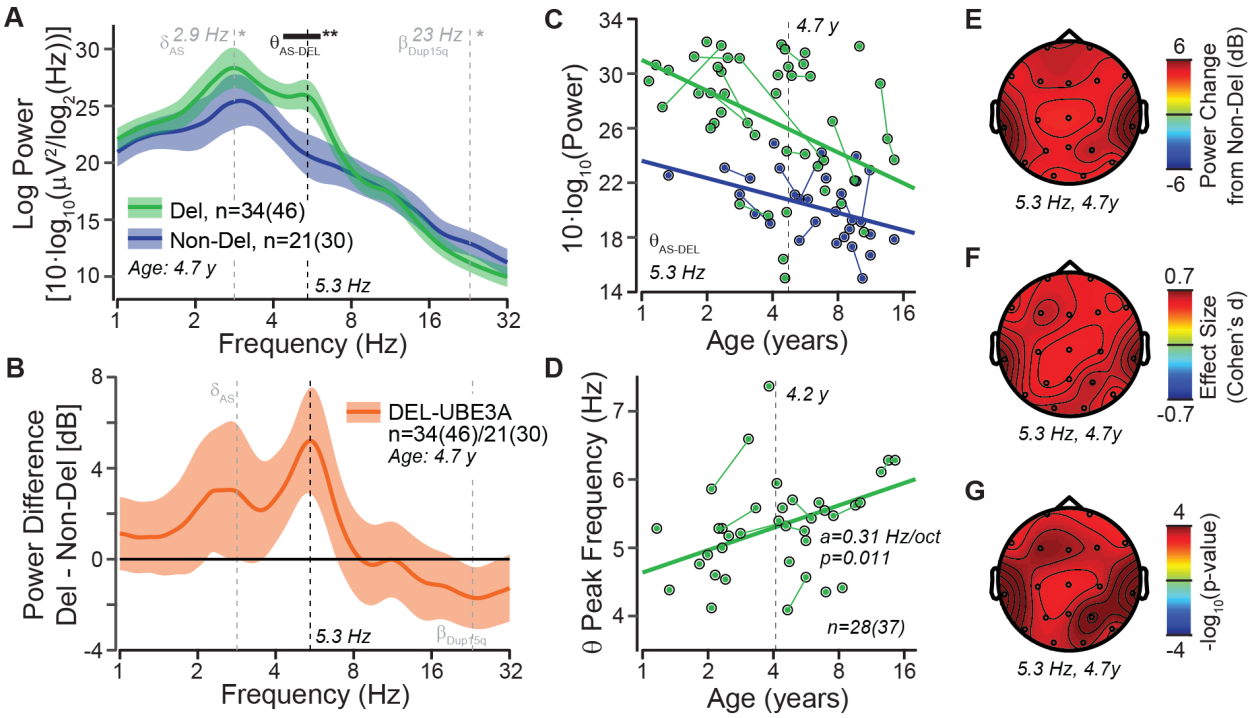


***Figure 5.8 Spectral power differs between AS genotypes.*** *(A) Grand average power spectral density derived from the LMM with age set to the mean log age of 4.7 years (average across all visits and electrodes). Deletion AS: green, non-deletion AS: blue. The colored bands show 95% confidence intervals. The black bar indicates frequency ranges with significant group differences (corrected for multiple testing across frequencies). The gray lines indicate the specific hypotheses tested in the delta and beta bands (see Figures 3 and 4). (B) Difference in spectral power between deletion AS and non-deletion AS. The colored bands show 95% confidence intervals. (C) Developmental trajectory of theta power (5.3 Hz)*

*derived from the LMM (average across all electrodes). Longitudinal visits are connected by solid lines. (D) Correlation between theta peak frequency and age. Longitudinal visits are connected by solid lines. (E-G) Scalp topography of power change in dB, effect size (Cohen's d) and p-values for t-tests between deletion AS and non-deletion AS derived from the LMM for 5.3 Hz and the mean log age of 4.7 years.*

| Name | Estimate | SE | t-stat | DF | p-value | Lower | Upper |
|---|---|---|---|---|---|---|---|
| **Intercept** | 20.76 | 0.92 | 22.80 | 50.70 | $<10^{-14}$ | 18.94 | 22.59 |
| **DEL_AS** | 5.17 | 1.14 | 4.57 | 50.78 | 3.0·10-5 | 2.90 | 7.45 |
| **LogAge** | -1.27 | 0.95 | -1.34 | 62.60 | 0.1847 | -3.16 | 0.62 |
| **DEL_AS:LogAge** | -0.99 | 1.13 | -0.88 | 66.21 | 0.3812 | -3.23 | 1.25 |

***Table 5.6 Deletion vs Non-deletion AS, LMM coefficients for theta peak power (5.34 Hz).*** *Fixed effects parameter for LMM POWER ~ 1 + GENOTYPE + AGE + GENOTYPE:AGE + (1|PARTICIPANT) with GENOTYPE being deletion AS or non-deletion AS and POWER being the power spectral density at 5.34 Hz in units 10·log10($\mu V^2/log_2(Hz)$). SE is the standard error of the mean, DF is the degrees of freedom estimated using the Satterwaite approximation, Lower and Upper and provide the lower and upper end for 95% confidence intervals.*

We then investigated the developmental trajectory of the theta-band deletion AS phenotype in terms of both power and peak frequency (Fig. 5.8C). We found a significant decrease in theta power (5.3 Hz) with age for deletion AS (slope -2.26 dB/oct, $p = 3.45 \times 10^{-4}$) but not for non-deletion AS (slope: -1.27 dB/oct, p = 0.185). This suggests a developmental decline of the deletion AS theta-band oscillation. However, slopes did not significantly differ between AS subgroups (difference in slope: -0.99 dB/oct, p = 0.381; see Fig. 5.9E for topography).

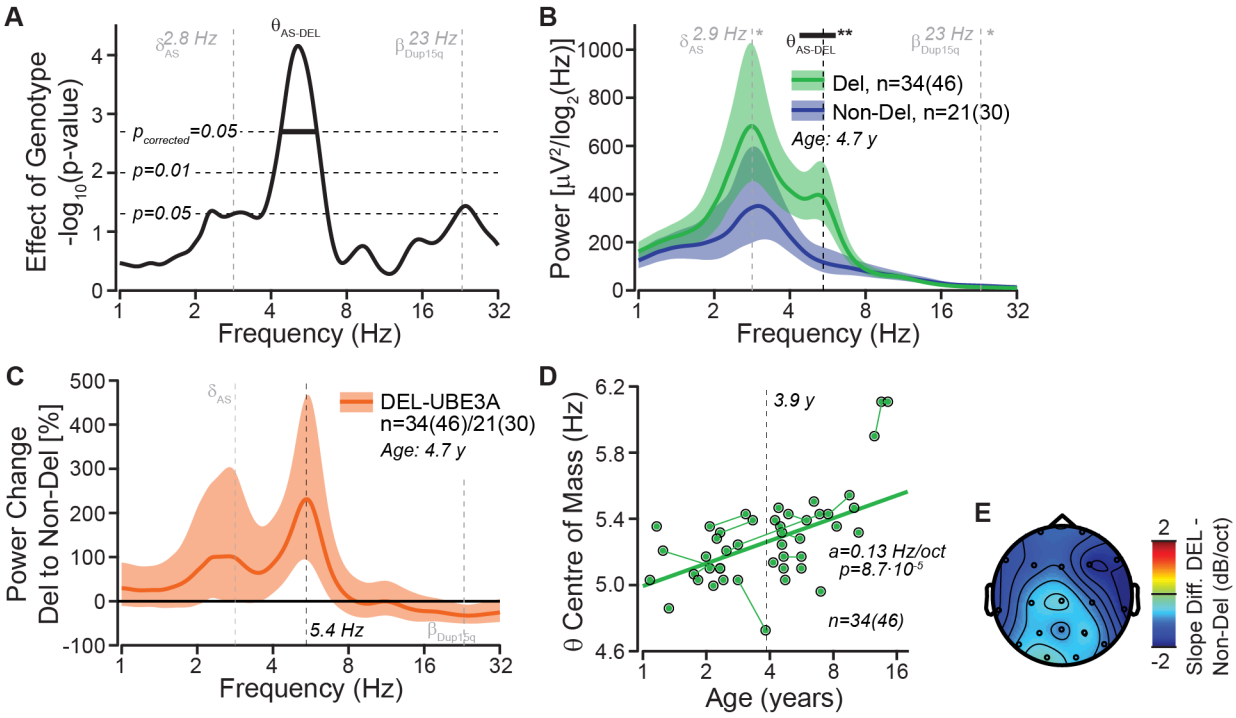


***Figure 5.9 Spectral power differs between AS genotype, continued.*** *(A) P-values for model comparisons (log-likelihood ratio tests) between models with and without AS genotype information (see Methods section). The horizontal lines depict different statistical threshold with and without correction for multiple testing across frequencies. (B) Grand average power spectral density derived from the LMM with age set to the mean log age of 4.7 years (average across all visits and electrodes). Same as Figure 3A but with power instead of log-power scaling. Deletion AS: green, non-deletion AS: blue. The colored bands show 95% confidence intervals. The black bar indicates frequency ranges with significant group differences (corrected for multiple testing across frequencies). The gray lines indicate the specific hypotheses tested in the delta and beta bands (see Figures 3 and 4). (C) Difference in spectral power of deletion AS relative to non-deletion AS in %-change. The colored bands show 95% confidence intervals. The gray lines indicate the specific hypotheses tested in the delta and beta bands (see Figures 3 and 4). (D) Correlation between age and the center of mass of electrode averaged power in the theta frequency*

*range (alternative metric to peak frequency, see Figure 5D). (E) Scalp topography of difference in developmental changes between deletion AS and non-deletion AS (i.e. difference of slopes of power change with age in $10 \cdot \log_{10}$(Pow)/oct), derived from the LMM for 5.3 Hz and the mean log age of 4.7 years.*

Clear theta peaks could be identified in 37 EEG recordings from 28 of 34 participants with class I or class II deletion AS (participants with atypical deletions were excluded; Fig. 5.4B). For participants with theta peaks, we found a significant increase of 0.31 dB/oct in peak frequency with age (LMM, log-likelihood ratio test of model with and without age, $p = 0.011$; Fig. 5.8D). This finding was confirmed using an alternative approach that quantifies the dominant frequency, i.e., center of mass, which can be derived for all deletion AS participants (metric: center of mass 4 – 8 Hz, $p = 8.7 \times 10^{-5}$, slope: 0.15 Hz/oct, see Fig. 5.9D). Thus, the deletion AS theta oscillation increases in frequency over the course of development.

Next, we analyzed deletion subgroups. The deletion group can be further broken down into subgroups with different deletion size (class I: ~6Mb; class II: ~5 Mb; we excluded rare atypical deletions from analysis (Buiting et al. 2016; Finucane et al. 2016)). Both deletion subgroups encompass *GABRA5*, *GABRB3*, and *GABRG3*. We tested if segregating the deletion group into these two subgroups would improve the model fit (log-likelihood ratio tests). We did not find any benefit of subgroup analysis, even when ignoring the correction for multiple testing across frequencies ($p > 0.05$). This suggests that the genes responsible for driving the differences between deletion AS and non-deletion AS reside in the region shared by deletion classes 1 and 2.

To examine potential confounds introduced by medication, we categorized all medications taken by participants that either (1) act principally on the CNS or (2) have incidental CNS side effects. Medications were classified by a physician, and further subcategories were established for CNS medications: antiepileptics, antipsychotics, alpha agonists, and stimulants. For each category and subcategory, we calculated the proportion of participants in each AS genotype taking a medication during at least one EEG recording used in our analysis (Table 5.7 and Fig. 5.10). Chi-squared tests were performed to test for different proportions between AS genotypes. We detected no significant difference in any medication category or subcategory, suggesting that differences in EEG between AS genotype reflect differences in pathophysiology rather than medication.

| Drug type | Non-del Participants (%) | Non-del Participants (#) | Non-del Recordings (#) | Deletion Participants (%) | Deletion Participants (#) | Deletion Recordings (#) | Chi-Square | P-value |
|---|---|---|---|---|---|---|---|---|
| CNS | 76.2 | 16 | 23 | 76 | 28 | 39 | 1.939 | 0.965 |
| AED | 52.4 | 11 | 17 | 70 | 26 | 36 | 1.856 | 0.173 |
| AP | 9.5 | 2 | 2 | 3 | 1 | 2 | 1.271 | 0.260 |
| CSE | 23.8 | 5 | 7 | 19 | 7 | 11 | 0.195 | 0.659 |
| AA | 14.3 | 3 | 4 | 8 | 3 | 5 | 0.551 | 0.458 |
| STM | 4.8 | 1 | 1 | 0 | 0 | 0 | 1.793 | 0.181 |

***Table 5.7 Medication overview.*** *This table summarizes the proportion of non-deletion AS and deletion AS participants on each of 6 different medications types: CNS: Central Nervous System; AED: Antiepileptic Drug; AP: Antipsychotic; CSE: CNS Side Effects; AA: Alpha Agonist; STM: Stimulant. Proportions are calculated from the number of unique participants in a group taking the medication at one or more EEG recording sessions used in the analysis. Number of affected participants and EEG recordings are reported*

*in separate columns. Test statistics and p-values from chi-squared tests are reported in the last two columns.*

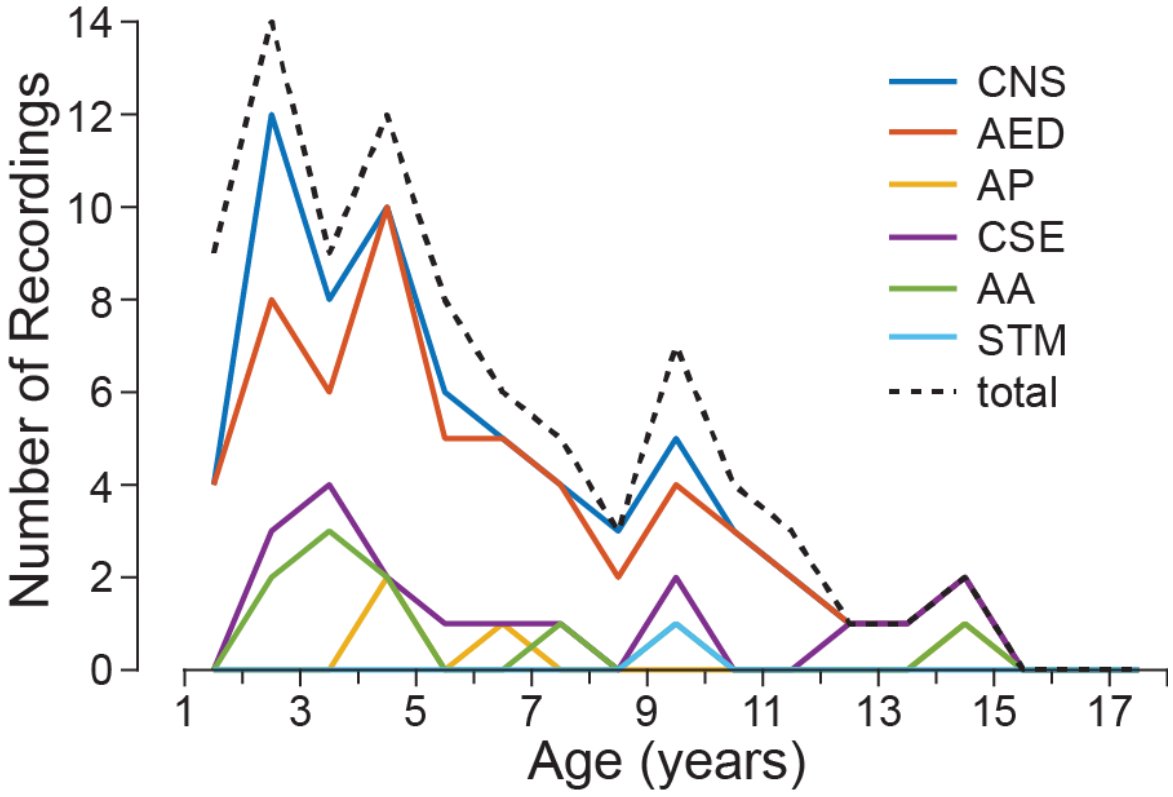


***Figure 5.10 Medication as a function of age.*** *6 different medications types: CNS: Central Nervous System; AED: Antiepileptic Drug; AP: Antipsychotic; CSE: CNS Side Effects; AA: Alpha Agonist; STM: Stimulant. The total number of available recordings in a given age bin is indicated by the black dotted line.*

## 5.4 Discussion

Our findings demonstrate a robust electrophysiological phenotype in children with AS comprising increased EEG power across all examined frequencies that is most pronounced in the delta frequency range centered at 2.8 Hz. Furthermore, our results reveal several

frequency-specific differences in the EEG phenotype between deletion and non-deletion AS. Our findings have important implications for both the basic understanding of AS disease pathophysiology, as well as for clinical applications. In the following, we summarize phenotypic differences, link them to GABAergic signaling, and discuss practical implications for the use of EEG as a biomarker.

### 5.4.1 Excess delta-band oscillations are a robust UBE3A-related AS phenotype

We found excess delta oscillations to be the most prominent AS EEG phenotype (peak frequency 2.8 Hz, 11.08 dB relative to TD controls). This result is well in line with clinical observations of qualitatively abnormal EEG activity in AS (Boyd et al. 1988; Laan and Vein 2005; Williams 2005) and a recent publication by Sidorov and colleagues that demonstrated a robust, quantitative increase in relative power in the delta frequency range (Sidorov et al. 2017). Our results extend previous work in several directions: (1) We showed that EEG power is elevated across a broad range of frequencies (i.e. all frequencies analyzed, 1 – 32 Hz) and, consequently, absolute delta power better separates AS and TD controls as compared to relative delta power. The origin of this unspecific increase of the EEG signal power is unknown, and it is unclear if it relates to neurophysiological or, alternatively, anatomical abnormalities (e.g., altered tissue conductivities). (2) We characterized the developmental trajectory across a broad age range (1 – 18 years) and showed that both the delta oscillation peak frequency and delta power increase (relative to TD controls) is stable across development. (3) We found that the delta-band AS phenotype is more pronounced for deletion as compared to non-deletion AS at young ages, though future studies with better age-matched data at younger ages are needed elaborate on this finding. (4) Finally, we showed the delta-band power increase in AS is wide-spread but

strongest at temporal electrodes. The pathophysiological mechanisms underlying the delta-band EEG phenotype are unknown; nonetheless, our results provide some insights. The observation that the delta EEG phenotype is present in both deletion and non-deletion AS suggests that it is driven by down-stream effects of *UBE3A* disruption. For instance, tonic GABAergic inhibition impaired through disruption of UBE3A-dependent GAT1 degradation (Egawa et al. 2012) might underlie the delta EEG phenotype.

### 5.4.2 Theta and beta-band oscillations index non-UBE3A specific pathophysiology in deletion AS

Deletion AS has a more severe clinical presentation than non-deletion AS (Gentile et al. 2010; Lossie et al. 2001; Minassian et al. 1998; Moncla et al. 1999). Our results reveal two electrophysiological signatures that differ between AS genotypes that may underlie the more severe symptomatology of deletion AS.

First, we confirmed the hypothesis – put forward in the introduction – that beta-band power is decreased in deletion AS compared to non-deletion AS. This builds on recent work in Dup15q syndrome (Frohlich et al. 2016; Urraca et al. 2013) suggesting that EEG beta-band activity reflects a gene-dose effect of the three $GABA_AR$ subunit genes (*GABRA5*, *GABRB3*, and *GABRG3*) manifesting in altered $GABA_AR$ density and, consequently, in altered network dynamics. Notably, the spatial topography of the beta-band modulation in Dup15q syndrome and AS are very different (Fig. 5.7B,C, *cf.* Fig. 2.2 (Frohlich et al. 2016)). This may be expected if certain brain areas start from a state where beta oscillations can be upregulated – but not downregulated, while other brain areas start from a state where beta oscillations can be down-regulated – but not further upregulated. While the anatomical generators underlying our

finding remain unknown, the observation of lower beta power in the deletion AS genotype nonetheless adds to the rationale for targeting $GABA_A$Rs in the group of neurodevelopmental disorders affecting the β3-α5-γ3 $GABA_A$R subunit gene cluster (i.e., Angelman syndrome, Prader-Will syndrome, and Dup15q syndrome).

The most prominent difference between AS genotypes, however, was not anticipated by our hypotheses: oscillatory activity in the theta frequency range, which is present only for the deletion AS genotype (peak frequency: f = 5.3 Hz). Rhythmic theta in AS has been described qualitatively in previous publications (Dan and Boyd 2003; Sugimoto et al. 1992; Valente et al. 2003; Vendrame et al. 2012), but to the best of our knowledge, our work is the first to quantify excess theta oscillations and to link them to the deletion AS genotype. Given that $GABA_A$Rs are critically involved in shaping neuronal dynamics, including most known oscillatory processes measured with EEG (Steriade and Timofeev 2003; X.-J. Wang 2010; Womelsdorf et al. 2014), deletions of *GABRA5*, *GABRB3*, and *GABRG3* are the most likely cause of the AS genotype differences observed in our study. Nonetheless, deletion AS is hemizygous for several other genes spared in non-deletion genotype. Thus, we cannot rule out contributions from genes common to both deletions classes beyond the β3-α5-γ3 $GABA_A$R subunit gene cluster, though EEG effects related to these other genes are unknown. Other important 15q11-q13 genes that are not shared by the two major deletion classes (class I and class II), e.g., *CYFIP1*, can be effectively ruled out as explanations for the EEG effect within the limits of the statistical power of our study.

### 5.4.3 $GABA_AR$ hypothesis provides testable predictions

As argued above, the $GABA_AR$ β3-α5-γ3 subunit gene cluster most likely underlies the electrophysiological differences between AS deletion and non-deletion genotypes. This $GABA_AR$ hypothesis provides specific, falsifiable predictions. Haploinsufficiency of the $GABA_AR$ β3-α5-γ3 subunit gene cluster should (1) be sufficient to induce the theta and beta EEG phenotype observed in deletion AS and (2) be insufficient to induce the AS delta phenotype. In fact, a population that allows one to test these hypotheses exists. Prader-Willi syndrome (PWS) is a neurogenetic disorder characterized by delayed development, hyperphagia, and obesity and generally caused by either a paternal 15q11-q13 deletion or maternal UPD of chromosome 15 (Cassidy and Driscoll 2009). Since *UBE3A* is expressed maternally, *UBE3A* expression levels are presumably normal in the PWS deletion genotype, whereas maternal UPD PWS cases should overexpress *UBE3A*. At the same time, individuals with deletion PWS (but not maternal UPD) have hemizygocity of the $GABA_AR$ β3-α5-γ3 subunit gene cluster, likely causing the same haploinsufficiency of these genes observed in deletion AS. Indeed, this speculation is supported by the finding of reduced $GABA_AR$ density in PWS (Lucignani et al. 2004). The foregoing makes the deletion PWS genotype an ideal *UBE3A*-normal-expression control group for testing our theta EEG hypothesis. Similarly, PWS caused by maternal UPD is also an ideal $GABA_AR$-normal control group for testing our beta EEG hypothesis.

Another avenue for testing our $GABA_AR$ hypothesis is pre-clinical experiments in knock-out animals. It has been reported that maternal *Ube3a* knockout mice have an EEG phenotype that resembles excessive low frequency oscillations seen in AS (Born et al. 2017; Judson et al. 2016; Sidorov et al. 2017), though further work is needed to understand differences between

mouse lines. DeLorey and colleagues reported abnormal EEG in a *gabrb3* knockout mouse line (DeLorey et al. 1998), but it remains to be established whether such mice have excessive theta and/or reduced beta-band oscillations and, moreover, would show all EEG features if crossed with *Ube3a* knock-out mice.

**5.4.4 EEG as a biomarker of AS**

For clinical development of treatments for AS, biomarkers that quantify the disease pathophysiology and index a treatment response are of critical importance. Our results corroborate previous work suggesting delta-band EEG power as a highly promising biomarker for AS. In particular, we provide groundwork on developmental trajectory, variances, effect sizes, genotype differences, and spatial topography that may help in planning future studies of EEG biomarkers. Moreover, our work identifies two new EEG signatures – theta-band and beta-band power – as additional biomarkers.

Our work provides evidence that the AS delta-band EEG signature indexes *UBE3A*-related pathophysiology, while the deletion AS theta-band and beta-band EEG signatures index contributions from other genes, most likely $GABA_AR$ β3-α5-γ3 subunit genes. Thus, the meaning and relevance of the biomarker depends on the target of the treatment. If re-expression of *UBE3A* is the main target of the treatment, EEG delta-band power should be the focus of investigation, whereas if the $GABA_ARs$ are the target, theta and beta power should be the focus of investigation. As such, quantitative EEG might provide surrogate endpoints in AS clinical trials.

We characterized delta, theta, and beta power at the group-level peak frequencies identified in the power spectral density. To derive robust EEG biomarkers, broader frequency

ranges around the peak frequencies may be defined (e.g. for theta: power in the range of 2.5 to 4.25 Hz instead of power at the peak at 2.8 Hz). Furthermore, one might utilize an individualized biomarker approach that takes the power at or around each patient's unique peak frequency (rather than the group-level averages identified herein).

The AS EEG signatures in delta, theta, and beta show substantial variability across participants. Some variance may be explained by the participant's state or reflect residual technical or physiological artifacts. However, a substantial portion of the variability is likely physiological. Such heterogeneity may imply a natural partition for stratifying AS patients. Future should investigate this variability and attempt to link it to symptom severity, including degree of intellectual disability, sleep problems, seizure vulnerability, and of onset and severity of epilepsy. Future work may also correlate the EEG phenotype with individual *GABRA5*, *GABRB3*, and *GABRG3* gene expression levels, e.g., as derived from induced pluripotent stem cells (iPSCs).

**5.5 Conclusions**

In conclusion, our results suggest that hemizygosity of $GABA_AR$ subunit genes modulates the *UBE3A*-related electrophysiological phenotype and causes widespread changes in cortical dynamics, manifesting as spectrally specific abnormalities in oscillatory neuronal activity. These electrophysiological abnormalities may underlie the more severe behavioral phenotype of deletion AS. Our work has direct implications for the use of EEG as a biomarker in the clinical development of AS treatments.

# Chapter 6: Summary and conclusions

## 6.1 Summary

In summary, EEG phenotypes, such as power in specific frequency bands, may be quantified as biomarkers that hold promise in guiding clinical trials for NDDs by indicating a treatment response or drug target engagement. To deploy EEG biomarkers in clinical trials for NDDs, the biomarkers must be understood in a developmental context. Thus, future studies should continue to examine the developmental trajectory of the delta EEG phenotype in AS using more longitudinal data (as most data points in Chapter 5 were cross sectional; see Fig. 5.2B). The beta EEG phenotype in Dup15q syndrome should also be examined longitudinally, as all data in this dissertation describe this phenotype cross-sectionally. EEG biomarkers must also be examined in the context of physiological state changes such as sleep and arousal, and test-retest reliability must be quantified by future work. With these broad considerations in mind, the preceding chapters have demonstrated several points:

(1) EEG frequency stability is inversely related to age in early childhood typical development. This is likely because synaptic pruning sculpts stable neurophysiological oscillations from neural noise in early brain development.

(2) Neurophysiological oscillations, which theoretically reflect biological processes such as synaptic pruning or neurotransmitter dysregulation in childhood development, may be utilized as markers of pathology in neurodevelopmental disorders.

(3) High amplitude spontaneous beta oscillations constitute an EEG phenotype of Dup15q syndrome that distinguishes children with this disorder from age-matched TD and age-and-IQ-matched ASD controls.

(4) The beta EEG phenotype in Dup15q syndrome is independent of *UBE3A* dysfunction and most likely reflects overexpression of $GABA_A$ receptor β3/α5/γ3 subunit genes.

(5) The delta EEG phenotype in AS reflects *UBE3A*-related pathology and is modulated by additional 15q genes.

(6) The theta EEG phenotype (characterized by high amplitude theta oscillations) and beta EEG phenotype (characterized by diminished beta oscillations) in AS most likely both reflect deletions of the $GABA_A$ receptor β3/α5/γ3 subunit genes.

(7) The theta EEG phenotype (characterized by high amplitude theta oscillations) and beta EEG phenotype (characterized by diminished beta oscillations) in AS most likely both reflect deletions of the $GABA_A$ receptor β3/α5/γ3 subunit genes.

(8) EEG phenotypes in Dup15q syndrome and AS may be utilized as quantitative biomarkers that serve as markers of disease pathology and target engagement in future clinical trials.

The foregoing conclusions point towards clinical trials for Dup15q syndrome and AS, guided by mechanism-based EEG biomarkers, as a new frontier of drug development. Such biomarkers would utilize neurophysiological oscillations as a readout of gene expression and circuit dysfunction in neurodevelopmental disorders. These conclusions are balanced by several important limitations, each of which may be addressed in future studies:

(1) EEG phenotypes described above have not yet been directly manipulated by gene knockdown studies in animals or iPSCs, nor have they been correlated with gene expression in patients.

(2) EEG phenotypes have not yet been correlated with clinical traits in patients. Identification of such statistical dependencies would strengthen the case that these EEG phenotypes may be used as surrogate endpoints in clinical trials for Dup15q syndrome or AS.

(3) EEG phenotypes in Dup15q syndrome and AS have not yet been directly compared in the same study. Such a comparison would allow investigators to establish that EEG phenotypes may be used for stratification across multiple disorders.

### 6.2 An evolving understanding of EEG biomarkers

Science is not a body of knowledge, but a process. As such, our scientific understanding of this work has evolved since the original publications of earlier chapters in peer-reviewed journals. Below, I list several conclusions that have evolved over the course of this work:

(1) Chapter 2 described the use of frequency variance ($f_v$) to capture abrupt transitions (or phase resets) between transiently stable oscillations in the resting EEG of children. As my Roche mentor and colleague Joerg Hipp has suggested to me following the original publication of this work, the third moment of the instantaneous frequency distribution (kurtosis) may capture phase resets better than the second moment of the distribution used in Chapter 2 (variance). This is because kurtosis is high for distributions with long tails, and phase resets expand the tails of the instantaneous frequency distribution. Thus, future work exploring metastability in EEG recordings as a marker of development should also examine frequency kurtosis.

(2) Chapter 3 reported a delta EEG phenotype of Dup15q syndrome in the form of deficient power as compared with TD and nonsyndromic ASD controls. Indeed, deletions of 15q11-q13 enhance delta power in AS, suggesting an elegant symmetry with our reported finding in duplications 15q11-q13. However, we reported relative power in Chapter 3, which creates normalization artifacts when other large oscillations are also present in the power spectrum. In the case of Dup15q syndrome, high amplitude beta oscillations result in a very large beta peak in the power spectrum, thus reducing the percentage of power accounted for by other frequency bands. The finding of reduced delta power in Dup15q syndrome may thus be a normalization artifact. The largest reduction of power in Dup15q syndrome relative to age-matched TD children is likely found in alpha power, as revealed by a one-tailed test at the TD alpha peak frequency in Chapter 4. However, Figure 4.1A does show qualitatively lower delta power in children with Dup15q syndrome without seizures relative to the age-matched TD cohort. However, we did not perform statistical tests at this frequency in Chapter 4, in part because there was no peak in delta to dictate which frequency bin a test should be performed at. Future studies with greater statistical power may reveal whether Dup15q syndrome truly displays an inverse of the delta EEG phenotype in AS; such a phenotype in Dup15q syndrome could be utilized as a biomarker of *UBE3A* pathology, following the conclusions of Chapter 5.

(3) Chapter 3 reported lower beta power in children with Dup15q syndrome and epilepsy. As discussed above, because we reported relative power in Chapter 3, some findings reported in this chapter may reflect normalization artifacts. Individuals with epilepsy

often have slowing in their interictal EEG (Noachtar and Rémi 2009) which manifests as higher power at lower frequencies. This slowing would artifactually reduce relative beta power in children with epilepsy. A forthcoming study by my group will address the relationship between epilepsy and Dup15q syndrome using absolute power.

(4) Chapter 3 did not find differences between Dup15q syndrome and controls in the theta band. However, Chapter 4 reveals the presence of highly prominent theta peaks in many participants with Dup15q syndrome. Because these participants did not have seizures and were not taking any antiepileptic medications, epilepsy and medication can be reasonably excluded as explanatory variables for these theta oscillations. Moreover, Chapter 5 revealed a theta EEG phenotype in children with deletion AS (the genetic converse of Dup15q syndrome) in the form of highly prominent theta oscillations. Intuitively, one might expect the opposite phenotype in Dup15q syndrome, but perhaps it is also feasible that both increases and decreases in $GABA_A$ receptor subunit gene copy number enhance theta amplitude. Future studies with greater statistical power should look for differences in theta power between Dup15q syndrome and appropriate controls. An ideal control group would be children with intellectual disability without GABAergic etiology, as other etiologies of cognitive impairment (e.g., institutionalization) are also linked to excessive theta power (Marshall et al. 2004).

(5) Chapter 3 did not report a significant effect of scalp region in the ANOVA. Indeed, the Dup15q syndrome beta EEG phenotype is diffuse and seen overly virtually all scalp regions. However, Fig. 4.1D, qualitatively shows that the largest effect sizes ($d > 1$) relative to TD controls at the Dup15q syndrome peak frequency are frontocentral.

Similarly, midazolam causes the largest increases in beta power in central scalp regions in healthy adults (Fig. 4.4D). Clinical trials for Dup15q syndrome that might use beta power as a surrogate endpoint should thus target scalp regions that show the largest difference referenced to controls. Future studies with greater statistical power should thus explore regional scalp effects in beta power between children with Dup15q syndrome and controls (TD children and children with nonsyndromic ASD).

## 6.3 Conclusions

Currently, there are no efficacious pharmaceutical treatments for the core symptoms of ASD. This failure is partly due to the tremendous heterogeneity and multiple etiologies of ASD (Farmer et al. 2013; West et al. 2009). Syndromic forms of ASD such as Dup15q syndrome may represent an entry point for targeted pharmaceutical interventions. Such interventions will be equipped with a mechanistic rationale rooted in GABAergic dysfunction. By characterizing GABAergic etiology in Dup15q syndrome, this work also facilitates progress towards targeted drug interventions in cases of nonsyndromic ASD with similar etiologies (e.g., idiopathic ASD featuring point mutations in *GABRB3*). The 15q11-q13 locus is thus a portal into meaningful understanding of ASD pathophysiology.

## 6.4 Coda

A targeted approach towards studying an ASD risk locus (i.e., 15q) in informative rare diseases has been crucial to the success of the research described herein. What role, however, has the technique of EEG played? EEG is an old technology dating back to 1929. While EEG is used in the diagnosis of several neurological disorders, including epilepsy, coma, and

encephalopathy (Smith 2005), its diagnostic use in psychiatry is currently limited. The FDA did not approve EEG in any psychiatric diagnosis until 2013, when the Neuropsychiatric EEG-Based Assessment Aid (NEBA) system was approved to guide the diagnosis of ADHD (Lenartowicz and Loo 2014). This test uses the ratio of EEG theta to beta power to guide ADHD diagnosis. Yet even this debut is asterisked by criticism from ADHD researchers who view the approval as premature (Lenartowicz and Loo 2014), in part due to failed replication attempts (Ogrim et al. 2012).

Given that EEG was invented before the vast majority of people alive today were born, its prospects of truly penetrating psychiatry may seem glum. However, Lenartowicz and Loo note that, with respect to ADHD, "the relatively high (>90%) sensitivities and specificities reported using EEG, far exceed the most advanced of classification attempts using anatomical and functional MRI data" (Lenartowicz and Loo 2014). MRI (magnetic resonance imaging) is a far newer technology (Hinshaw et al. 1978), yet it provides very different information than EEG. The temporal precision of EEG is essential for observing neurophysiological oscillations that, as this dissertation has demonstrated, yield valuable information concerning circuit and molecular level pathophysiology (e.g., GABAergic or *UBE3A*-related dysfunction). Furthermore, EEG has undergone incredible refinement since the era of Hans Berger from an analog, pen-and-needle technology to a digital technology amendable to many mathematical tools (Nuwer 1997). These mathematical tools include Hilbert transforms, Fourier transforms, and wavelet convolutions such as those described in this dissertation.

New mathematical tools will continue to shape the future of EEG and neuroimaging research. Perhaps the most promising of these new tools is machine learning (Iniesta et al.

2016), a technique not mentioned yet in this dissertation. Machine learning is a field of artificial intelligence that allows computers to learn and find patterns in data. Identification of these patterns often uses multivariate feature vectors constructed from many measures (e.g., EEG measures from many channels, or EEG combined with MRI and genomics data). Recently, machine learning has shown promise in classifying infants according to ASD risk from EEG and MRI data (Bosl et al. 2011; Hazlett et al. 2017). Similarly, in the field of ADHD research, Lenartowicz and Loo advocate for multivariate measures to be used for ADHD classification (Lenartowicz and Loo 2014), as these approaches better capture variability within a heterogenous sample as compared with a univariate measure (e.g., that used by the NEBA system).

Indeed, machine learning may be the officiant presiding over the marriage of behavior and the brain. This process, however, will not be an outsourcing of all intellectual work to computers. Rather, it will still require quality data, careful hypotheses, and good science. I hope the hypotheses laid forth in this dissertation will guide future investigations of new ASD biomarkers, far too subtle to be observed in a raw EEG trace, detectable perhaps only using large datasets and the newest machine learning algorithms. With the right data, the right hypotheses, and the right science, we may better understand the brain-behavior relationship in neurodevelopmental disorders. In the words of Buzsáki, “It may turn out that the rhythms of the brain are also the rhythms of the mind” (Buzsáki 2006).

**References**


Abrahams, B. S., & Geschwind, D. H. (2008). Advances in autism genetics: on the threshold of a new neurobiology. *Nature reviews. Genetics*, *9*(5), 341.

Al Ageeli, E., Drunat, S., Delanoë, C., Perrin, L., Baumann, C., Capri, Y., et al. (2014). Duplication of the 15q11-q13 region: clinical and genetic study of 30 new cases. *European journal of medical genetics*, *57*(1), 5–14.

Albrecht, U., Sutcliffe, J. S., Cattanach, B. M., Beechey, C. V., Armstrong, D., Eichele, G., & Beaudet, A. L. (1997). Imprinted expression of the murine Angelman syndrome gene, Ube3a, in hippocampal and Purkinje neurons. *Nature genetics*, *17*(1), 75–78.

Amari S-I, Cichocki A, & Yang HH. (1996). A new learning algorithm for blind source seperation. *Advances in Neural Informaton Processing Systems*, (8), 757–763.

American Psychiatric Association. (2013). *The Diagnostic and Statistical Manual of Mental Disorders: DSM 5* (5th edition.). bookpointUS.

Bak P, Tang C, & Wiesenfeld K. (1987). Self-organized criticality: an explanation of 1/f noise. *Physical Review Letters*, *59*(4), 381–384.

Bak P, Tang C, & Wiesenfeld K. (1988). Self-organized criticality. *Physical Review A*, *38*(1), 364–374.

Baker, S. N. (2007). Oscillatory interactions between sensorimotor cortex and the periphery. *Current opinion in neurobiology*, *17*(6), 649–655.

Battaglia, A. (2008). The inv dup (15) or idic (15) syndrome (Tetrasomy 15q). *Orphanet journal of rare diseases*, *3*(1), 30.

Beck, A. (1890). Die ströme der nervencentren. *Centralbl Physiol*, *4*, 572–573.

Beggs, J. M., & Plenz, D. (2003). Neuronal avalanches in neocortical circuits. *The Journal of neuroscience: the official journal of the Society for Neuroscience*, *23*(35), 11167–11177.

Beggs, J. M., & Plenz, D. (2004). Neuronal avalanches are diverse and precise activity patterns that are stable for many hours in cortical slice cultures. *The Journal of neuroscience: the official journal of the Society for Neuroscience*, *24*(22), 5216–5229. doi:10.1523/JNEUROSCI.0540-04.2004

Bell, A. J., & Sejnowski, T. J. (1995). An information-maximization approach to blind separation and blind deconvolution. *Neural computation*, *7*(6), 1129–1159.

Berens, P. (2009). CircStat: A MATLAB toolbox for circular statistics. *Journal of Statistical Software*, *31*(10), 1–21.

Berger, H. (1929). Über das elektrenkephalogramm des menschen. *European Archives of Psychiatry and Clinical Neuroscience*, *87*(1), 527–570.

Berrios, J., Stamatakis, A. M., Kantak, P. A., McElligott, Z. A., Judson, M. C., Aita, M., et al. (2016). Loss of UBE3A from TH-expressing neurons suppresses GABA co-release and enhances VTA-NAc optical self-stimulation. *Nature communications*, *7*, 10702.

Bianchi, S., Stimpson, C. D., Duka, T., Larsen, M. D., Janssen, W. G. M., Collins, Z., et al. (2013). Synaptogenesis and development of pyramidal neuron dendritic morphology in the chimpanzee neocortex resembles humans. *Proceedings of the National Academy of Sciences of the United States of America*, *110 Suppl 2*, 10395–10401. doi:10.1073/pnas.1301224110

Biomarkers Definitions Working Group, Atkinson Jr, A. J., Colburn, W. A., DeGruttola, V. G., DeMets, D. L., Downing, G. J., et al. (2001). Biomarkers and surrogate endpoints:

preferred definitions and conceptual framework. *Clinical Pharmacology & Therapeutics*, *69*(3), 89–95.

Bird, L. M. (2014). Angelman syndrome: review of clinical and molecular aspects. *The application of clinical genetics*, *7*, 93.

Bishop, K. M. (2017). Progress and promise of antisense oligonucleotide therapeutics for central nervous system diseases. *Neuropharmacology*, *120*, 56–62.

Bliss, T. V., & Collingridge, G. L. (1993). A synaptic model of memory: long-term potentiation in the hippocampus. *Nature*, *361*(6407), 31–39. doi:10.1038/361031a0

Born, H. A., Dao, A. T., Levine, A. T., Lee, W. L., Mehta, N. M., Mehra, S., et al. (2017). Strain-dependence of the Angelman Syndrome phenotypes in Ube3a maternal deficiency mice. *Scientific Reports*, *7*(1), 8451.

Bosl, W., Tierney, A., Tager-Flusberg, H., & Nelson, C. (2011). EEG complexity as a biomarker for autism spectrum disorder risk. *BMC medicine*, *9*, 18. doi:10.1186/1741-7015-9-18

Boyd, S., Harden, A., & Patton, M. (1988). The EEG in early diagnosis of the Angelman (happy puppet) syndrome. *European journal of pediatrics*, *147*(5), 508–513.

Bruining, H., Passtoors, L., Goriounova, N., Jansen, F., Hakvoort, B., de Jonge, M., & Poil, S.-S. (2015). Paradoxical benzodiazepine response: a rationale for bumetanide in neurodevelopmental disorders? *Pediatrics*, peds-2014.

Buchsbaum, M. S., Hazlett, E., Sicotte, N., Stein, M., Wu, J., & Zetin, M. (1985). Topographic EEG changes with benzodiazepine administration in generalized anxiety disorder. *Biological psychiatry*, *20*(8), 837–842.

Buiting, K., Williams, C., & Horsthemke, B. (2016). Angelman syndrome—insights into a rare neurogenetic disorder. *Nature Reviews Neurology*, *12*(10), nrneurol-2016.

Buxbaum, J., Silverman, J., Smith, C., Greenberg, D., Kilifarski, M., Reichert, J., et al. (2002). Association between a GABRB3 polymorphism and autism. *Molecular psychiatry*, *7*(3), 311.

Buzsáki, G. (2006). *Rhythms of the Brain*. New York: Oxford University Press.

Buzsáki, G., & Draguhn, A. (2004). Neuronal oscillations in cortical networks. *Science*, *304*(5679), 1926–1929.

Buzsáki, G., & Wang, X.-J. (2012). Mechanisms of gamma oscillations. *Annual review of neuroscience*, *35*, 203–225.

Cantor, D. S., Thatcher, R. W., Hrybyk, M., & Kaye, H. (1986). Computerized EEG analyses of autistic children. *Journal of autism and developmental disorders*, *16*(2), 169–187.

Cassidy, S. B., & Driscoll, D. J. (2009). Prader–Willi syndrome. *European Journal of Human Genetics*, *17*(1), 3.

Catarino, A., Churches, O., Baron-Cohen, S., Andrade, A., & Ring, H. (2011). Atypical EEG complexity in autism spectrum conditions: a multiscale entropy analysis. *Clinical Neurophysiology: Official Journal of the International Federation of Clinical Neurophysiology*, *122*(12), 2375–2383. doi:10.1016/j.clinph.2011.05.004

Chamberlain, S. J., & Lalande, M. (2010). Angelman syndrome, a genomic imprinting disorder of the brain. *Journal of Neuroscience*, *30*(30), 9958–9963.

Chan, A. S., Sze, S. L., & Cheung, M. (2007). Quantitative electroencephalographic profiles for children with autistic spectrum disorder. *Neuropsychology*, *21*(1), 74.

Chen, C.-H., Huang, C.-C., Cheng, M.-C., Chiu, Y.-N., Tsai, W.-C., Wu, Y.-Y., et al. (2014). Genetic analysis of GABRB3 as a candidate gene of autism spectrum disorders. *Molecular autism*, *5*(1), 36.

Chez, M. G., Chang, M., Krasne, V., Coughlan, C., Kominsky, M., & Schwartz, A. (2006). Frequency of epileptiform EEG abnormalities in a sequential screening of autistic patients with no known clinical epilepsy from 1996 to 2005. *Epilepsy & Behavior*, *8*(1), 267–271.

Cimino, G. (1999). Reticular theory versus neuron theory in the work of Camillo Golgi.

Clayton-Smith, J. (1993). Clinical research on Angelman syndrome in the United Kingdom: observations on 82 affected individuals. *American journal of medical genetics*, *46*(1), 12–15.

Clayton-Smith, J., & Laan, L. (2003). Angelman syndrome: a review of the clinical and genetic aspects. *Journal of medical genetics*, *40*(2), 87–95.

Coenen, A., Fine, E., & Zayachkivska, O. (2014). Adolf Beck: A forgotten pioneer in electroencephalography. *Journal of the History of the Neurosciences*, *23*(3), 276–286.

Coffey, D. S. (1998). Self-organization, complexity and chaos: the new biology for medicine. *Nature medicine*, *4*(8), 882–885.

Cook Jr, E. H., Courchesne, R. Y., Cox, N. J., Lord, C., Gonen, D., Guter, S. J., et al. (1998). Linkage-disequilibrium mapping of autistic disorder, with 15q11-13 markers. *The American Journal of Human Genetics*, *62*(5), 1077–1083.

Cook Jr, E. H., Lindgren, V., Leventhal, B. L., Courchesne, R., Lincoln, A., Shulman, C., et al. (1997). Autism or atypical autism in maternally but not paternally derived proximal 15q duplication. *American journal of human genetics*, *60*(4), 928.

Cox, A., Klein, K., Charman, T., Baird, G., Baron-Cohen, S., Swettenham, J., et al. (1999). Autism spectrum disorders at 20 and 42 months of age: stability of clinical and ADI-R

diagnosis. *Journal of child psychology and psychiatry, and allied disciplines*, *40*(5), 719–732.

Crunelli, V., & Leresche, N. (2002). Childhood absence epilepsy: genes, channels, neurons and networks. *Nature Reviews Neuroscience*, *3*(5), 371.

Dagli, A., Buiting, K., & Williams, C. (2011). Molecular and clinical aspects of Angelman syndrome. *Molecular syndromology*, *2*(3–5), 100–112.

Dan, B., & Boyd, S. (2003). Angelman syndrome reviewed from a neurophysiological perspective. The UBE3A-GABRB3 hypothesis. *Neuropediatrics*, *34*(04), 169–176.

de la Torre-Ubieta, L., Won, H., Stein, J. L., & Geschwind, D. H. (2016). Advancing the understanding of autism disease mechanisms through genetics. *Nature medicine*, *22*(4), 345.

De Luca, C., & Leventer, R. (2010). Developmental trajectories of executive funtions across the lifespan. In *Executive Functions and the Frontal Lobes: A Lifespan Perspective* (pp. 23–56). New York: Taylor & Francis.

DeLorey, T., Handforth, A., Anagnostaras, S., Homanics, G., Minassian, B., Asatourian, A., et al. (1998). Mice lacking the β3 subunit of the GABAA receptor have the epilepsy phenotype and many of the behavioral characteristics of Angelman syndrome. *Journal of Neuroscience*, *18*(20), 8505–8514.

Delorme, A., & Makeig, S. (2004). EEGLAB: an open source toolbox for analysis of single-trial EEG dynamics including independent component analysis. *Journal of neuroscience methods*, *134*(1), 9–21. doi:10.1016/j.jneumeth.2003.10.009

Dindot, S. V., Antalffy, B. A., Bhattacharjee, M. B., & Beaudet, A. L. (2007). The Angelman syndrome ubiquitin ligase localizes to the synapse and nucleus, and maternal deficiency

results in abnormal dendritic spine morphology. *Human molecular genetics*, *17*(1), 111–118.

DiStefano, C., Gulsrud, A., Huberty, S., Kasari, C., Cook, E., Reiter, L. T., et al. (2016). Identification of a distinct developmental and behavioral profile in children with Dup15q syndrome. *Journal of neurodevelopmental disorders*, *8*(1), 19.

Dixon, J. B., Dixon, M. E., & O'brien, P. E. (2003). Depression in association with severe obesity: changes with weight loss. *Archives of internal medicine*, *163*(17), 2058–2065.

Domino, E., French, J., Pohorecki, R., Galus, C., & Pandit, S. (1989). Further observations on the effects of subhypnotic doses of midazolam in normal volunteers. *Psychopharmacology bulletin*, *25*(3), 460–465.

DuBose, A. J., Johnstone, K. A., Smith, E. Y., Hallett, R. A., & Resnick, J. L. (2010). Atp10a, a gene adjacent to the PWS/AS gene cluster, is not imprinted in mouse and is insensitive to the PWS-IC. *Neurogenetics*, *11*(2), 145–151.

Egawa, K., Asahina, N., Shiraishi, H., Kamada, K., Takeuchi, F., Nakane, S., et al. (2008). Aberrant somatosensory-evoked responses imply GABAergic dysfunction in Angelman syndrome. *Neuroimage*, *39*(2), 593–599.

Egawa, K., Kitagawa, K., Inoue, K., Takayama, M., Takayama, C., Saitoh, S., et al. (2012). Decreased Tonic Inhibition in Cerebellar Granule Cells Causes Motor Dysfunction in a Mouse Model of Angelman Syndrome. *Science Translational Medicine*, *4*(163), 163ra157-163ra157. doi:10.1126/scitranslmed.3004655

Eldridge, J., Lane, A. E., Belkin, M., & Dennis, S. (2014). Robust features for the automatic identification of autism spectrum disorder in children. *Journal of Neurodevelopmental Disorders*, *6*(1), 12. doi:10.1186/1866-1955-6-12

Elliot, C.D. (2007). *Differential Abilitity Scales (2nd Ed)*. San Antonio: Harcourt Assessment.

Errington, A. C., Di Giovanni, G., Crunelli, V., & Cope, D. W. (2011). mGluR control of interneuron output regulates feedforward tonic GABAA inhibition in the visual thalamus. *Journal of Neuroscience*, *31*(23), 8669–8680.

Fain, G. L. (1999). *Molecular and cellular physiology of neurons*. Harvard University Press.

Fallon, J. (2013). *The psychopath inside: A neuroscientist's personal journey into the dark side of the brain*. Penguin.

Farmer, C., Thurm, A., & Grant, P. (2013). Pharmacotherapy for the core symptoms in autistic disorder: current status of the research. *Drugs*, *73*(4), 303–314.

Fatemi, S. H., Folsom, T. D., Kneeland, R. E., & Liesch, S. B. (2011). Metabotropic glutamate receptor 5 upregulation in children with autism is associated with underexpression of both Fragile X mental retardation protein and GABAA receptor beta 3 in adults with autism. *Anatomical record (Hoboken, N.J.: 2007)*, *294*(10), 1635–1645. doi:10.1002/ar.21299

Fatemi, S. H., Reutiman, T. J., Folsom, T. D., Rooney, R. J., Patel, D. H., & Thuras, P. D. (2010). mRNA and protein levels for GABAAalpha4, alpha5, beta1 and GABABR1 receptors are altered in brains from subjects with autism. *Journal of autism and developmental disorders*, *40*(6), 743–750. doi:10.1007/s10803-009-0924-z

Feinberg, I. (1982). Schizophrenia: caused by a fault in programmed synaptic elimination during adolescence? *Journal of psychiatric research*, *17*(4), 319–334.

Fell, J., Röschke, J., & Beckmann, P. (1993). Deterministic chaos and the first positive Lyapunov exponent: a nonlinear analysis of the human electroencephalogram during sleep. *Biological Cybernetics*, *69*(2), 139–146.

Feshchenko, V. A., Veselis, R. A., & Reinsel, R. A. (1997). Comparison of the EEG effects of midazolam, thiopental, and propofol: the role of underlying oscillatory systems. *Neuropsychobiology*, *35*(4), 211–220.

Feucht, M., Fuchs, K., Pichlbauer, E., Hornik, K., Scharfetter, J., Goessler, R., et al. (1999). Possible association between childhood absence epilepsy and the gene encoding GABRB3. *Biological psychiatry*, *46*(7), 997–1002.

Finucane, B. M., Lusk, L., Arkilo, D., Chamberlain, S., Devinsky, O., Dindot, S., et al. (2016). 15q duplication syndrome and related disorders.

Fontaine, M. (2013). On Being Sane in an Insane Place–The Rosenhan Experiment in the Laboratory of Plautus' Epidamnus. *Current Psychology*, *32*(4), 348–365.

Fountain, C., King, M. D., & Bearman, P. S. (2011). Age of diagnosis for autism: individual and community factors across 10 birth cohorts. *Journal of epidemiology and community health*, *65*(6), 503–510. doi:10.1136/jech.2009.104588

Freeman, W J, Burke, B., & Holmes, M. (2003). Aperidoic phase re-setting in scalp EEG of beta-gamma oscillations by state transitions at alpha-theta rates. *Human brain mapping*, (19), 248–272.

Freeman, W.J., & Kozma, R. (2010). Freeman's mass action. *Scholarpedia*, *5*(1), 8040.

Freeman, W. J. (2003). Evidence from human scalp electroencephalograms of global chaotic itinerancy. *Chaos (Woodbury, N.Y.)*, *13*(3), 1067–1077. doi:10.1063/1.1596553

Freeman, W. J. (2004). Origin, structure, and role of background EEG activity. Part 1. Analytic amplitude. *Clinical neurophysiology: official journal of the International Federation of Clinical Neurophysiology*, *115*(9), 2077–2088. doi:10.1016/j.clinph.2004.02.029

Freeman, W. J, & Holmes, M. D. (2005). Metastability, instability, and state transition in neocortex. *Neural networks: the official journal of the International Neural Network Society*, *18*(5–6), 497–504. doi:10.1016/j.neunet.2005.06.014

Freeman, W. J., Holmes, M. D., West, G. A., & Vanhatalo, S. (2006). Fine spatiotemporal structure of phase in human intracranial EEG. *Clinical neurophysiology: official journal of the International Federation of Clinical Neurophysiology*, *117*(6), 1228–1243. doi:10.1016/j.clinph.2006.03.012

Freeman, W.J. (2004). Origin, Structure, and Role of Background EEG Activity. Part 2: Analytic Phase. *Clinical Neurophysiology*, (115), 2089–2107.

Freemon, F. R. (1994). Galen's ideas on neurological function. *Journal of the History of the Neurosciences*, *3*(4), 263–271.

Fries, P. (2015). Rhythms for cognition: communication through coherence. *Neuron*, *88*(1), 220–235.

Friston, K. J. (1996). Theoretical neurobiology and schizophrenia. *British medical bulletin*, *52*(3), 644–655.

Friston, K. J. (2000). The labile brain. I. Neuronal transients and nonlinear coupling. *Philosophical transactions of the Royal Society of London. Series B, Biological sciences*, *355*(1394), 215–236. doi:10.1098/rstb.2000.0560

Fritschy, J.-M. (2008). Epilepsy, E/I balance and GABAA receptor plasticity. *Frontiers in molecular neuroscience*, *1*, 5.

Frohlich, J., Senturk, D., Saravanapandian, V., Golshani, P., Reiter, L. T., Sankar, R., et al. (2016). A quantitative electrophysiological biomarker of duplication 15q11. 2-q13. 1 syndrome. *PloS one*, *11*(12), e0167179.

Frohlich, J., & van Horn, J. D. (2014). Reviewing the ketamine model for schizophrenia. *Journal of psychopharmacology (Oxford, England)*, *28*(4), 287–302. doi:10.1177/0269881113512909

Gaetz, W., Edgar, J. C., Wang, D., & Roberts, T. P. (2011). Relating MEG measured motor cortical oscillations to resting γ-aminobutyric acid (GABA) concentration. *Neuroimage*, *55*(2), 616–621.

Gaugler, T., Klei, L., Sanders, S. J., Bodea, C. A., Goldberg, A. P., Lee, A. B., et al. (2014). Most genetic risk for autism resides with common variation. *Nature genetics*, *46*(8), 881.

Gentile, J. K., Tan, W.-H., Horowitz, L. T., Bacino, C. A., Skinner, S. A., Barbieri-Welge, R., et al. (2010). A neurodevelopmental survey of Angelman syndrome with genotype-phenotype correlations. *Journal of developmental and behavioral pediatrics: JDBP*, *31*(7), 592.

Geschwind, D. H. (2008). Autism: many genes, common pathways? *Cell*, *135*(3), 391–395.

Ghanbari, Y., Bloy, L., Christopher Edgar, J., Blaskey, L., Verma, R., & Roberts, T. P. L. (2013). Joint Analysis of Band-Specific Functional Connectivity and Signal Complexity in Autism. *Journal of Autism and Developmental Disorders*. doi:10.1007/s10803-013-1915-7

Granger, B. (1996). [Synaptogenesis and synaptic pruning: role in triggering schizophrenia]. *Presse médicale (Paris, France: 1983)*, *25*(33), 1595–1598.

Greenblatt, D. J., Ehrenberg, B. L., Culm, K. E., Scavone, J. M., Corbett, K. E., Friedman, H. L., et al. (2004). Kinetics and EEG Effects of Midazolam during and after 1-Minute, 1-Hour, and 3-Hour Intravenous Infusions. *The Journal of Clinical Pharmacology*, *44*(6), 605–611.

Greenblatt, D. J., Ehrenberg, B. L., Gunderman, J., Locniskar, A., Scavone, J. M., Harmatz, J. S., & Shader, R. I. (1989). Pharmacokinetic and electroencephalographic study of intravenous diazepam, midazolam, and placebo. *Clinical Pharmacology & Therapeutics*, *45*(4), 356–365.

Greer, P. L., Hanayama, R., Bloodgood, B. L., Mardinly, A. R., Lipton, D. M., Flavell, S. W., et al. (2010). The Angelman Syndrome protein Ube3A regulates synapse development by ubiquitinating arc. *Cell*, *140*(5), 704–716.

Gross, C. G. (1987). Early history of neuroscience. *Encyclopedia of neuroscience*, *2*, 843–846.

Guffanti, G., Lievers, L. S., Bonati, M. T., Marchi, M., Geronazzo, L., Nardocci, N., et al. (2011). Role of UBE3A and ATP10A genes in autism susceptibility region 15q11-q13 in an Italian population: a positive replication for UBE3A. *Psychiatry research*, *185*(1–2), 33–38.

Hazlett, H. C., Gu, H., Munsell, B. C., Kim, S. H., Styner, M., Wolff, J. J., et al. (2017). Early brain development in infants at high risk for autism spectrum disorder. *Nature*, *542*(7641), 348.

He, B. J. (2014). Scale-free brain activity: past, present, and future. *Trends in cognitive sciences*. doi:10.1016/j.tics.2014.04.003

Hebb, D. (1949). *The Organization of Behavior: a Neuropsychological Theory*. New York: Wiley.

Hertz-Picciotto, I., & Delwiche, L. (2009). The rise in autism and the role of age at diagnosis. *Epidemiology (Cambridge, Mass.)*, *20*(1), 84–90. doi:10.1097/EDE.0b013e3181902d15

Hinshaw, W., Andrew, E., Bottomley, P., Holland, G., Moore, W., & Worthington, B. (1978). Display of cross sectional anatomy by nuclear magnetic resonance imaging. *The British journal of radiology*, *51*(604), 273–280.

Hofstadter, D. (1979). *Gödel, Escher, Bach: An Eternal Golden Braid*. New York: Basic Books.

Hogart, A., Patzel, K. A., & LaSalle, J. M. (2008). Gender influences monoallelic expression of ATP10A in human brain. *Human genetics*, *124*(3), 235–242.

Hogart, A., Wu, D., LaSalle, J. M., & Schanen, N. C. (2010). The comorbidity of autism with the genomic disorders of chromosome 15q11. 2-q13. *Neurobiology of disease*, *38*(2), 181–191.

Holopainen, I. E., Metsähonkala, E. L., Kokkonen, H., Parkkola, R. K., Manner, T. E., Någren, K., & Korpi, E. R. (2001). Decreased binding of [11C]flumazenil in Angelman syndrome patients with GABA(A) receptor beta3 subunit deletions. *Annals of Neurology*, *49*(1), 110–113.

Hughes, J. R. (1958). Post-tetanic potentiation. *Physiological reviews*, *38*(1), 91–113.

Huttenlocher, P., & de Courten, C. (1987). The development of synapses in striate cortex of man. *Human neurobiology*, *6*(1), 1–9.

Huttenlocher, P. R. (1979). Synaptic density in human frontal cortex - developmental changes and effects of aging. *Brain research*, *163*(2), 195–205.

Huttenlocher, P. R., & Dabholkar, A. S. (1997). Regional differences in synaptogenesis in human cerebral cortex. *The Journal of comparative neurology*, *387*(2), 167–178.

Hyvarinen, A. (1999a). Fast and robust fixed-point algorithms for independent component analysis. *IEEE transactions on Neural Networks*, *10*(3), 626–634.

Hyvarinen, A. (1999b). Fast ICA for noisy data using Gaussian moments (Vol. 5, pp. 57–61). Presented at the Circuits and Systems, 1999. ISCAS'99. Proceedings of the 1999 IEEE International Symposium on, IEEE.

Iniesta, R., Stahl, D., & McGuffin, P. (2016). Machine learning, statistical learning and the future of biological research in psychiatry. *Psychological medicine*, *46*(12), 2455–2465.

Inoki, K., Corradetti, M. N., & Guan, K.-L. (2005). Dysregulation of the TSC-mTOR pathway in human disease. *Nature genetics*, *37*(1), 19.

Insel, T. (2013, April 29). Post by Former NIMH Director Thomas Insel: Transforming Diagnosis. *Blog posts by Thomas Insel*. https://www.nimh.nih.gov/about/directors/thomas-insel/blog/2013/transforming-diagnosis.shtml. Accessed 26 June 2018

Insel, T., Cuthbert, B., Garvey, M., Heinssen, R., Pine, D. S., Quinn, K., et al. (2010). Research domain criteria (RDoC): toward a new classification framework for research on mental disorders.

Isles, A. R., Ingason, A., Lowther, C., Walters, J., Gawlick, M., Stöber, G., et al. (2016). Parental origin of interstitial duplications at 15q11. 2-q13. 3 in schizophrenia and neurodevelopmental disorders. *PLoS genetics*, *12*(5), e1005993.

Janjarasjitt, S., Scher, M. S., & Loparo, K. A. (2008). Nonlinear dynamical analysis of the neonatal EEG time series: the relationship between neurodevelopment and complexity. *Clinical Neurophysiology: Official Journal of the International Federation of Clinical Neurophysiology*, *119*(4), 822–836. doi:10.1016/j.clinph.2007.11.012

Jeste, Shafali S., Frohlich, J., & Loo, S. K. (2015). Electrophysiological biomarkers of diagnosis and outcome in neurodevelopmental disorders. *Current Opinion in Neurology*. doi:10.1097/WCO.0000000000000181

Jeste, Shafali S, & Geschwind, D. H. (2016). Clinical trials for neurodevelopmental disorders: At a therapeutic frontier. *Science translational medicine*, *8*(321), 321fs1-321fs1.

Jeste, Shafali Spurling, & Tuchman, R. (2015). Autism spectrum disorder and epilepsy: two sides of the same coin? *Journal of child neurology*, *30*(14), 1963–1971.

Jones, K. A., Han, J. E., DeBruyne, J. P., & Philpot, B. D. (2016). Persistent neuronal Ube3a expression in the suprachiasmatic nucleus of Angelman syndrome model mice. *Scientific Reports*, *6*, 28238.

Judson, M. C., Sosa-Pagan, J. O., Del Cid, W. A., Han, J. E., & Philpot, B. D. (2014). Allelic specificity of Ube3a expression in the mouse brain during postnatal development. *Journal of Comparative Neurology*, *522*(8), 1874–1896.

Judson, M. C., Wallace, M. L., Sidorov, M. S., Burette, A. C., Gu, B., van Woerden, G. M., et al. (2016). GABAergic neuron-specific loss of Ube3a causes Angelman syndrome-like EEG abnormalities and enhances seizure susceptibility. *Neuron*, *90*(1), 56–69.

Jung, T.-P., Makeig, S., Westerfield, M., Townsend, J., Courchesne, E., & Sejnowski, T. J. (2000). Removal of eye activity artifacts from visual event-related potentials in normal and clinical subjects. *Clinical Neurophysiology*, *111*(10), 1745–1758.

Kang, J.-Q., & Barnes, G. (2013). A common susceptibility factor of both autism and epilepsy: functional deficiency of GABA A receptors. *Journal of autism and developmental disorders*, *43*(1), 68–79. doi:10.1007/s10803-012-1543-7

Kaplan, T., Fingelkurts, A., Fingelkurts, A., Borisov, SV, & Darkhovsky, B. (2005). Nonstationary nature of the brain activity as revealed by EEG/MEG: Methodological, practical and conceptual challenges. *Signal Processing*, *85*(11), 2190–2212.

Kehrer, C., Maziashvili, N., Dugladze, T., & Gloveli, T. (2008). Altered Excitatory-Inhibitory Balance in the NMDA-Hypofunction Model of Schizophrenia. *Frontiers in molecular neuroscience*, *1*, 6. doi:10.3389/neuro.02.006.2008

Kishino, T., Lalande, M., & Wagstaff, J. (1997). UBE3A/E6-AP mutations cause Angelman syndrome. *Nature genetics*, *15*(1), 70–73.

Koenig, T., Prichep, L., Lehmann, D., Sosa, P. V., Braeker, E., Kleinlogel, H., et al. (2002). Millisecond by millisecond, year by year: normative EEG microstates and developmental stages. *NeuroImage*, *16*(1), 41–48. doi:10.1006/nimg.2002.1070

Laan, L. A., & Vein, A. A. (2005). Angelman syndrome: is there a characteristic EEG? *Brain and Development*, *27*(2), 80–87.

Lancel, M., Cro, T. A., Mu, P., & Holsboer, F. (1994). Pregnenolone enhances EEG delta activity during non-rapid eye movement sleep in the rat, in contrast to midazolam. *Brain research*, *646*(1), 85–94.

Lee, E., Lee, J., & Kim, E. (2017). Excitation/inhibition imbalance in animal models of autism spectrum disorders. *Biological psychiatry*, *81*(10), 838–847.

Lee, T. W., Girolami, M., & Sejnowski, T. J. (1999). Independent component analysis using an extended infomax algorithm for mixed subgaussian and supergaussian sources. *Neural computation*, *11*(2), 417–441.

Lehmann, D., Pascual-Marqui, R. D., & Michel, C. (2009). EEG microstates. *Scholarpedia*, *4*(3), 7632.

Lenartowicz, A., & Loo, S. K. (2014). Use of EEG to diagnose ADHD. *Current psychiatry reports*, *16*(11), 498.

Letellier, C., & Rössler, O. (2007). Hyperchaos. *Scholarpedia*, *2*(8), 1936.

Levisohn, P. M. (2007). The autism-epilepsy connection. *Epilepsia*, *48*, 33–35.

Li, J., Cai, T., Jiang, Y., Chen, H., He, X., Chen, C., et al. (2016). Genes with de novo mutations are shared by four neuropsychiatric disorders discovered from NPdenovo database. *Molecular psychiatry*, *21*(2), 290.

Lindsley, D. B. (1939). A longitudinal study of the occipital alpha rhythm in normal children: Frequency and amplitude standards. *The Pedagogical Seminary and Journal of Genetic Psychology*, *55*(1), 197–213.

Linkenkaer-Hansen, K., Nikouline, V. V., Palva, J. M., & Ilmoniemi, R. J. (2001). Long-range temporal correlations and scaling behavior in human brain oscillations. *The Journal of neuroscience: the official journal of the Society for Neuroscience*, *21*(4), 1370–1377.

Lippé, S., Kovacevic, N., & McIntosh, A. R. (2009). Differential maturation of brain signal complexity in the human auditory and visual system. *Frontiers in Human Neuroscience*, *3*, 48. doi:10.3389/neuro.09.048.2009

Little, M. A., McSharry, P. E., Roberts, S. J., Costello, D. A. E., & Moroz, I. M. (2007). Exploiting nonlinear recurrence and fractal scaling properties for voice disorder detection. *Biomedical engineering online*, *6*, 23. doi:10.1186/1475-925X-6-23

Löscher, W., & Rogawski, M. A. (2012). How theories evolved concerning the mechanism of action of barbiturates. *Epilepsia*, *53*(s8), 12–25.

Lossie, A., Whitney, M., Amidon, D., Dong, H., Chen, P., Theriaque, D., et al. (2001). Distinct phenotypes distinguish the molecular classes of Angelman syndrome. *Journal of medical genetics*, *38*(12), 834–845.

Lowen, S. B., Cash, S. S., Poo, M., & Teich, M. C. (1997). Quantal neurotransmitter secretion rate exhibits fractal behavior. *The Journal of neuroscience: the official journal of the Society for Neuroscience*, *17*(15), 5666–5677.

Lucignani, G., Panzacchi, A., Bosio, L., Moresco, R. M., Ravasi, L., Coppa, I., et al. (2004). GABAA receptor abnormalities in Prader–Willi syndrome assessed with positron emission tomography and [11C] flumazenil. *Neuroimage*, *22*(1), 22–28.

Macdonald, R. L., & Twyman, R. E. (1991). Biophysical properties and regulation of GABAA receptor channels (Vol. 3, pp. 219–230). Presented at the Seminars in Neuroscience, Elsevier.

Manor, B., & Lipsitz, L. A. (2012). Physiologic complexity and aging: Implications for physical function and rehabilitation. *Progress in neuro-psychopharmacology & biological psychiatry*. doi:10.1016/j.pnpbp.2012.08.020

Marshall, P. J., Fox, N. A., & Group, B. C. (2004). A comparison of the electroencephalogram between institutionalized and community children in Romania. *Journal of Cognitive Neuroscience*, *16*(8), 1327–1338.

Matrisciano, F., Bonaccorso, S., Ricciardi, A., Scaccianoce, S., Panaccione, I., Wang, L., et al. (2009). Changes in BDNF serum levels in patients with major depression disorder (MDD) after 6 months treatment with sertraline, escitalopram, or venlafaxine. *Journal of Psychiatric Research*, *43*(3), 247–254.

Matsuura, T., Sutcliffe, J. S., Fang, P., Galjaard, R.-J., Jiang, Y., Benton, C. S., et al. (1997). De novo truncating mutations in E6-AP ubiquitin-protein ligase gene (UBE3A) in Angelman syndrome. *Nature genetics*, *15*(1), 74.

McCauley, J. L., Olson, L. M., Delahanty, R., Amin, T., Nurmi, E. L., Organ, E. L., et al. (2004). A linkage disequilibrium map of the 1-Mb 15q12 GABA(A) receptor subunit cluster and association to autism. *American journal of medical genetics. Part B, Neuropsychiatric genetics: the official publication of the International Society of Psychiatric Genetics*, *131B*(1), 51–59. doi:10.1002/ajmg.b.30038

McEvoy, K., Hasenstab, K., Senturk, D., Sanders, A., & Jeste, S. S. (2015). Physiologic artifacts in resting state oscillations in young children: methodological considerations for noisy data. *Brain imaging and behavior*, *9*(1), 104–114.

McGinnity, C. J., Barros, D. A. R., Rosso, L., Veronese, M., Rizzo, G., Bertoldo, A., et al. (2017). Test-retest reproducibility of quantitative binding measures of [11C] Ro15-4513, a PET ligand for GABAA receptors containing alpha5 subunits. *NeuroImage*, *152*, 270–282.

McIntosh, A. R., Kovacevic, N., & Itier, R. J. (2008). Increased brain signal variability accompanies lower behavioral variability in development. *PLoS computational biology*, *4*(7), e1000106. doi:10.1371/journal.pcbi.1000106

Meng, L., Ward, A. J., Chun, S., Bennett, C. F., Beaudet, A. L., & Rigo, F. (2015). Towards a therapy for Angelman syndrome by targeting a long non-coding RNA. *Nature*, *518*(7539), 409–412. doi:10.1038/nature13975

Menold, M. M., Shao, Y., Wolpert, C. M., Donnelly, S. L., Raiford, K. L., Martin, E. R., et al. (2001). Association analysis of chromosome 15 gabaa receptor subunit genes in autistic disorder. *Journal of neurogenetics*, *15*(3–4), 245–259. doi:10.3109/01677060109167380

Mesbah-Oskui, L., Penna, A., Orser, B. A., & Horner, R. L. (2017). Reduced expression of α5GABAA receptors elicits autism-like alterations in EEG patterns and sleep-wake behavior. *Neurotoxicology and teratology*, *61*, 115–122.

Meyer-Lindenberg, A. (1996). The evolution of complexity in human brain development: an EEG study. *Electroencephalography and Clinical Neurophysiology*, *99*(5), 405–411.

Miao, S., Chen, R., Ye, J., Tan, G.-H., Li, S., Zhang, J., et al. (2013). The Angelman syndrome protein Ube3a is required for polarized dendrite morphogenesis in pyramidal neurons. *Journal of Neuroscience*, *33*(1), 327–333.

Minassian, B. A., Delorey, T. M., Olsen, R. W., Philippart, M., Bronstein, Y., Zhang, Q., et al. (1998). Angelman syndrome: correlations between epilepsy phenotypes and genotypes. *Annals of neurology*, *43*(4), 485–493.

Mitchell, D. J., McNaughton, N., Flanagan, D., & Kirk, I. J. (2008). Frontal-midline theta from the perspective of hippocampal "theta." *Progress in neurobiology*, *86*(3), 156–185.

Mody, I, De Koninck, Y., Otis, T. S., & Soltesz, I. (1994). Bridging the cleft at GABA synapses in the brain. *Trends in neurosciences*, *17*(12), 517–525.

Mody, Istvan. (2001). Distinguishing between GABAA receptors responsible for tonic and phasic conductances. *Neurochemical research*, *26*(8–9), 907–913.

Moeschler, J. B., Mohandas, T., Hawk, A. B., & Noll, W. W. (2002). Estimate of prevalence of proximal 15q duplication syndrome. *American journal of medical genetics*, *111*(4), 440–442.

Møller, R. S., Wuttke, T. V., Helbig, I., Marini, C., Johannesen, K. M., Brilstra, E. H., et al. (2017). Mutations in GABRB3 From febrile seizures to epileptic encephalopathies. *Neurology*, 10–1212.

Moncla, A., Malzac, P., Voelckel, M.-A., Auquier, P., Girardot, L., Mattei, M.-G., et al. (1999). Phenotype–genotype correlation in 20 deletion and 20 non-deletion Angelman syndrome patients. *European Journal of Human Genetics*, *7*(2).

Moreno-De-Luca, D., Sanders, S., Willsey, A., Mulle, J., Lowe, J., Geschwind, D., et al. (2013). Using large clinical data sets to infer pathogenicity for rare copy number variants in autism cohorts. *Molecular psychiatry*, *18*(10), 1090.

Mullen, E. (1995). *Mullen Scales of Early Learning: AGS edition*. Circle Pines, MN: American Guidance Service.

Nichols, T. E., & Holmes, A. P. (2002). Nonparametric permutation tests for functional neuroimaging: a primer with examples. *Human brain mapping*, *15*(1), 1–25.

Nickel, B., & Szelenyi, I. (1989). Comparison of changes in the EEG of freely moving rats induced by enciprazine, buspirone and diazepam. *Neuropharmacology*, *28*(8), 799–803.

Noachtar, S., & Rémi, J. (2009). The role of EEG in epilepsy: a critical review. *Epilepsy & Behavior*, *15*(1), 22–33.

Nunez, P., & Srinivasan, R. (2006). *Electric Fields of the Brain: The Neurophysics of EEG* (second.). Oxford: Oxford University Press.

Nurmi, E. L., Bradford, Y., Chen, Y., Hall, J., Arnone, B., Gardiner, M. B., et al. (2001). Linkage disequilibrium at the Angelman syndrome gene UBE3A in autism families. *Genomics*, *77*(1), 105–113.

Nutt, D. J., & Malizia, A. L. (2001). New insights into the role of the GABAA—benzodiazepine receptor in psychiatric disorder. *The British Journal of Psychiatry*, *179*(5), 390–396.

Nuwer, M. (1997). Assessment of digital EEG, quantitative EEG, and EEG brain mapping: report of the American Academy of Neurology and the American Clinical Neurophysiology Society. *Neurology*, *49*(1), 277–292.

Ogrim, G., Kropotov, J., & Hestad, K. (2012). The quantitative EEG theta/beta ratio in attention deficit/hyperactivity disorder and normal controls: sensitivity, specificity, and behavioral correlates. *Psychiatry research*, *198*(3), 482–488.

Oguro-Ando, A., Rosensweig, C., Herman, E., Nishimura, Y., Werling, D., Bill, B., et al. (2015). Increased CYFIP1 dosage alters cellular and dendritic morphology and dysregulates mTOR. *Molecular psychiatry*, *20*(9), 1069.

Olney, J. W., & Farber, N. B. (1997). Discussion of Bogerts' temporolimbic system theory of paranoid schizophrenia. *Schizophrenia bulletin*, *23*(3), 533–536.

Onton, J., Westerfield, M., Townsend, J., & Makeig, S. (2006). Imaging human EEG dynamics using independent component analysis. *Neuroscience and biobehavioral reviews*, *30*(6), 808–822. doi:10.1016/j.neubiorev.2006.06.007

Oostenveld, R., Fries, P., Maris, E., & Schoffelen, J.-M. (2011). FieldTrip: open source software for advanced analysis of MEG, EEG, and invasive electrophysiological data. *Computational intelligence and neuroscience*, *2011*, 1.

Parikshak, N. N., Swarup, V., Belgard, T. G., Irimia, M., Ramaswami, G., Gandal, M. J., et al. (2016). Genome-wide changes in lncRNA, splicing, and regional gene expression patterns in autism. *Nature*, *540*(7633), 423.

Pennisi, E. (2012). ENCODE project writes eulogy for junk DNA.

Pfurtscheller, G., Neuper, C., Andrew, C., & Edlinger, G. (1997). Foot and hand area mu rhythms. *International Journal of Psychophysiology*, *26*(1–3), 121–135.

Pillai, J., & Sperling, M. R. (2006). Interictal EEG and the diagnosis of epilepsy. *Epilepsia*, *47*(s1), 14–22.

Plenz, D., & Thiagarajan, T. C. (2007). The organizing principles of neuronal avalanches: cell assemblies in the cortex? *Trends in neurosciences*, *30*(3), 101–110. doi:10.1016/j.tins.2007.01.005

Poil, S.-S., Hardstone, R., Mansvelder, H. D., & Linkenkaer-Hansen, K. (2012). Critical-state dynamics of avalanches and oscillations jointly emerge from balanced excitation/inhibition in neuronal networks. *Journal of Neuroscience*, *32*(29), 9817–9823.

Poldrack, R. A. (2006). Can cognitive processes be inferred from neuroimaging data? *Trends in cognitive sciences*, *10*(2), 59–63.

Pop-Jordanova, N., Zorcec, T., Demerdzieva, A., & Gucev, Z. (2010). QEEG characteristics and spectrum weighted frequency for children diagnosed as autistic spectrum disorder. *Nonlinear Biomedical Physics*, *4*(1), 4.

Poyares, D., Guilleminault, C., Ohayon, M. M., & Tufik, S. (2004). Chronic benzodiazepine usage and withdrawal in insomnia patients. *Journal of psychiatric research*, *38*(3), 327–334.

Pritchard, W. S. (1992). The brain in fractal time: 1/f-like power spectrum scaling of the human electroencephalogram. *The International journal of neuroscience*, *66*(1–2), 119–129.

Puffenberger, E. G., Jinks, R. N., Wang, H., Xin, B., Fiorentini, C., Sherman, E. A., et al. (2012). A homozygous missense mutation in HERC2 associated with global developmental delay and autism spectrum disorder. *Human mutation*, *33*(12), 1639–1646.

Rabinovich, M. I., Huerta, R., Varona, P., & Afraimovich, V. S. (2008). Transient cognitive dynamics, metastability, and decision making. *PLoS computational biology*, *4*(5), e1000072. doi:10.1371/journal.pcbi.1000072

Ritter, P., Moosmann, M., & Villringer, A. (2009). Rolandic alpha and beta EEG rhythms' strengths are inversely related to fMRI-BOLD signal in primary somatosensory and motor cortex. *Human brain mapping*, *30*(4), 1168–1187.

Roberts, E. (2007). Gamma-aminobutyric acid. *Scholarpedia*, *2*(10), 3356.

Robinson, A. A., Goldman, S., Barnes, G., Goodpaster, L., & Malow, B. A. (2015). Electroencephalogram (EEG) duration needed to detect abnormalities in angelman syndrome: is 1 hour of overnight recording sufficient? *Journal of child neurology*, *30*(1), 58–62.

Roden, W. H., Peugh, L. D., & Jansen, L. A. (2010). Altered GABAA receptor subunit expression and pharmacology in human Angelman syndrome cortex. *Neuroscience letters*, *483*(3), 167–172.

Roid, G. H. (2003). *Stanford-Binet intelligence scales*. Riverside Pub.

Roid, G. H., & Miller, L. J. (2011). Leiter international performance scale-revised (Leiter-R). *Madrid: Psymtec*.

Rosenhan, D. L. (1973). On being sane in insane places. *Science*, *179*(4070), 250–258.

Rössler, O. (1979). An equation for hyperchaos. *Physics Letters A*, *71*, 155–157.

Roux, F., Wibral, M., Singer, W., Aru, J., & Uhlhaas, P. J. (2013). The phase of thalamic alpha activity modulates cortical gamma-band activity: evidence from resting-state MEG recordings. *The Journal of neuroscience: the official journal of the Society for Neuroscience*, *33*(45), 17827–17835. doi:10.1523/JNEUROSCI.5778-12.2013

Rubenstein, J., & Merzenich, M. M. (2003). Model of autism: increased ratio of excitation/inhibition in key neural systems. *Genes, Brain and Behavior*, *2*(5), 255–267.

Sagan, C. (2011). *The demon-haunted world: Science as a candle in the dark*. Ballantine Books.

Schaefer, G. B., & Mendelsohn, N. J. (2013). Clinical genetics evaluation in identifying the etiology of autism spectrum disorders: 2013 guideline revisions. *Genetics in Medicine*, *15*(5), 399.

Scoles, H. A., Urraca, N., Chadwick, S. W., Reiter, L. T., & LaSalle, J. M. (2011). Increased copy number for methylated maternal 15q duplications leads to changes in gene and protein expression in human cortical samples. *Molecular autism*, *2*(1), 19.

Sharma, A., Hoeffer, C. A., Takayasu, Y., Miyawaki, T., McBride, S. M., Klann, E., & Zukin, R. S. (2010). Dysregulation of mTOR signaling in fragile X syndrome. *Journal of Neuroscience*, *30*(2), 694–702.

Sidorov, M. S., Deck, G. M., Dolatshahi, M., Thibert, R. L., Bird, L. M., Chu, C. J., & Philpot, B. D. (2017). Delta rhythmicity is a reliable EEG biomarker in Angelman syndrome: a parallel mouse and human analysis. *Journal of neurodevelopmental disorders*, *9*(1), 17.

Simon, C. W., & Emmons, W. H. (1956). EEG, consciousness, and sleep. *Science*, *124*(3231), 1066–1069.

Smith, S. (2005). EEG in the diagnosis, classification, and management of patients with epilepsy. *Journal of Neurology, Neurosurgery & Psychiatry*, *76*(suppl 2), ii2–ii7.

Smith, S. E., Zhou, Y.-D., Zhang, G., Jin, Z., Stoppel, D. C., & Anderson, M. P. (2011). Increased gene dosage of Ube3a results in autism traits and decreased glutamate synaptic transmission in mice. *Science translational medicine*, *3*(103), 103ra97-103ra97.

Soong, A. C., & Stuart, C. I. (1989). Evidence of chaotic dynamics underlying the human alpha-rhythm electroencephalogram. *Biological cybernetics*, *62*(1), 55–62.

Souchet, B., Guedj, F., Penke-Verdier, Z., Daubigney, F., Duchon, A., Herault, Y., et al. (2015). Pharmacological correction of excitation/inhibition imbalance in Down syndrome mouse models. *Frontiers in behavioral neuroscience*, *9*, 267.

Souchet, B., Guedj, F., Sahún, I., Duchon, A., Daubigney, F., Badel, A., et al. (2014). Excitation/inhibition balance and learning are modified by Dyrk1a gene dosage. *Neurobiology of disease*, *69*, 65–75.

Sporns, O. (2011). *Networks of the Brain*. Cambridge, MA: MIT Press.

Stam, C. J. (2005). Nonlinear dynamical analysis of EEG and MEG: review of an emerging field. *Clinical neurophysiology: official journal of the International Federation of Clinical Neurophysiology*, *116*(10), 2266–2301. doi:10.1016/j.clinph.2005.06.011

Steriade, M., & Timofeev, I. (2003). Neuronal plasticity in thalamocortical networks during sleep and waking oscillations. *Neuron*, *37*(4), 563–576.

Stief, F., Zuschratter, W., Hartmann, K., Schmitz, D., & Draguhn, A. (2007). Enhanced synaptic excitation–inhibition ratio in hippocampal interneurons of rats with temporal lobe epilepsy. *European Journal of Neuroscience*, *25*(2), 519–528.

Stiles, J., & Jernigan, T. L. (2010). The basics of brain development. *Neuropsychology review*, *20*(4), 327–348.

Stroganova, T. A., Nygren, G., Tsetlin, M. M., Posikera, I. N., Gillberg, C., Elam, M., & Orekhova, E. V. (2007). Abnormal EEG lateralization in boys with autism. *Clinical Neurophysiology*, *118*(8), 1842–1854.

Sugimoto, T., Yasuhara, A., Ohta, T., Nishida, N., Saitoh, S., Hamabe, J., & Niikawa, N. (1992). Angelman syndrome in three siblings: characteristic epileptic seizures and EEG abnormalities. *Epilepsia*, *33*(6), 1078–1082.

Tallon-Baudry, C., & Bertrand, O. (1999). Oscillatory gamma activity in humans and its role in object representation. *Trends in cognitive sciences*, *3*(4), 151–162.

Tallon-Baudry, C., Bertrand, O., Delpuech, C., & Pernier, J. (1997). Oscillatory γ-band (30–70 Hz) activity induced by a visual search task in humans. *Journal of Neuroscience*, *17*(2), 722–734.

Tammimies, K., Marshall, C. R., Walker, S., Kaur, G., Thiruvahindrapuram, B., Lionel, A. C., et al. (2015). Molecular diagnostic yield of chromosomal microarray analysis and whole-exome sequencing in children with autism spectrum disorder. *Jama*, *314*(9), 895–903.

Tanaka, M., DeLorey, T. M., Delgado-Escueta, A., & Olsen, R. W. (2012). GABRB3, epilepsy, and neurodevelopment.

Tanaka, M., Olsen, R. W., Medina, M. T., Schwartz, E., Alonso, M. E., Duron, R. M., et al. (2008). Hyperglycosylation and reduced GABA currents of mutated GABRB3 polypeptide in remitting childhood absence epilepsy. *The American Journal of Human Genetics*, *82*(6), 1249–1261.

Teich, M. C., Heneghan, C., Lowen, S. B., Ozaki, T., & Kaplan, E. (1997). Fractal character of the neural spike train in the visual system of the cat. *Journal of the Optical Society of America. A, Optics, image science, and vision*, *14*(3), 529–546.

Thatcher, R W, North, D. M., & Biver, C. J. (2008). Intelligence and EEG phase reset: a two compartmental model of phase shift and lock. *NeuroImage*, *42*(4), 1639–1653. doi:10.1016/j.neuroimage.2008.06.009

Thatcher, R. W, North, D. M., Neubrander, J., Biver, C. J., Cutler, S., & Defina, P. (2009). Autism and EEG phase reset: deficient GABA mediated inhibition in thalamo-cortical circuits. *Developmental neuropsychology*, *34*(6), 780–800. doi:10.1080/87565640903265178

Thatcher, R. W., North, D. M., & Biver, C. J. (2009). Self-organized criticality and the development of EEG phase reset. *Human brain mapping*, *30*(2), 553–574. doi:10.1002/hbm.20524

Thibert, R. L., Larson, A. M., Hsieh, D. T., Raby, A. R., & Thiele, E. A. (2013). Neurologic manifestations of Angelman syndrome. *Pediatric neurology*, *48*(4), 271–279.

Toib, A., Lyakhov, V., & Marom, S. (1998). Interaction between duration of activity and time course of recovery from slow inactivation in mammalian brain Na+ channels. *The Journal of neuroscience: the official journal of the Society for Neuroscience*, *18*(5), 1893–1903.

Tononi, G., & Edelman, G. M. (1998). Consciousness and complexity. *Science (New York, N.Y.)*, *282*(5395), 1846–1851.

Trillingsgaard, A., & Østergaard, J. R. (2004). Autism in Angelman syndrome: an exploration of comorbidity. *Autism*, *8*(2), 163–174.

Tsuda, I. (2013). Chaotic itinerancy. *Scholarpedia*, *8*(1), 4459.

Uhlhaas, P. J., Roux, F., Rodriguez, E., Rotarska-Jagiela, A., & Singer, W. (2010). Neural synchrony and the development of cortical networks. *Trends in cognitive sciences*, *14*(2), 72–80.

Uhlhaas, P. J., Roux, F., Singer, W., Haenschel, C., Sireteanu, R., & Rodriguez, E. (2009). The development of neural synchrony reflects late maturation and restructuring of functional

networks in humans. *Proceedings of the National Academy of Sciences*, *106*(24), 9866–9871.

Urraca, N., Cleary, J., Brewer, V., Pivnick, E. K., McVicar, K., Thibert, R. L., et al. (2013). The Interstitial Duplication 15q11. 2-q13 Syndrome Includes Autism, Mild Facial Anomalies and a Characteristic EEG Signature. *Autism Research*, *6*(4), 268–279.

Valente, K. D., Andrade, J. Q., Grossmann, R. M., Kok, F., Fridman, C., Koiffmann, C. P., & Marques-Dias, M. J. (2003). Angelman syndrome: difficulties in EEG pattern recognition and possible misinterpretations. *Epilepsia*, *44*(8), 1051–1063.

van Lier, H., Drinkenburg, W. H., van Eeten, Y. J., & Coenen, A. M. (2004). Effects of diazepam and zolpidem on EEG beta frequencies are behavior-specific in rats. *Neuropharmacology*, *47*(2), 163–174.

Varela, F. J. (1995). Resonant cell assemblies: a new approach to cognitive functions and neuronal synchrony. *Biological research*, *28*(1), 81–95.

Veauthier, J., Haettig, H., & Meencke, H.-J. (2009). Impact of levetiracetam add-on therapy on different EEG occipital frequencies in epileptic patients. *Seizure-European Journal of Epilepsy*, *18*(6), 392–395.

Vendrame, M., Loddenkemper, T., Zarowski, M., Gregas, M., Shuhaiber, H., Sarco, D. P., et al. (2012). Analysis of EEG patterns and genotypes in patients with Angelman syndrome. *Epilepsy & Behavior*, *23*(3), 261–265.

Voytek, B., Kramer, M. A., Case, J., Lepage, K. Q., Tempesta, Z. R., Knight, R. T., & Gazzaley, A. (2015). Age-related changes in 1/f neural electrophysiological noise. *Journal of Neuroscience*, *35*(38), 13257–13265.

Wang, J., Barstein, J., Ethridge, L. E., Mosconi, M. W., Takarae, Y., & Sweeney, J. A. (2013). Resting state EEG abnormalities in autism spectrum disorders. *Journal of neurodevelopmental disorders*, *5*(1), 24.

Wang, X., Meng, J., Tan, G., & Zou, L. (2010). Research on the relation of EEG signal chaos characteristics with high-level intelligence activity of human brain. *Nonlinear Biomedical Physics*, *4*(1), 2. doi:10.1186/1753-4631-4-2

Wang, X.-J. (2010). Neurophysiological and computational principles of cortical rhythms in cognition. *Physiological reviews*, *90*(3), 1195–1268.

Welch, P. (1967). The use of fast Fourier transform for the estimation of power spectra: a method based on time averaging over short, modified periodograms. *IEEE Transactions on audio and electroacoustics*, *15*(2), 70–73.

Werner, G. (2007). Metastability, criticality and phase transitions in brain and its models. *Bio Systems*, *90*(2), 496–508. doi:10.1016/j.biosystems.2006.12.001

West, B. T., Welch, K. B., & Galecki, A. T. (2014). *Linear mixed models: a practical guide using statistical software*. Chapman and Hall/CRC.

West, L., Waldrop, J., & Brunssen, S. (2009). Pharmacologic treatment for the core deficits and associated symptoms of autism in children. *Journal of Pediatric Health Care*, *23*(2), 75–89.

Whitford, T. J., Rennie, C. J., Grieve, S. M., Clark, C. R., Gordon, E., & Williams, L. M. (2007). Brain maturation in adolescence: concurrent changes in neuroanatomy and neurophysiology. *Human brain mapping*, *28*(3), 228–237.

Williams, C. A. (1995). Angelman syndrome: consensus for diagnostic criteria. *American journal of medical genetics*, *56*(2), 237–238.

Williams, C. A. (2005). Neurological aspects of the Angelman syndrome. *Brain and Development*, *27*(2), 88–94.

Wisor, J. P., DeLorey, T. M., Homanics, G. E., & Edgar, D. M. (2002). Sleep states and sleep electroencephalographic spectral power in mice lacking the β3 subunit of the GABAA receptor. *Brain research*, *955*(1–2), 221–228.

Womelsdorf, T., Valiante, T. A., Sahin, N. T., Miller, K. J., & Tiesinga, P. (2014). Dynamic circuit motifs underlying rhythmic gain control, gating and integration. *Nature neuroscience*, *17*(8), 1031.

Yamasaki, K., Joh, K., Ohta, T., Masuzaki, H., Ishimaru, T., Mukai, T., et al. (2003). Neurons but not glial cells show reciprocal imprinting of sense and antisense transcripts of Ube3a. *Human molecular genetics*, *12*(8), 837–847.

Yang, Y., & Raine, A. (2009). Prefrontal structural and functional brain imaging findings in antisocial, violent, and psychopathic individuals: a meta-analysis. *Psychiatry Research: Neuroimaging*, *174*(2), 81–88.

Zaitsev, M., Maclaren, J., & Herbst, M. (2015). Motion artifacts in MRI: a complex problem with many partial solutions. *Journal of Magnetic Resonance Imaging*, *42*(4), 887–901.

Zimmerman, I., Steiner, V., & Pond, R. (2011). PLS-5: Preschool language scale-5 [measurement instrument]. *San Antonio, TX: Psychological Corporation*.

Zurek, A. A., Kemp, S. W., Aga, Z., Walker, S., Milenkovic, M., Ramsey, A. J., et al. (2016). α5GABAA receptor deficiency causes autism-like behaviors. *Annals of clinical and translational neurology*, *3*(5), 392–398.